Université des Sciences et Technologies de Lille
Laboratoire de Mécanique de Lille (UMR CNRS 8107)
Ecole Doctorale régionale Sciences Pour l'Ingénieur Lille Nord-de-France
Année 2009 - N° d'ordre : 40131

THESE

Pour obtenir le grade de

Docteur de l'Université des Sciences et Technologies de Lille

Discipline : Génie Civil

Présentée par

Tao JIANG

Contributions à la modélisation micromécanique des comportements anélastiques des géomatériaux hétérogènes

Soutenue publiquement le 09 Décembre 2009

devant le jury composé de

MM.	A. GIRAUD	Professeur, Université Metz	Rapporteur
	D. LYDZBA	Professeur, Université Polytechnique Wroclaw Pologne	Rapporteur
	D. KONDO	Professeur, Université Lille 1 Sciences et Technologies	Examinateur
	A. POUYA	Directeur de recherche CNRS, Laboratoire central des ponts et chaussées	Examinateur
	W.Y. XU	Professeur, Université de HOHAI, Chine	Examinateur
	J.F. SHAO	Professeur, Université Lille 1 Sciences et Technologies	Directeur de thèse

Acknowledgement

I would like to gratefully and sincerely thank Prof. Jianfu Shao for his guidance, understanding, patience, and most importantly, his friendship during my doctoral studies at Université de Lille-1. This dissertation work would have never been accomplished without his valuable guidance and support. His mentorship was paramount in providing a well rounded experience consistent my long-term career goals.

I would also like to thank Prof. Weiya Xu in Hohai University, as the director of my first PhD in China, for his help and encouragement.

My gratitude goes to Prof. Jean-Claude Michel and Prof. Pierre Suquet in LMA for their valuable help and advices about the NTFA calculation. My thanks also go to Prof. Djimédo Kondo and Dr. Ariane Abou-Chakra Guery for many helpful suggestions about the incremental method.

I am grateful for the presence of Prof. Ahmad Pouya as the president of the defence committee. I am also thankful to Prof. Albert Giraud and Prof. Dariusz Lydzba for their modification and comment of my dissertation.

I would also like to thank all the members of the research group ER4 in LML, including Dr. Shouyi Xie, Qizhi Zhu, Yun Jia, Jian Lin, Liang Chen, Dawei Hu… They gave me not only many help in the doctoral research, but also provide much humor and entertainment to relax me the stressful laboratory environment.

Finally, and most importantly, I would like to thank my wife Ningzhi Zhou. Her support, encouragement, quiet patience and unwavering love are undeniably the bedrock upon which I have built. I also thank our parents, for their faith in me and unending encouragement and support to me.

Contents

Introduction générale:

La modélisation du comportement mécanique non linéaire des géomatériaux est un aspect essentiel pour l'analyse de la stabilité et de la durabilité des structures et des ouvrages dans de divers domaines d'application d'ingénieur comme la construction des espaces souterrain, le stockage des déchets radioactifs et des gaz résiduels, l'exploitation des hydrocarbures, la construction des infrastructures dans les transports etc. Dans ces domaines d'application, les géomatériaux concernés (sols, roches et matériaux cimentaires) sont souvent soumis à des sollicitations couplées d'origines différentes telles que mécanique, hydraulique, hydrique, thermique et chimique. Il convient alors de prendre en compte ces différents phénomènes de couplage. La maîtrise du comportement mécanique des géomatériaux sous sollicitations complexes est le point de départ pour la modélisation des couplages.

Par ailleurs, par leur histoire de formation et procédure de fabrication, les géomatériaux sont quasi exclusivement des matériaux hétérogènes dans des échelles variées. Le comportement macroscopique de ces matériaux est intimement lié à leur microstructure et son évolution. Par exemple, le comportement mécanique d'une roche est fortement dépendent de sa composition minéralogique. Afin d'étudier et de modéliser le comportement mécanique des géomatériaux, des essais en laboratoires conventionnels comme compression triaxiale fournissent une base de données indispensables pour la caractérisation du comportement macroscopique. Ces essais sont généralement réalisés dans des échantillons de tailles différentes permettant de représenter un volume élémentaire représentatif (VER) du matériau. Cependant, afin de mieux cerner des mécanismes de déformation et de la rupture des géomatériaux, des observations et des expérimentations microscopiques s'avèrent de plus en plus utiles et indispensables. De nombreuses méthodes expérimentales nouvelles ont été développées pendant les dernières décennies visant à caractériser les déformations locales, les évolutions de la microstructure comme microfissuration et variation de porosité. L'amélioration de ces méthodes expérimentales microscopique représente encore un challenge largement ouvert dans le domaine expérimental.

Dans le domaine de la modélisation, de nombreux et divers modèles ont été proposés pour décrire le comportement mécanique des géomatériaux. D'une manière simplifiée, on peut distinguer deux types de modèles. Les modèles macroscopiques ou phénoménologiques sont formulés essentiellement en se basant sur des données expérimentales en laboratoire et in situ et

en utilisant le cadre théorique de la thermodynamique des processus irréversibles. On peut citer par exemple des modèles plastiques isotropes ou anisotropes, des modèles d'endommagement isotropes et anisotropes, des modèles viscoplastiques, des modèles couplés etc. Des propres récents et significatifs ont également été réalisés quant à la précision des simulations fournies par de tels modèles. On est maintenant capable de décrire des réponses complexes des géomatériaux sous sollicitations très variées. Les modèles macroscopiques sont également utilisés dans des applications industrielles et fournissent ainsi un outil de modélisation numérique efficace. Cependant, les modèles macroscopiques ne permettent pas de prendre en compte directement des effets de l'hétérogénéité et des mécanismes physiques mis en jeu à différentes échelles de la microstructure des géomatériaux. A titre d'exemple, il n'est pas possible d'inclure directement des effets de la composition minéralogique dans un modèle macroscopique. Pour compléter ainsi les modélisations macroscopiques, des modèles micromécaniques ont également proposés notamment pour des matériaux fragiles et des matériaux granulaires. Par exemple, différents modèles d'endommagement micromécaniques ont été formulés pour des matériaux quasi fragiles (roches et bétons), soit en utilisant les principes de la mécanique de la rupture linéaire, soit en utilisant les techniques d'homogénéisation des milieux périodiques ou aléatoires. D'une manière générale, il s'agit souvent d'étudier à une échelle microscopique pertinente la nucléation et la propagation de microfissures. Les outils mathématiques utilisés dans les techniques d'homogénéisation des milieux élastiques comme la solution d'Eshelby d'un problème d'inclusion ont été adaptées. En revanche, lorsqu'il s'agit de la modélisation micromécanique du comportement des matériaux hétérogènes composés des constituants ayant un comportement inélastique, le problème devient largement plus complexe et reste encore largement ouvert. Dans le domaine des matériaux composites à matrice métallique (ou céramique) ou polycristallins, d'importants progrès de modélisation micromécanique ont été accomplis pendant des dernières décennies ; on peut citer les méthodes incrémentales, les méthodes sécantes, tangentes et affines, les méthodes d'analyse de champs de transformation uniformes (transformation field analysis – TFA) et non uniformes (non–uniform transformation analysis – NTFA), et les modèles auto cohérentes pour polycristallins etc. L'adaptation de ces méthodes d'homogénéisation non linéaire est un sujet de recherche d'actualité et prometteuse pour la modélisation micromécanique des géomatériaux non linéaires. C'est dans ce contexte général que le présent travail de thèse est proposé.

Nous proposons d'aborder la question de modélisation micromécanique d'une classe de géomatériaux hétérogènes ayant une morphologie matrice/inclusion ou matrice/pores (matériaux poreux) ; le comportement mécanique de la matrice étant anélastique. On s'intéressera notamment à la modélisation du comportement mécanique d'une roche argileuse raide dite argilite de Meuse-

Haute Marne (MHM), qui est largement étudiée dans le cadre des études de faisabilité du stockage des déchets radioactifs menées par l'ANDRA (agence nationale de gestion des déchets radioactifs). Le présente travail représente la poursuite d'une série de travaux effectués dans l'équipe de recherche « couplages THMC » du laboratoire de mécanique de Lille (UMR 8107 CNRS), notamment de la thèse de doctorat d'Abou-Chakra Guéry (2007). Dans ladite thèse, la méthode incrémentale de Hill (1965) a été adptée pour la modélisation du comportement mécanique à court et à long terms de l'argilite de MHM. La roche a été considérée comme un composite à trois phases : matrice argileuse plastique, grains de calcite élastiques endommageables et grains de quartz élastisques. Dans la première partie de notre travail, nous présenterons quelques extensions de ce travail. L'argillite sera éttudiée comme un composite à deux phases; matrice argileuse plastique endommageable et les inclisons minéralogiques (calcite et quartz). En plus, des études numériques complémentaires seront effectuées sur la qualité redictive de la méthode incrémentales en terme de la technique d'isotropisation et de la nature du comportement local. Des comparaisons entre des prédictions numériques et données expérimentales et entre les deux modèles micromécaniques seront également présentées.

Le modèle incrémentale fait partie des approches dites de « champs moyens ». La principale hypothèse et également le principal défaut de ces approches est le fait qu'on suppose que les champs locaux sont unifomes dans chaque phase. Dans le cas des métriaux hétérogènes non linéaires, cette hypothèse est à toute évident trop forte et ne reflète pas des champs locaux qui peuvent être fortement non-uniformes. Pour prendre en compte cette hétéronégéité des champs locaux, différentes méthodes ont été proposées pour des matériaux composites, on cite notamment les méthodes «transformation field analysis- TFA» (Dvorak, 1992) et «non-uniform transformation field analysis- NTFA » (Michel et Suquet, 2003). Les principaux de ces deux méthodes seront présentés dans le chapitre 1 de ce mémoire. Dans la deuxième partie du présent travail, nous proposons une adaptation de la méthode (NTFA) à la modélisation micromécanique des géomatériaux. Le principe de base est d'approcher le champ de déformation plastique locale par une combinaison linéaire des modes de déformations plastiques orthgonaux. La formulation et la mise en œuvre de cette méthode sera présentée dans le chapitre 4. Des applications numériques à des composites matrice/inclusion et des matériaux poreux seront présentées et comparées avec l'approche incrémentale. Enfin dans le dernier chapitre, une epremière phase d'application de la méthode (NTFA) à la modélisation de l'argilite de MHM sera aborée.

Principal Notations

Notations of tensorial operations:

a	scalar	.	simple contraction
$\underline{a}$	first order tensor (vector)	:	double contraction
$\underline{\underline{a}}$	second order tensor	$\otimes$	tensor product
$\mathbb{A}$	fourth order tensor	$\overset{s}{\otimes}$	symmetric tensor product
$\underline{\underline{\delta}}$	second order unit tensor	$tr\underline{\underline{a}}$	trace of second order tensor

$\mathbb{I}$ fourth order unit tensor, $I_{ijkl} = \frac{1}{2}(\delta_{ik}\delta_{jl} + \delta_{il}\delta_{jk})$

$\mathbb{J}$ volumetric projection operator of fourth order tensor, $J_{ijkl} = \frac{1}{3}\delta_{ij}\delta_{kl}$

$\mathbb{K}$ deviatoric projection operator of fourth order tensor, $K_{ijkl} = I_{ijkl} - J_{ijkl}$

Notations of main variables:

$\underline{\underline{\sigma}}$ microscopic stress tensor

$\underline{\underline{\varepsilon}}$ microscopic strain tensor

$\underline{\xi}$ microscopic displacement vector

$\underline{\underline{s}}$ deviator stress

σ_m microscopic hydrostatic (or mean) stress, $\sigma_m = \frac{1}{3}tr\underline{\underline{\sigma}}$

σ_{eq} microscopic equivalent stress, $\sigma_{eq} = \sqrt{\frac{3}{2}\underline{\underline{s}} : \underline{\underline{s}}}$

$\underline{\underline{\Sigma}}$ macroscopic stress tensor

$\underline{\underline{E}}$ macroscopic strain tensor

Σ_m macroscopic hydrostatic (or mean) stress

Σ_{eq} microscopic equivalent stress

E Young's modulus

ν Poisson's ratio

k bulk modulus

G shear modulus

a^{hom} homogenized quantity

a_r value in phase r

$\mathbb{C}$ fourth order elastic stiffness tensor

$\mathbb{L}$ fourth order tangent stiffness tensor

$\mathbb{A}$ localization tensor

$\mathbb{P}$ Hill's tensor

$\mathbb{S}^E$ Eshelby tensor

Chapter 1:
Introduction to multiscale analyses of nonlinear heterogeneous materials and basic mechanical behavior of argillites

In this chapter, we propose to give a short review of main homogenization techniques developed for multiscale modeling of nonlinear heterogeneous materials. The emphasis will be put on the Hill's incremental method and non-uniform transformation field analysis (NTFA), which are used and adapted to geomaterials in this work. A short summary will also be given on the basic mechanical behavior of a hard clay rock (the argillites MHM) to which the two aforementioned methods will be applied.

1.1 Principles and general procedures of nonlinear homogenization

The primary assumption of mechanics of continuous media is that the medium is homogeneous, whose geometry and mechanical characteristics can be described by continuous functions. However, almost all the natural engineering materials, such as rocks, soils, woods, and many man-made engineering materials, such as concrete, mortar, alloy, ceramics, etc., are multiphase and multi-scale material systems. They are not homogeneous in microscopic scale, actually with complicated constituents and microstructures, even though some homogeneous properties are revealed in macroscopic scale.

Mostly, the details of individual component properties and geometrical arrangement of constituents are not concerned in engineering practice. Instead the overall effective or homogenized material properties are used to evaluate the performance of the heterogeneous material and predict the macroscopic structure responses. However, those effective or homogenized properties are usually difficult to measure directly. Therefore the development of homogenization method is motivated to derive the homogenized material properties directly from the property of each individual constituent and their microstructures (Kanouté et al. 2009).

It has been widely studied in great deal of literatures of various homogenization methods to forecast the overall properties of heterogeneous materials with linear elastic properties based on micromechanics. Most of them own good abilities to predict the effective properties very accurately taking account of different shapes and spatial distribution of constituents (Nemat-Nasser & Hori, 1999; Torquato, 2001; Segurado & Llorca, 2001; Milton, 2004; Li and Wang, 2008), or even extended to simulate multi-phase or linear thermo-elasticity heterogeneous

materials (Lielens, 1999; Pierard et al., 2004). However, the situation for nonlinear heterogeneous materials is much more complicated, and many difficulties emerge when these methods are extended to predicting nonlinear heterogeneous materials because the strain localization during plastic deformation is more difficult to capture. Various approaches dealing with nonlinear homogenization method are proposed in the latest decades, some of which are extended directly from the linear homogenization method, others are specially created for nonlinear heterogeneous materials.

In this section, a short review will be given to introduce the principles of nonlinear homogenization methods and some most common approaches applied to obtain the equivalent properties of nonlinear heterogeneous materials.

1.1.1 Basic principles of nonlinear homogenization

In the framework of micromechanics, the mechanical properties of a macroscopic material point $M(\underline{X})$ regarded as a regular homogeneous medium, are equivalent to the overall properties of a representative volumetric element (RVE) in microscopic scale. $\underline{\underline{\Sigma}}$ and $\underline{\underline{E}}$ are macroscopic stress and strain tensor at the material point M, respectively. In fact, the choice of the RVE must satisfy such scale conditions (Zaoui, 2000; Zaoui, 2002):

$$d_0 \ll d \ll l \ll L, \quad l \ll \lambda \tag{1.1}$$

where l, L, d, d_0, λ are respectively the sizes of RVE, macroscopic structure, microscopic heterogeneities (i.e. inclusions, grains, pores), molecular structure, and load fluctuate. The geometrical domain of the RVE is denoted by Ω, and each microscopic point in the RVE is represented by the its position vector $\underline{z}$. $\underline{\underline{\sigma}}(\underline{z})$ and $\underline{\underline{\varepsilon}}(\underline{z})$ are microscopic stress and strain tensor at the microscopic point $\underline{z}$. In order to estimate local stress and strain distribution inside the RVE, two kinds of boundary conditions, uniform stress condition and uniform strain condition, are generally prescribed on the exterior boundaries of the RVE, noted by $\partial\Omega$. These two loading conditions are expressed as:

- Uniform stress boundary condition (Figure 1-1 (a)):

$$\underline{T}^d(\underline{z}) = \underline{\underline{\sigma}}(\underline{z}).\underline{n}(\underline{z}) = \underline{\underline{\Sigma}}.\underline{n}(\underline{z}) \quad (\forall \underline{z} \in \partial\Omega) \tag{1.2}$$

where $\underline{n}(\underline{z})$ is the outward unit normal to the boundary of the RVE at microscopic point $\underline{z}$. From this uniform boundary condition, we can deduce the condition that the volumetric average of microscopic stress field in RVE must be equal to the prescribed macroscopic stress $\underline{\underline{\Sigma}}$ (Dormieux et al. 2006):

$$\left\langle \underline{\underline{\sigma}}(\underline{z}) \right\rangle_{\Omega} = \underline{\underline{\Sigma}} \tag{1.3}$$

$<.>_{\Omega}$ denotes the volumetric average operator defined as:

$$\langle x \rangle = \frac{1}{|\Omega|} \int_{\Omega} x dV \tag{1.4}$$

- Uniform strain boundary condition (Figure 1-1(b)):

$$\underline{\xi}(\underline{z}) = \underline{\underline{E}}.\underline{z} \quad (\forall \underline{z} \in \partial\Omega) \tag{1.5}$$

$\underline{\xi}(\underline{z})$ is the displacement vector at the microscopic point $\underline{z}$. We can derive in this case the condition that the volumetric average of microscopic strain field in RVE must be equal to the prescribed macroscopic strain $\underline{\underline{E}}$:

$$\left\langle \underline{\underline{\varepsilon}}(\underline{z}) \right\rangle_{\Omega} = \underline{\underline{E}} \tag{1.6}$$

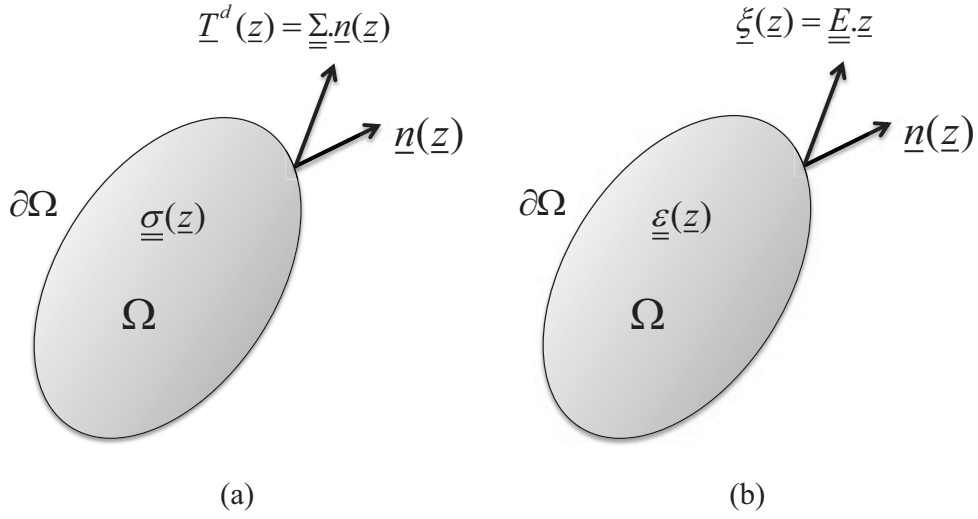

(a) (b)

Figure 1-1: Two types of boundary conditions applied to RVE

(a) Uniform stress boundary condition; (b) Uniform strain boundary condition.

Nonlinear homogenization methods deal with heterogeneous materials composed of nonlinear material phases; which, when deformed have a partly reversible and partly irreversible response (Lahellec & Suquet, 2007). Generally, reversible effects are associated with a free energy density depending only on the state variables of the material which consists of all the energy available in a given state of the system (at a given material point). The evolution of the system is characterized by the changes of state variables, and controlled by the thermodynamic forces which are obtained by derivation of the free energy with respect to the state variables. Meanwhile, the irreversible effects are characterized by dissipation along an evolution path of the system. The evolution equations for state variables can be derived in a commonly used formulation from the dissipation potential (Lahellec & Suquet, 2007). Different homogenization methods for nonlinear materials have so far been developed. In the following sections, some typical approaches will be shortly reviewed and discussed.

1.1.2 Mean filed approaches for nonlinear homogenization method

Different mean field approaches are largely used to determine the overall properties of nonlinear heterogeneous materials. All of them assume that the stress and strain fields in each constituent phase can be adequately represented by some kind of averaged values or eigenvalues, though they differ in the way they account for the elastic interaction between the phases. They are usually based on the generalization of Eshelby inclusion solution (Eshelby, 1957) and particularly useful for situations with random microstructures. Generally they deliver only average values of local stress and strain and are not formulated in order to obtain the local stress and strain fields (Chaboche et al., 2001). According to the different methods for the linearization of local constitutive laws, mean filed approaches can be categorized in to some specific classes. Three mainly used mean field approaches are briefly reviewed here.

- Hill's tangent incremental method

In 1965 Hill (Hill, 1965) proposed a method to transform the nonlinear homogenization problem to a multi linear one in an incremental form:

$$\dot{\underline{\underline{\sigma}}}(\underline{z}) = \mathbb{L}(\underline{z}) : \dot{\underline{\underline{\varepsilon}}}(\underline{z}) \tag{1.7}$$

where $\mathbb{L}(\underline{z})$ is the tangent operator (related to local constitutive relations) at each microscopic point. Then the macroscopic tangent operator can be determined in such a form, where it is assumed that the local tangent operator is uniform inside each phase and is calculated by means of some average strain of the phase at the current loading step:

$$\dot{\underline{\underline{\sigma}}}_r = \mathbb{L}_r : \dot{\underline{\underline{\varepsilon}}}_r \tag{1.8}$$

Where the fourth order tensor, $\mathbb{L}_r$, is the local tangent operator of the r^{th} material phase. $\underline{\underline{\varepsilon}}_r$ is the average value of local strain field in this phase, which is used as a reference strain state to evaluate $\mathbb{L}_r$. Then the macroscopic effective tangent operator to the reference homogeneous medium can be formulated by such expression:

$$\mathbb{L}^{\text{hom}} = \left\langle \mathbb{L}(\underline{z}) : \mathbb{A}(\underline{z}) \right\rangle = \sum_r c_r \mathbb{L}_r : \mathbb{A}_r \tag{1.9}$$

in which c_r is the volume fraction of the phase r, and $\mathbb{A}_r$ is the localization tensor of instantaneous tangent strain, which should be determined at each increment with an appropriate homogenization scheme, such as the dilute scheme, Mori-Tanaka scheme (Mori & Tanaka, 1973) etc. Finally, the overall tangent behavior can be expressed as:

$$\dot{\underline{\underline{\Sigma}}} = \mathbb{L}^{\text{hom}} : \dot{\underline{\underline{E}}} \tag{1.10}$$

It is the actual starting point of a whole range of schemes using linearization of the constitutive relations of the phases. This incremental formulation has been considered for a long time the standard for deriving nonlinear estimates of heterogeneous materials (Masson et al., 2000). This kind of methods have been largely applied to two phase nonlinear composite materials, for instance Chaboche (2005) for metals with von-Mises type plasticity theory, Doghri (2003) for cyclic plasticity with non linear kinematical hardening.

- Secant method

Following Hill's works, many researchers proposed other ways to linearize local nonlinear constitutive equations other than the tangent form. One of them is called "secant" approach (Berveiller & Zaoui, 1979; Tandon & Weng, 1988), in which the secant modulus tensor $\mathbb{L}^{\text{sec}}$ is defined in order to replace the local constitutive equation of each material phase by the following linear secant form:

$$\sigma(\underline{z}) = \mathbb{L}(\underline{z}) : (\varepsilon(\underline{z}) - \varepsilon^p(\underline{z})) \quad \Rightarrow \quad \underline{\underline{\sigma}}_r = \mathbb{L}_r^{\text{sec}} : \underline{\underline{\varepsilon}}_r \tag{1.11}$$

$\mathbb{L}_r^{\text{sec}}$ is the secant modulus tensor of the phase r. After volumetric averaging, the macroscopic constitutive equation can be obtained and also written in secant form:

$$\underline{\underline{\Sigma}} = \mathbb{L}^{\text{sec}} : \underline{\underline{E}} \tag{1.12}$$

$\mathbb{L}^{\text{sec}}$ is the macroscopic secant modulus tensor for the equivalent homogenized medium.

- Affine approach

More recently, Masson (1998), Masson et al. (2000) proposed an "affine" approximation using the tangent stiffness tensor but in a non-incremental form to linearize the local constitutive equation:

$$\underline{\underline{\sigma}}_r = \mathbb{L}_r : \underline{\underline{\varepsilon}}_r + \underline{\underline{\sigma}}_r^0 \tag{1.13}$$

Then the overall constitutive equation is obtained as:

$$\underline{\underline{\Sigma}}_r = \mathbb{L} : \underline{\underline{E}}_r + \underline{\underline{\Sigma}}_r^0 \tag{1.14}$$

Chaboche et al. (2001) gave a schematic diagram (Figure 1-2) illustrating the three different mean field localization approaches to describe the instantaneous local behavior of nonlinear heterogeneous materials.

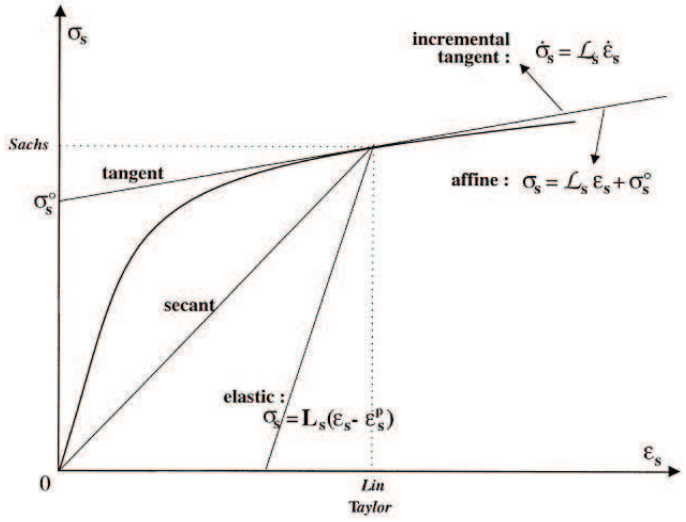

Figure 1-2: Schematic illustration of different methods for linearization of local constitutive relation used in nonlinear homogenization techniques (Chaboche et al., 2001)

1.1.3 Transformation field analysis (TFA)

The most important assumption of mean filed approaches is that the local stress and strain fields in each phase are uniform. However, these physical fields are heterogeneously distributed in every phase. It has been long recognized that for nonlinear heterogeneous materials the exact determination of the effective constitutive relations requires the accurate description of all microscopic plastic strain fields in RVE (Rice, 1970; Mandel, 1972; Suquet, 1985). The consequence of this theoretical result is that the number of macroscopic internal variable required for determining the macroscopic effective behavior is equal to the product of the number of integration points at all scales, which is nearly infinite. Therefore some approximations need to be made to derive a useable and reasonably accurate macroscopic constitutive model. The "Transformation field analysis" (TFA) proposed by Dvorak (Dvorak & Benveniste, 1992; Dvorak, 1992) is an elegant way to reduce the number of macroscopic internal variables by assuming the microscopic fields of internal variables to be piecewise uniform. Many scholars including Dvorak himself developed this method for complex behaviors, such as thermo-visco-plasticity, damage, or interface debonding (Dvorak et al., 1994; Chaboche et al., 2001; Dvorak & Zhang, 2001; Fish & Yu, 2002; Fish et al., 1997; Kattan & Voyiadjiis, 1993). There are two main assumptions with the "Transformation Field Analysis" (TFA):

- H1: The plastic strain field is piecewise uniform

Considering a RVE of a heterogeneous material occupying a domain denoted by V, subdivide the volume V into several local sub-domains $V_r\ (r=1,2,....,N)$. The plastic strain field $\underline{\underline{\varepsilon}}^{an}(\underline{x})$ is uniform in each sub-domain, that is:

$$\underline{\underline{\varepsilon}}^{an}(\underline{x})=\sum_{r=1}^{N}\underline{\underline{\varepsilon}}_r^{an}\chi^{(r)}(\underline{x}) \tag{1.15}$$

$$\chi^{(r)}(\underline{x})=\begin{cases}1 & if\ \underline{x}\in V_r\\ 0 & if\ \underline{x}\notin V_r\end{cases} \tag{1.16}$$

where $\underline{\underline{\varepsilon}}_r^{an}$ is a constant tensor in V_r, independent of coordinates. Under this assumption the average strain and stress in V_r can be derived as:

$$\underline{\underline{E}}_r=\mathbb{A}_r:\underline{\underline{E}}+\sum_{s=1}^{N}\mathbb{D}_{rs}:\underline{\underline{\varepsilon}}_s^{an}\qquad (r=1,2,....,N) \tag{1.17}$$

$$\underline{\underline{\Sigma}}_r=\mathbb{C}^{(r)}:(\underline{\underline{E}}_r-\underline{\underline{\varepsilon}}_r^{an}) \tag{1.18}$$

in which $\mathbb{A}_r$ and $\mathbb{D}_{rs}$ are the average strain localization tensor and influence tensor, respectively. The components of these two tensors can be obtained by the following integrations:

$$\mathbb{A}_r=\frac{1}{c_r}\frac{1}{|V|}\int_V\mathbb{A}(\underline{x})\chi^{(r)}(\underline{x})d\underline{x} \tag{1.19}$$

$$\mathbb{D}_{rs}=\frac{1}{c_r}\frac{1}{|V|}\frac{1}{|V|}\int_V\int_V\chi^{(r)}(\underline{x})\mathbb{G}(\underline{x},\underline{x}'):\mathbb{C}(\underline{x}')\chi^{(s)}(\underline{x}')d\underline{x}'d\underline{x} \tag{1.20}$$

where $c_r=|V_r|/|V|$, representing the volumetric fraction of phase r; $\mathbb{G}(\underline{x},\underline{x}')$ is the non local elastic Green operator.

- H2: Internal variables in each sub-domain can be replaced by an average value

This assumption means that the evolution of the internal variables in sub-domain r follows exactly the constitutive relations of a particular phase containing such sub-domain, and all the internal variables can be replaced by average value, as a homogeneous material.

1.1.4 Non-uniform transformation field analysis (NTFA)

Compared with the mean field approaches which treat the heterogeneous plastic strain field in RVE as a uniform distribution, the TFA takes account of in some extent the heterogeneity of plastic strain distribution. However, it has been recognized by many scholars (Suquet, 1997; Chaboche et al., 2001; Michel et al., 2000) that the TFA may require, for nonlinear heterogeneous materials, a relative dense subdivision of each individual phase into several sub-domains to obtain a satisfactory description of the effective behavior. As a consequence, the number of macroscopic internal variables needed in the effective constitutive relations to obtain an acceptable result, although finite, can be still prohibitively high (Michel & Suquet, 2004).

In order to better describe the plastic strain distribution in the RVE and obtain more accurate solutions with less internal variables, Michel and Suquet (2003; 2004) proposed and Rossete (2008) improved a new approach based on the TFA, named "Non-uniform transformation field analysis" (NTFA), expressing the heterogeneous plastic strain field with a linear combination of some predefined plastic modes, which owns a better ability to describe the heterogeneity of plastic field and the overall behavior of nonlinear heterogeneous materials.

The basic hypothesis of NTFA is that the heterogeneous plastic strain field can be expressed as a linear combination of a set of pre-calculated fields $\underline{\underline{\mu}}^{(k)}$, named "plastic modes" (Michel & Suquet, 2003; 2004):

$$\underline{\underline{\varepsilon}}^{an}(\underline{x}) = \sum_{k=1}^{M} \varepsilon_k^{an} \underline{\underline{\mu}}^{(k)}(\underline{x}) \tag{1.21}$$

where M is the total number of plastic modes. According to Michel & Suquet (2004), further assumptions should be satisfied such that the plastic modes are incompressible, i.e. $tr(\underline{\underline{\mu}}^{(k)}) = 0$; orthogonal, i.e. $\left\langle \underline{\underline{\mu}}^{(k)} : \underline{\underline{\mu}}^{(l)} \right\rangle = 0$ (if $k \neq l$) and normalized, i.e. $\left\langle \mu_{eq}^{(k)} \right\rangle = 1$. All the related variables and constitutive equations can be decomposed in such a space.

Moreover, it is proposed to define a group of reduced variables to represent total strain, plastic strain, stress, strain localization tensor, and Green's operator, listed as follows respectively:

$$e_k = \left\langle \underline{\underline{\varepsilon}}(\underline{x}) : \underline{\underline{\mu}}^{(k)}(\underline{x}) \right\rangle, \quad e_k^{an} = \left\langle \underline{\underline{\varepsilon}}^{an}(\underline{x}) : \underline{\underline{\mu}}^{(k)}(\underline{x}) \right\rangle \tag{1.22}$$

$$\tau_k = \left\langle \underline{\underline{\sigma}}(\underline{x}) : \underline{\underline{\mu}}^{(k)}(\underline{x}) \right\rangle \tag{1.23}$$

$$\underline{\underline{a}}^{(k)} = \left\langle {}^{T}\mathbb{A}(\underline{x}) : \underline{\underline{\mu}}^{(k)}(\underline{x}) \right\rangle, \quad D_{kl} = \left\langle \underline{\underline{\mu}}^{(k)}(\underline{x}) : (\mathbb{D} * \underline{\underline{\mu}}^{(l)})(\underline{x}) \right\rangle \tag{1.24}$$

where the operator "*" is defined as:

$$(\mathbb{D} * \underline{\underline{\mu}}^{(l)})(\underline{x}) = \frac{1}{|V|} \int_V \mathbb{D}(\underline{x}, \underline{x}') : \underline{\underline{\mu}}^{(l)}(\underline{x}') d\underline{x}' \tag{1.25}$$

and $\mathbb{D}(\underline{x}, \underline{x}')$ is the non-local operator gives the strain at the point $\underline{x}$ created by a transformation strain $\underline{\underline{\mu}}^{(l)}$ at the point $\underline{x}'$. The reduced strain is then expressed as:

$$e_k = \underline{\underline{a}}^{(k)} : \underline{\underline{E}} + \sum_{l=1}^{M} D_{kl} \varepsilon_l^{an} \tag{1.26}$$

Considering the isotropy of the studied material, the stress-strain function expressed by the reduced variables can be obtained as:

$$\tau_k = 2G^{(r)}(e_k - e_k^{an}) \tag{1.27}$$

It should be noted that $G^{(r)}$ is the shear modulus of phase r, which the k^{th} plastic mode fully occupied.

To express the Mises yield criterion in the material phase r with the reduced variables previously defined, an approximation was made in (Michel & Suquet, 2003) to define a new variable, which described a total effect of the Mises stress in all the $M(r)$ modes supported in this material phase r:

$$\bar{\sigma}_{eq}^{r} = \left(\sum_{k=1}^{M(r)} {\tau_k}^2 \right)^{\frac{1}{2}} \tag{1.28}$$

Then the Mises yield criterion in each material phase r is transformed as:

$$f_p^r = \bar{\sigma}_{eq}^{r} - R^r(p_r) = 0 \tag{1.29}$$

where p_r is the plastic hardening scale in the material phase r. Thus the evolution of internal variables Eq. is formulated as:

$$\dot{e}_k^{an} = \frac{3}{2} \dot{p}_r \frac{\tau_k}{\sigma_{eq}^{r}} \tag{1.30}$$

1.1.5 Comparison of different approaches

As mentioned above, a theoretical result has been widely accepted that the accuracy of homogenization method for determining the effective mechanical behavior of nonlinear heterogeneous materials mostly depends on whether the heterogeneous plastic strain field can be well described. The mean field approaches are based on the hypothesis that the plastic strain is uniform distributed. Obviously the hypothesis is far from the reality.

1.2 Summary of mechanical behavior of argillite

This thesis is devoted to the micromechanical modeling of nonlinear heterogeneous materials. In particular, the proposed models will be applied to constitutive modeling of a typical nonlinear heterogeneous geomaterial called Callovo-Oxford argillite. This is a sedimentary hard clay rock from the East Paris basin in France.

The Callovo-Oxford argillite has been largely investigated in the framework of feasibility study for geological storage of nuclear waste storage in France. Due to its high mechanical strength and very low permeability, this rock is studied as potential geological barrier for nuclear waste storage. In this framework, an underground research laboratory (URL) is constructed in the East region of France by the national agency for radioactive waste management (ANDRA). Extensive experimental investigations including laboratory testing and in situ experiments both in microscopic and macroscopic scale have being been performed. A short review is given here mainly on the engineering and geological context, mineralogical compositions and basic mechanical behaviors of this material.

1.2.1 Engineering and geological context

In November 1999, after completing the preliminary investigation phases, Andra started the construction work of the URL in the village of Bure (Meuse District) on the border of the Meuse and Haute-Marne departments in eastern France (Figure 1-3). The research activities of the URL are dedicated to study the feasibility of reversible, deep geological disposal of high-activity,

long-lived radioactive wastes in the host rock. The Callovo-Oxford argillite is chosen as potential geological barrier due to its excellent mechanical and permeability properties.

The extent for the URL is a 130m thick layer of argillite that lies between about 420 and 550m below the surface. The clays, constituting 40 to 45% of the Callovo-Oxford argillite, isolate the ground waters. Silica and carbonate-rich sedimentary components reinforce the rock and promote stability for underground construction (Delay et al., 2007).

The Laboratory consists of two shafts, an experimental drift at 445m depth, and a set of technical and experimental drifts at the main level at 490m depth (Figure 1-4). The main shaft has a 5m diameter and allows access for personnel and equipment, material extraction and ventilation. The 4m auxiliary shaft located 100m away from the main shaft serves the ventilation system and provides not only mine safety, but also a second access for lowering equipment. Detailed monitoring of hydraulic and mechanical responses made the construction phase an important part of the experimental program for the URL From the shafts (Delay et al., 2007).

There are three major aspects in the URL drifts to be investigated. The first topic is the capacity of rock to contain the radioactive liquid. The second is the reaction of rock to the excavation of shafts and drifts, and the associated development of the damaged and disturbed zone. And the last is the technique of sealing of a drift (Delay et al., 2007). As the host rock of the radioactive waste deposal, the argillite will be submitted to various complicated perturbations, including mechanical loadings, hydraulic infiltration, and chemical erodes, temperature variation, and so on. All the perturbations directly impact the long term safety of the storage facilities.

This thesis focuses on the constitutive modeling for the mechanical properties of argillite. There have been various proposed phenomenological constitutive models for the argillite, and most of which can simulate the mechanical responses in a satisfactory way (Chiarelli et al., 2003; Conil et al., 2004; Hoxha et al. 2007 and others). However, it has been shown in many geological tests that the mineralogical compositions vary significantly between rock layers in different depth (Figure 1-5). The phenomenological constitutive models have to identify the material parameters for each rock layer. Moreover, the interactions between mineral composites of argillite can not be well considered in these macroscopic models. The physical mechanisms involved in deformation and failure process of the argillite are not clearly identified. Therefore, there is a need for the formulation of multi-scale models in order to link physical mechanisms at the microscopic scale to overall responses at macroscopic scale, by taking into account influences of mineralogical compositions.

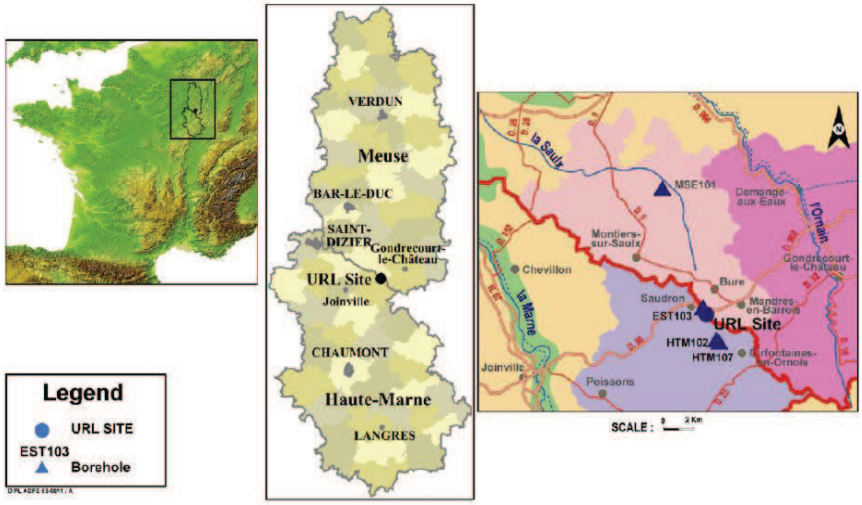

Figure 1-3: Location of the underground research laboratory (URL) at the Meuse/Haute-Marne site (Delay et al., 2007)

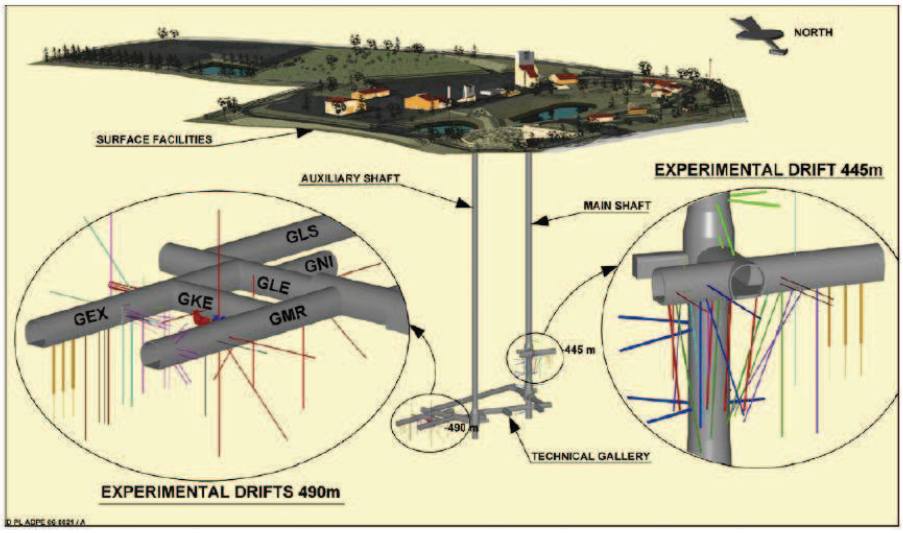

Figure 1-4: General layout drawing of the URL drifts (Delay et al., 2007)

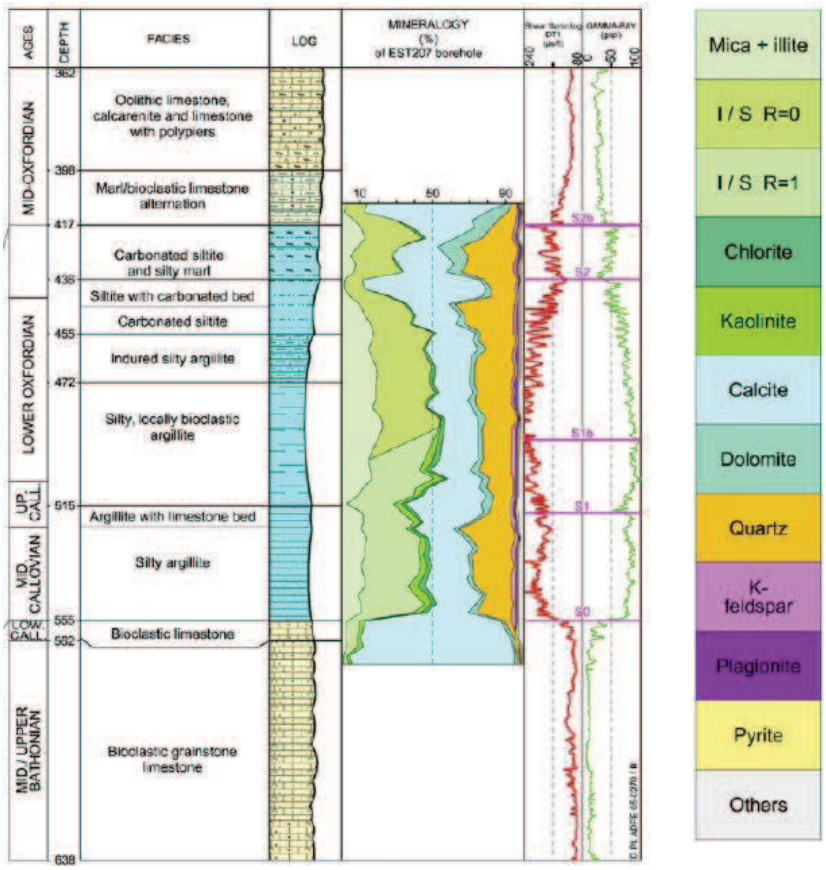

Figure 1-5: Variation of mineralogical compositions of the Callovo-Oxford formation (Delay et al., 2007)

1.2.2 Microscopic analyses and mineralogical composition of argillite

In order to study influences of mineralogical compositions on hydromechanical behaviors of argillite, specimens from three different depths between 450m and 485m have been investigated. Mineralogical compositions were determined from the analyses of X-ray diffractometry and calcimetry (Chiarelli, 2000). It is shown that the argillite is main composed of three main phases: quartz (23% average), calcite (27% average) and clay minerals (45% average) together with subordinate feldspars, pyrite and iron oxides (total 5% average). The clay minerals composition is relatively constant at 65% I/S (ilite-smectite interstratifield minerals), 30% illite and 5% kaolinite and chlorite. The variation of mineralogical composition with the depth is shown in Table 1-1. Further observations in microscopic scale reveal that the grains of quartz and calcite are approximately ellipsoidal shape, and scattered in a fine matrix of clay minerals which acts as the cement phase.

Generally the elastic modulus of calcite and quartz are around 100GPa, and that of clay matrix is about 10GPa. Due to the significant contrast, the material studied exhibits strongly heterogeneous mechanical behaviors. According to microscopic extensometer analyses (Bornert et al., 2001) strongly heterogeneous strain fields are observed inside the different material phases of the argillite sample subjected to mechanical loading. The quartz and calcite grains generally deform in an elastic way. In some cases, a few microcracks may be observed inside calcite grains. The deformation of the clay matrix is more complex. Indeed, this matrix is itself a heterogeneous at smaller scales composed of clay particles and various pores. However, as a first approximation and at the scale of grains, it may be simplified as a homogeneous matrix. Its mechanical responses are mainly characterized by plastic deformation related to sliding of clay sheets. However, significant microcracks have also been observed inside the clay matrix. Finally, the interfaces between the clay matrix and mineral grains constituent important weakness zones in which growth and coalescence of microcracks can take place. In this thesis, the emphasis is to develop a micromechanical approach for modeling macroscopic behavior of argillite by taking into account the influences of mineralogical compositions. A simplified schematization the representative volume element (RVE) will be adopted. The argillite is considered as a two phase composite: the clay matrix and inclusion grains of quartz and calcite.

Table 1-1: Mineral compositions in different depths of Callovo-Oxford argillite

No.	Depth (m)	Calcite Content (%)	Quartz Content (%)	Clays content (%)
1	451.4-466.8	20-40	20-30	40-55
2	468.9-469.1	25-55	20-30	35-55
3	482.1-482.4	25-35	15-20	45-60

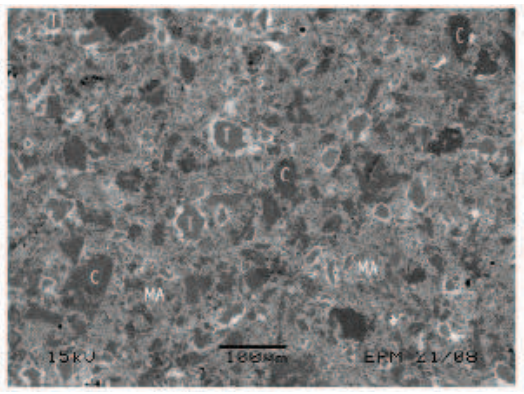

Figure 1-6: Micrography of a typical Callovo-Oxford argillite structure: calcite grains (C), quartz grains (tectosilicates) (T) and clay matrix (MA)

1.2.3 Basic mechanical properties of argillite

To investigate the macroscopic mechanical properties of the argillite, triaxial compression tests including the unloading-reloading paths have been performed on cylinder sample seen as the RVE. The size of sample is large enough with respect to that of heterogeneities considered here but small enough comparing with the characteristic length of structure. Different confining pressures varying from 0 to 20MPa have been used, and chosen according to the estimation of in situ stresses. Basic mechanical properties of the material have been investigated. First, the argillites may be regarded as initially isotropic material, as the structural anisotropy of this material plays is not very significant and can be neglected as a first approximation. Secondly, the argillites studied here exhibit significant plastic deformation upon unloading of deviatoric stress, and the plastic deformation is as more important as the confining pressure is higher (Chiarelli et al., 2003; Abou-Chakra Guéry et al., 2008). Therefore, there is an important pressure dependency of mechanical responses and transition from brittle to ductile behavior when the confining pressure increases. Further, significant volumetric plastic strains have also been obtained. During triaxial compression tests with given confining pressure, there is the transition from volumetric compressibility to dilatancy when the deviatoric stress increases. The compressibility/dilatancy transition point also depends on the confining pressure. Elastic properties have been determined through unloading-reloading cycles during triaxial compression tests. There is progressive deterioration of elastic modulus with the increase of deviatoric stress. Making the connection with the microstructure of argillite studied here, this deterioration of elastic properties is related to the growth of microcracks inside the clay matrix and on the interfaces. The growth of microcracks is further correlated with the increase of permeability (Bossart et al., 2002; Shao et al., 2005). On the other hand, the macroscopic plastic deformation is mainly related to irreversible sliding of clay sheets inside the matrix phase. Moreover, time-dependent deformation has also been observed in the argillite. The creep deformation may be related to two basic phenomena: viscoplastic sliding of clay matrix and sub-critical propagation of microcracks (Shao et al., 1999). However, this feature is not discussed in the thesis, and the emphasis is put on the time-independent deformation of argillite only.

Therefore, based on the review of microstructure and basic macroscopic mechanical behavior of argillite, the following micromechanical modeling framework will be adopted. The RVE of argillite is composed of the clay matrix and quartz and calcite grains. The clay matrix is described by an elastoplastic damage model. The quartz and calcite grains are combined into a single

inclusion phase which exhibits a linear elastic behavior.

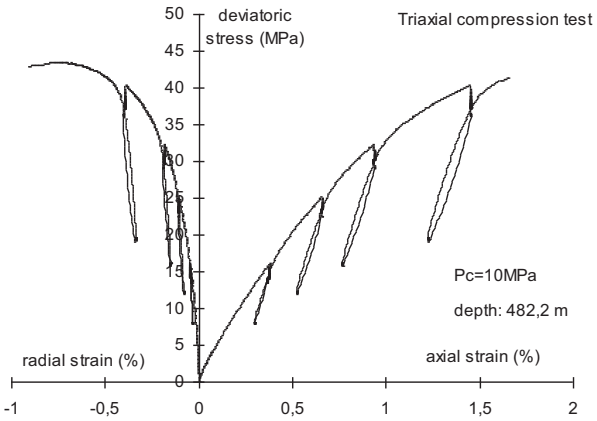

Figure 1-7: Typical stress strain curves of the argillite during triaxial compression test with unloading-reloading paths (Chiarelli, 2000)

Chapter 2:
Numerical simulation of heterogeneous with periodic microstructures

In this chapter, we present some numerical results from direct finite element simulations of heterogeneous materials with periodic structures. These simulations are performed for double purposes: on the one hand, such direct simulations will be used for the validation of non linear homogenization methods in some specific cases. And on the other hand, such the direct simulation of periodic representative volume element is a key step in various numerical techniques for multi-scale modeling of heterogeneous materials such as square finite element method.

Indeed, the direct numerical simulations consist in determining effective properties of linear or nonlinear heterogeneous materials by solving boundary values problems on the representative volume element by taking into account as close as possible the real microstructures of materials. The direct simulations are generally computationally expensive compared with homogenization methods. However, they provide the possibility of computing the macroscopic responses of heterogeneous materials with different configurations of constituents or microstructures. Theoretically all kinds of heterogeneous materials can be simulated by direct numerical approaches. Secondly, the relatively accurate results obtained can be regarded as the reference solutions, which will be used for the validation of different homogenization methods. Moreover, besides the effective properties of heterogeneous materials, the direct simulations can also give distributions of local fields (stresses, strains, plastic deformation, damage etc) inside each material phase. Such information may be very useful to capture local deformation and failure mechanisms and then provides relevant elements for the formulation and improvement of various homogenization techniques (Michel et al., 1999).

The numerical approach by finite element method (FEM) for periodic heterogeneous materials was firstly developed in 1960s (Adams & Doner, 1967; Needleman, 1972). During recent years many significant progresses have been achieved including the simulation of heterogeneous materials composed of elastoplastic or viscoelastoplastic constituents (Gonzalez et al., 2004; Pierard et al., 2007), or composite with complicated microstructures (Moulinec & Suquet, 1998; Segurado & Llorca, 2002; Segurado & Llorca, 2006; Pierard et al., 2007), or considering the interface effect to deal with fractures (Segurado & Llorca, 2004; Segurado & Llorca, 2005)

In this chapter, the direct numerical approaches for one of the mostly used heterogeneous materials, periodic heterogeneous materials are studied. The principles of simulations are firstly presented in section 2.1. Then the numerical algorithms are discussed in section 2.2. Finally, in

section 2.3, some examples are presented.

2.1 Principles of direct simulations

As discussed above, the macroscopic effective properties of heterogeneous materials are determined from the direct numerical study of RVE using given geometrical (microstructural) and boundary conditions as well as material properties of each phase. Compared with random materials that the geometrical and materials properties are only partially known through statistical information, all the geometrical and material information of periodic heterogeneous materials are completely determined by periodically repeating a unit cell to form the whole microstructure. The unit cell can be selected in different shape as shown in Figure 2-1, and the effective properties obtained from any type of unit cell should coincide (Michel and al., 1999).

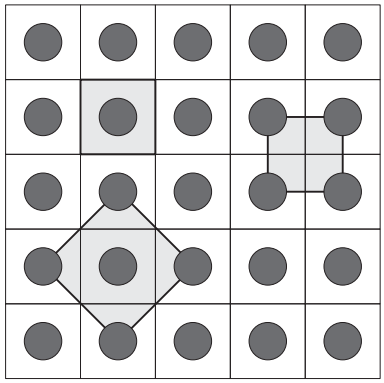

Figure 2-1: Different choices of unit cell for quadrangular array

Consider a large sample of periodic heterogeneous material composed of a large number of unit cells submitted to an arbitrary loading. Each unit cell can be either regarded as a material point in macroscopic scale, submitted to a macroscopic strain tensor $\underline{\underline{E}}$, or be considered as a microscopic structure (occupying a domain of Ω) where a local strain field $\underline{\underline{\varepsilon}}(\underline{z})$ distributes. According to the basic principles of micromechanics, the macroscopic strain $\underline{\underline{E}}$ is the volumetric average value of microscopic strain field $\underline{\underline{\varepsilon}}(\underline{z})$ as defined in equation(1.6) , as well as the uniform strain boundary condition as in equation(1.5). Decompose the microscopic strain field $\underline{\underline{\varepsilon}}(\underline{z})$ into two part, $\underline{\underline{E}}$ as the volumetric average value, and $\underline{\underline{\varepsilon}}'(\underline{z})$ the fluctuation:

$$\underline{\underline{\varepsilon}}(\underline{z}) = \underline{\underline{E}} + \underline{\underline{\varepsilon}}'(\underline{z}) \tag{2.1}$$

and accordingly the microscopic displacement field $\underline{u}(\underline{z})$ can be also decomposed into two parts, displacement due to average strain and due to fluctuation:

$$\underline{u}(\underline{z}) = \underline{\underline{E}}.\underline{z} + \underline{u}'(\underline{z}) \tag{2.2}$$

Substitute Eq.(2.1) into Eq. (1.6) the following relation that the microscopic strain fluctuation must satisfied can be obtained:

$$\left\langle \underline{\underline{\varepsilon}}'(\underline{z}) \right\rangle_{\Omega} = 0 \tag{2.3}$$

It should be noted that $\underline{u}'(\underline{z})$ is periodic, which means all components of $\underline{u}'(\underline{z})$ take the same values on points of the boundary $\partial\Omega$ of the unit cell which are deduced by translation parallel to the directions of invariance of the lattice (Michel et al., 1999; Bornert et al., 2001), as illustrated in Figure 2-2.

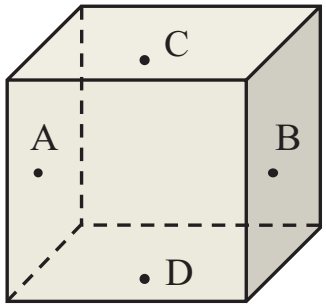

$$\underline{u}'(\mathrm{A}) = \underline{u}'(\mathrm{B})$$
$$\underline{u}'(\mathrm{C}) = \underline{u}'(\mathrm{D})$$
$$\underline{\underline{\sigma}}(\mathrm{A}).\underline{n}(\mathrm{A}) = -\underline{\underline{\sigma}}(\mathrm{B}).\underline{n}(\mathrm{B})$$
$$\underline{\underline{\sigma}}(\mathrm{C}).\underline{n}(\mathrm{C}) = -\underline{\underline{\sigma}}(\mathrm{D}).\underline{n}(\mathrm{D})$$

Figure 2-2: Periodic displacement boundary condition of unit cell

When the periodic displacement boundary condition is satisfied, the condition Eq. (2.3) is met automatically. It can be proved as follows:

$$\begin{aligned}\left\langle \underline{\underline{\varepsilon}}'(\underline{z}) \right\rangle_{\Omega} &= \frac{1}{|\Omega|}\int_{\Omega} \underline{\underline{\varepsilon}}'(\underline{z}) d\Omega \\ &= \frac{1}{|\Omega|}\int_{\Omega} \frac{1}{2}(u'_{i,j} + u'_{j,i}) d\Omega \\ &= \frac{1}{|\Omega|}\int_{\partial\Omega} \underline{u}' \overset{s}{\otimes} \underline{n} d\Omega\end{aligned}$$

Since the $\underline{u}'$ takes the same values and $\underline{n}$ takes opposite value on the opposite sides of $\partial\Omega$,

the integral above results zero. Another periodic boundary condition is obvious considering the third Newton law that $\underline{\underline{\sigma}}.\underline{n}$ take the opposite value on the opposite side of unit cell, as illustrated in Figure 2-2. Then the numerical analysis for unit cell of periodic heterogeneous material can be concluded as such a boundary value:

$$div\,\underline{\underline{\sigma}}(\underline{z}) = 0, \quad \forall \underline{z} \in \Omega \tag{2.4}$$

$$\underline{\underline{\varepsilon}}'(\underline{z}) = \frac{1}{2}(u'_{i,j} + u'_{j,i}) \tag{2.5}$$

$$\underline{\underline{\sigma}}(\underline{z}) = \mathbb{C}(\underline{z}) : \left(\underline{\underline{E}} + \underline{\underline{\varepsilon}}'(\underline{z})\right) \tag{2.6}$$

$$\underline{u}'(\underline{z}) \text{ periodic}, \ \underline{\underline{\sigma}}.\underline{n}(\underline{z}) \text{ opposite periodic}, \quad \forall \underline{z} \in \partial\Omega \tag{2.7}$$

In this boundary value problem defined by Eq. (2.4) to Eq.(2.7), the periodic displacement fluctuation $\underline{u}'(\underline{z})$ can be regarded as the independent unknown value, and the macroscopic strain $\underline{\underline{E}}$ is the uniform strain boundary strain condition. Generally the stress opposite periodic condition can be satisfied automatically, while the periodic condition for $\underline{u}'$ should be imposed by some techniques. The implementation in details will be discussed in the following sections.

When dealing with nonlinear heterogeneous materials, the local constitutive law Eq. (2.6) can be also rewritten for elastoplastic materials as Eq.(2.8), or in an incremental form as Eq.(2.9).

$$\underline{\underline{\sigma}}(\underline{z}) = \mathbb{C}(\underline{z}) : \left(\underline{\underline{E}} + \underline{\underline{\varepsilon}}'(\underline{z}) - \underline{\underline{\varepsilon}}^{p}(\underline{z})\right) \tag{2.8}$$

$$\dot{\underline{\underline{\sigma}}}(\underline{z}) = \mathbb{L}^{\tan}(\underline{z}) : \left(\dot{\underline{\underline{E}}} + \dot{\underline{\underline{\varepsilon}}}'(\underline{z})\right) \tag{2.9}$$

The fourth order tensors, $\mathbb{C}(\underline{z})$ and $\mathbb{L}^{\tan}(\underline{z})$, respectively denote local elastic stiffness tensor and elastoplastic tangent operator at the point $\underline{z}$ of the unit cell.

2.2 Numerical algorithm for stress controlled unit cell

In the previous section, the numerical analysis for unit cell of periodic heterogeneous material has been concluded into a boundary value problem in which periodic displacement fluctuation $\underline{u}'(\underline{z})$ is the independent unknown value, and macroscopic strain $\underline{\underline{E}}$ is the specified boundary

strain condition. However, in many loading processes the macroscopic strain $\underline{\underline{E}}$ cannot be specified in advance. For example, in the triaxial compression tests (including the uniaxial test) the confining pressure is prescribed while the lateral strain is an undetermined value. So in this section the numerical algorithm of stress controlled problem of the unit cell is studied based on the Newton-Raphson method in incremental form.

Consider a unit cell of heterogeneous material which can be either regarded as a microscopic structure or a macroscopic material point. The macroscopic stress and strain in the current load step m are $\underline{\underline{\Sigma}}_m$ and $\underline{\underline{E}}_m$, respectively. In the next load step $m+1$, a prescribed macroscopic stress increment $\Delta\underline{\underline{\Sigma}}_{m+1}$ is applied to the unit cell. The problem then becomes to solve the boundary value problem presented in section 2.1 for the corresponding macroscopic strain increment $\Delta\underline{\underline{E}}_{m+1}$ (or equivalently $\underline{\underline{E}}_{m+1}$) and the microscopic stress and strain distribution $\underline{\underline{\sigma}}_{m+1}(\underline{z})$, $\underline{\underline{\varepsilon}}_{m+1}(\underline{z})$ in the load step $m+1$. Denote the superscript i to be the iteration number $(i \geq 0)$. When $i=0$, the variables are initiated as follows:

$$\underline{\underline{E}}^0_{m+1} = \underline{\underline{E}}_m, \quad \left(\mathbb{L}^{\tan}(\underline{z})\right)^0_{m+1} = \left(\mathbb{L}^{\tan}(\underline{z})\right)_m$$
$$\underline{\underline{\sigma}}^0_{m+1}(\underline{z}) = \underline{\underline{\sigma}}_m(\underline{z}), \quad \left\langle \underline{\underline{\sigma}}^0_{m+1}(\underline{z}) \right\rangle = \left\langle \underline{\underline{\sigma}}_m(\underline{z}) \right\rangle = \underline{\underline{\Sigma}}_m$$

Thus the uniform strain boundary condition applied to the unit cell in the iteration $i=1$ can be obtained as:

$$\begin{cases} \underline{\underline{E}}^1_{m+1} = \underline{\underline{E}}_m + \Delta\underline{\underline{E}}^0_{m+1} \\ \Delta\underline{\underline{E}}^0_{m+1} = \left\langle \left(\mathbb{L}^{\tan}(\underline{z})\right)^0_{m+1} \right\rangle^{-1} : \Delta\underline{\underline{\Sigma}}_{m+1} \end{cases} \tag{2.10}$$

It should be noted that $\left\langle \mathbb{L}^{\tan}(\underline{z}) \right\rangle$ cannot be understood as the equivalent homogeneous stiffness tensor $\mathbb{L}^{\hom}$. $\left\langle \mathbb{L}^{\tan}(\underline{z}) \right\rangle$ is used just to obtain a better rate of convergence. Indeed, the equivalent macroscopic stiffness tensor $\mathbb{L}^{\hom}$ should be obtained as follows (Dormieux et al. 2006):

$$\mathbb{L}^{\hom-\tan} = \left\langle \mathbb{L}^{\tan}(\underline{z}) : \mathbb{A}(\underline{z}) \right\rangle$$

A simplified iterative procedure can also be proposed by replacing $\left\langle \mathbb{L}^{\tan}(\underline{z}) \right\rangle$ by $\left\langle \mathbb{C}(\underline{z}) \right\rangle$, which does not vary in terms of loading process; this leads to a modified Newton-Raphson algorithm in which it is not needed to solve the inverse matrix during every iteration. But in general, a slower rate of convergence is obtained.

After $\underline{\underline{E}}^{1}_{m+1}$ is obtained, the boundary value problem can be then solved for the microscopic strain field $\underline{\underline{\varepsilon}}^{1}_{m+1}(\underline{z})$, stress field $\underline{\underline{\sigma}}^{1}_{m+1}(\underline{z})$, and tangent stiffness tensor at every microscopic point $\left(\mathbb{L}^{\tan}\right)^{1}_{m+1}(\underline{z})$ by finite element method (FEM) or any other numerical methods such as Fast Fourier Transform (FFT) (Moulinec & Suquet, 1994). For $i \geq 1$, $\underline{\underline{E}}^{i+1}_{m+1}$ can be updated as:

$$\begin{cases} \underline{\underline{E}}^{i+1}_{m+1} = \underline{\underline{E}}^{i}_{m+1} + \Delta\underline{\underline{E}}^{i}_{m+1} \\ \Delta\underline{\underline{E}}^{i}_{m+1} = \left\langle \left(\mathbb{L}^{\tan}(\underline{z}) \right)^{i}_{m+1} \right\rangle^{-1} : \left(\underline{\underline{\Sigma}}_{m+1} - \left\langle \underline{\underline{\sigma}}^{i}_{m+1} \right\rangle \right) \end{cases} \tag{2.11}$$

Then the microscopic strain field $\underline{\underline{\varepsilon}}^{i+1}_{m+1}(\underline{z})$, stress field $\underline{\underline{\sigma}}^{i+1}_{m+1}(\underline{z})$, and tangent stiffness tensor at every microscopic point $\left(\mathbb{L}^{\tan}\right)^{i+1}_{m+1}(\underline{z})$ can be determined.

The convergence criterion is as follows:

$$\left\| \underline{\underline{\Sigma}}_{m+1} - \left\langle \underline{\underline{\sigma}}^{i}_{m+1} \right\rangle \right\| < c_f \left\| \underline{\underline{\Sigma}}_{m+1} \right\| \tag{2.12}$$

and

$$\left\| \Delta\underline{\underline{E}}^{i}_{m+1} \right\| < c_d \left\| \underline{\underline{E}}^{i}_{m+1} \right\| \tag{2.13}$$

where c_f and c_d are two tolerance values. $\|\bullet\|$ denotes the norm of a matrix. Eq. (2.12) defines the stress criterion while Eq.(2.13) the strain criterion. When the convergence conditions are met, the macroscopic stress, the microscopic stress and strain fields can be obtained.

2.3 Numerical examples

Some examples are now presented to show the application of direct simulation approaches to modeling of heterogeneous materials using the principles and algorithms discussed above. These examples are also regarded as the preliminary bases for some more complicated computations in Chapter 4.

2.3.1 Example I

The first example aims the estimation of macroscopic and microscopic mechanical behaviors of a unit cell in plain strain condition for a heterogeneous material composed of plastic matrix and elastic inclusions. The volumetric fraction of inclusion is 25%. The numerical simulation is performed by ABAQUS with user subroutines UEXTERNALDB, UMAT, URDFIL. The element type CPE8R (8-node biquadratic plane strain quadrilateral, reduced integration) is used to mesh the geometric domain into 546 elements and 1703 nodes. The FEM mesh is illustrated in Figure 2-3. The plastic matrix is described by a non associated flow rule based on the classic Drucker-Prager yield criterion. The plastic yield function and plastic potential are given by:

$$\begin{aligned} f_p &= \alpha\sigma_m + \sigma_{eq} - (\sigma_0 + H\gamma^a) = 0 \\ g &= \psi\sigma_m + \sigma_{eq} - (\sigma_0 + H\gamma^a) \end{aligned} \tag{2.14}$$

The parameter α is the internal frictional coefficient and β the volumetric dilation coefficient; σ_0 denotes the initial plastic yield threshold; H and γ are two parameters for plastic hardening law and p is the equivalent plastic shear strain. The parameters of matrix and inclusion are listed in Table 2-1 and Table 2-2.

A pure shear loading is applied to the unit cell:

$$\underline{\underline{\Sigma}} = \Sigma_4(\underline{e}_1 \otimes \underline{e}_2 + \underline{e}_2 \otimes \underline{e}_1) + \Sigma_3(\underline{e}_3 \otimes \underline{e}_3)$$

The component Σ_3 cannot be prescribed but are determined as the reaction of the plain strain reaction. As discussed in the previous section, the independent variable in the FEM calculation is the periodic displacement fluctuation $\underline{u}'(\underline{z})$, which is imposed in the periodic condition by '*Equation' command in ABAQUS. The uniform boundary condition $\underline{\underline{E}}$ is determined by Newton-Raphson iteration using the user subroutine 'UEXTERNALDB' in ABAQUS.

Table 2-1: Parameters of Drucker-Prager matrix in example I

E_m(Pa)	υ_m	σ_0(Pa)	H(Pa)	a	α	ψ
1.0×10^{10}	0.25	3.0×10^{7}	1.0×10^{8}	0.3	0.15	0.15

Table 2-2: Parameters of linear inclusion in example I

E_I (Pa)	υ_I
5.0×10^{10}	0.20

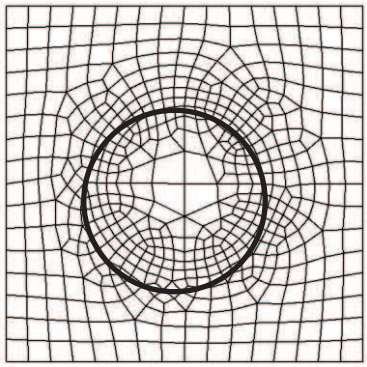

Figure 2-3: Illustrations of the FEM mesh in example I

The macroscopic mechanical responses are illustrated in Figure 2-4. Besides the macroscopic shearing strain and shearing stress curve, the relation between shearing strain and normal strain due to plastic flow is also included in this figure. The microscopic fields can also be obtained by the FEM calculation. The periodic displacement fluctuation $\underline{u}'(\underline{z})$ and the corresponding $\underline{\underline{\varepsilon}}'(\underline{z})$ (only shear component of the strain tensor) are illustrated in Figure 2-5. The microscopic strain field $\underline{\underline{\varepsilon}}(\underline{z})$ and displacement field $\underline{u}(\underline{z})$ for each load step can be then calculated by Eq.(2.1) and Eq. (2.2).

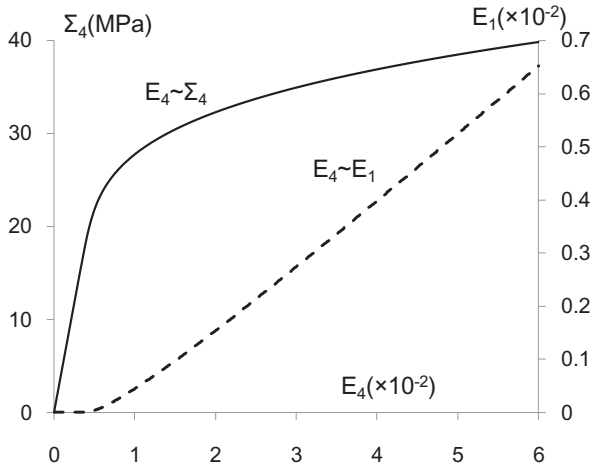

Figure 2-4: Results of macroscopic mechanical responses: shearing strain vs. shearing stress and shearing strain vs. normal strain

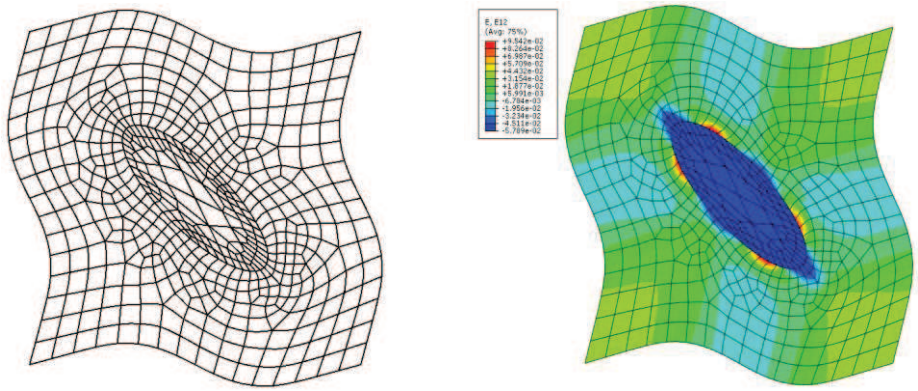

(a) (b)

Figure 2-5: Microscopic fields on deformed configuration of the unit cell

(a) Periodic displacement fluctuation $\underline{u}'(\underline{z})$; (b) corresponding strain fluctuation $\varepsilon_4'(\underline{z})$

2.3.2 Example II

The second example is the simulation of a porous material subjected to a uniaxial tension loading. For the sake of simplicity and clear illustration, a plain strain model with 25% porosity is considered in this example (Figure 2-6). The matrix of the simulated material obeys the Mises criterion as Eq.(2.15), and the parameters are listed in

Table 2-3.

$$f_p = \sigma_{eq} - (\sigma_0 + Hp^a) = 0 \tag{2.15}$$

Table 2-3: Parameters of Mises type matrix in example II

E_m(Pa)	υ_m	σ_0(Pa)	H(Pa)	a
1.0×10^{10}	0.20	3.0×10^{7}	1.5×10^{8}	0.35

Figure 2-7 shows a usually used but incorrect method to simulate this problem. Figure 2-7(a) is the matrix of unit cell submitted to a macroscopic uniaxial tension loading. Then a single unit cell is separated, and a uniaxial loading is applied to the unit cell directly. In particular, the boundary condition in one dimension is imposed a uniform displacement loading, and the

boundary condition in another dimension is free of charge as Figure 2-7(b). The results are illustrated in Figure 2-7(c) and (d). One can see that the matrix of unit cell is no longer continuous, but appears some discontinuities, because the free boundaries of the unit cell can not keep uniform deformation. This is obviously incompatible with the reality. So the approach presented above in this work for periodic heterogeneous materials is applied to solve this problem. The macroscopic and microscopic results are illustrated in Figure 2-8 and Figure 2-9, respectively. It can be seen from the microscopic results that the microstructure keeps a periodic shape during the loading process. So the matrix of unit cell as Figure 2-7(a) will be always continuous.

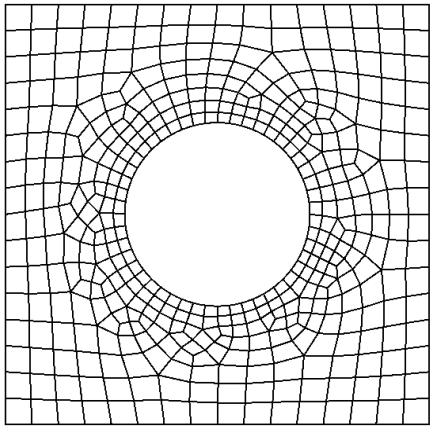

Figure 2-6: Illustrations of the FEM mesh in example II

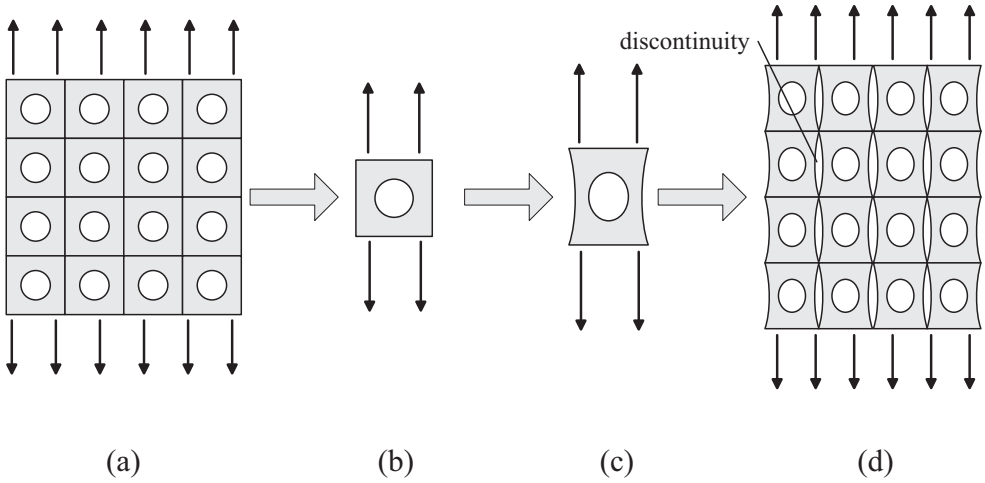

Figure 2-7: Incorrect computation process of porous material submitted to uniaxial tension

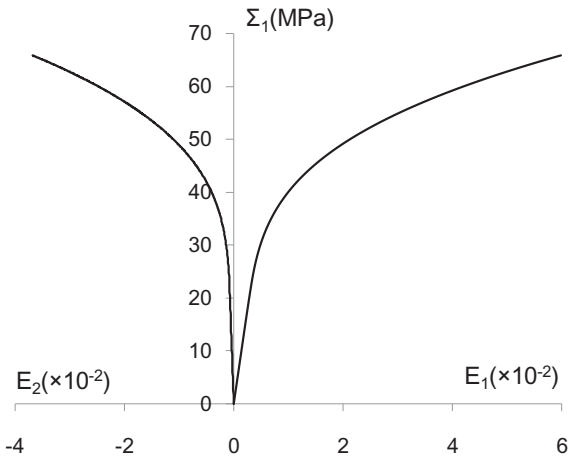

Figure 2-8: Macroscopic stress strain curves in uniaxial tension test of porous medium

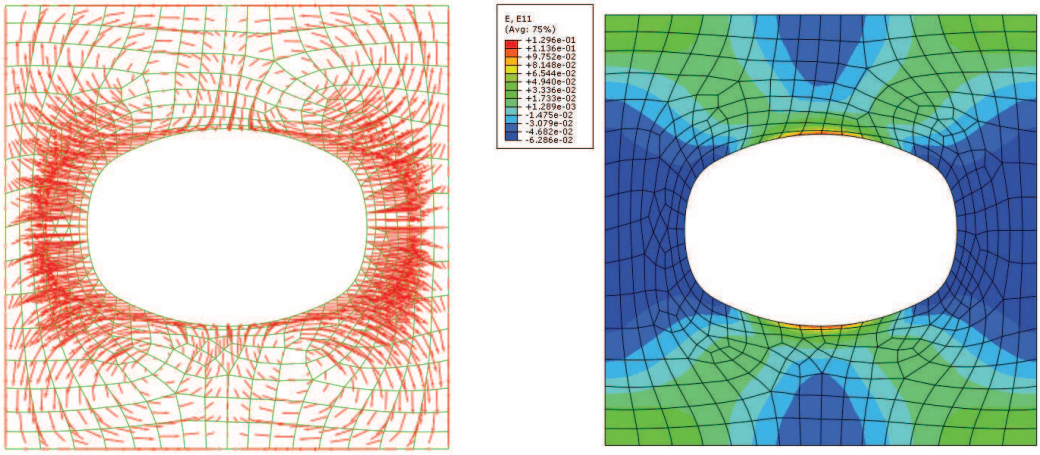

(a) (b)

Figure 2-9: Microscopic fields on deformed configuration of the unit cell

(a) Vector of periodic displacement fluctuation $\underline{u}'(\underline{z})$; (b) corresponding strain fluctuation $\varepsilon_1'(\underline{z})$

2.4 Conclusions

In this chapter we focus on the direct computational approaches for heterogeneous materials with periodic microstructures. As a general numerical modeling method, despite this direct approach is not the final aim of the present work, it still deserves our attention because of its capacity of solving non linear problems with complex microstructures, its accuracy of results to be used as reference solution to validate homogenization methods, and its ability of exploring the microscopic fields distributions. Moreover, the direct computational approach is studied here to be a preliminary phase for the following sections in this thesis.

The periodic boundary conditions were discussed as a key point in section 2.1. Then the numerical analysis for the unit cell of periodic heterogeneous material was concluded as a boundary value problem. For some macroscopic strain controlled problem, this problem can be directly solved. But for the other stress controlled or stress-strain mixed controlled problem (such as the triaxial tension or compression), a Newton-Raphson iterative procedure is necessary to determine the suitable macroscopic strain boundary condition. Specific numerical algorithms are presented. Finally, two examples were presented to show the validity and advantage of the proposed direct computational approach.

Chapter 3:
Incremental approach for nonlinear heterogeneous materials and its application to argillite

This chapter focuses on one of the most commonly used approaches of nonlinear homogenization methods for nonlinear heterogeneous materials, Hill's incremental approach. In spite of some limitations, the incremental method is easy to implement in standard computer codes and it is particularly suitable for complex loading paths with unloading cycles. In particular, combined with suitable isotropization procedure, the incremental method seems to provide efficient predictions of macroscopic responses of non linear heterogeneous materials. Further, it is also useful to note that the numerical implementation of the incremental method is very easy and it can be easily used as a user defined material subroutine in any computer codes. Therefore, we adopt the incremental approach in this chapter, give the homogenization scheme and algorithm for numerical simulation in section 3.1, and then make a further study for the efficiency of isotropization methods based on the incremental approach for describe nonlinear heterogeneous materials in section 3.2.

As mentioned above, besides studying the general method of nonlinear homogenization, the second aim of this thesis is devoted to the micromechanical modeling of cohesive geomaterials, in particular the Callovo-Oxford hard clays (argillite) which is chosen as one of the possible geological barriers for the underground storage of radioactive wastes. To fulfill this target, an application of Hill's incremental approach based on Mori-Tanaka scheme on modeling the argillite is implemented in section 3.3. Taking account of the microscopic constituent character of argillite, a local elastoplastic damage constitutive model for clay matrix is proposed in section 3.3. At last, the calibration and verification of the micromechanical model are performed in section 3.5 by comparing numerical simulations and experimental data on the argillite for various loading paths.

3.1 Fundamentals of Hill's incremental approach

As the standard steps of micromechanical modeling, the representative volumetric element (RVE) should be firstly defined. In this section, the heterogeneous material is taken as a composite composed of nonlinear matrix and elastic inclusions. The RVE is illustrated as Figure 3-1, which occupies the geometrical domain Ω, and is subjected to a uniform strain boundary

condition on $\partial\Omega$. In this context, $|\Omega|$ denotes the volume of the RVE, V_m (V_I) and f_m (f_I) are the volume and volume fraction of matrix (inclusion), respectively. The volumetric average operator is denoted as follows,

$$\langle x \rangle = \frac{1}{|\Omega|} \int_{\Omega} (x) dV \tag{3.1}$$

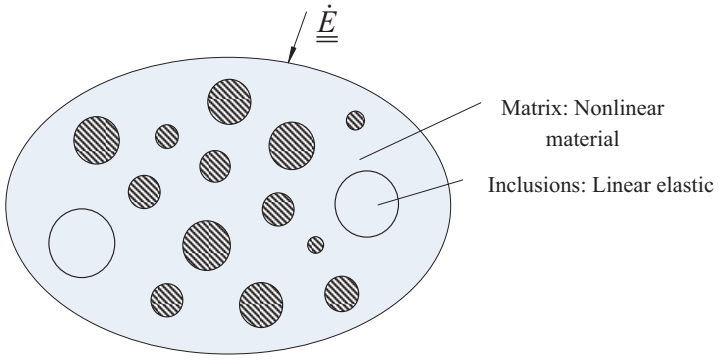

Figure 3-1: Illustration of RVE of a random matrix-inclusion composite

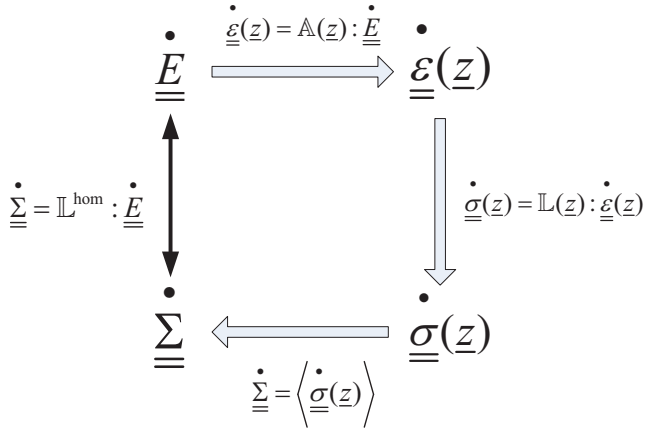

Figure 3-2: Main steps of non homogenization method using incremental approach

The main steps of non linear homogenization method for micromechanical modeling of heterogeneous materials are illustrated in Figure 3-2 in incremental form. The basic principle of the incremental method proposed by (Hill, 1965) consists in the determination of the overall tangent stiffness tensor for each incremental loading step, based on the knowledge of local constitutive behaviors. This method thus requires a rate formulation of the local constitutive relations for each phase:

$$\dot{\underline{\underline{\sigma}}}(\underline{z}) = \mathbb{L}(\underline{z}) : \dot{\underline{\underline{\varepsilon}}}(\underline{z}) \tag{3.2}$$

$\dot{\underline{\underline{\sigma}}}$ and $\dot{\underline{\underline{\varepsilon}}}$ denotes respectively local fields of stress and strain rates while $\mathbb{L}(\underline{z})$ is the local

tangent stiffness tensor which depends on the position of material point in each material phase. Due to the fact that the local constitutive relations Eq. (3.2) take the form of an incrementally linearized law with nonlinear tangent operator, the classical Eshelby-based homogenization procedures (Eshelby, 1957) can be used for the resolution of this problem. For this purpose, a tangent localization tensor $\mathbb{A}(\underline{z})$ is introduced to relate the local strain rate to that of macroscopic strain rate:

$$\dot{\underline{\underline{\varepsilon}}}(\underline{z}) = \mathbb{A}(\underline{z}) : \dot{\underline{\underline{E}}} \tag{3.3}$$

Substituting (3.3) for (3.2) and defining the macroscopic stress tensor by $\dot{\underline{\underline{\Sigma}}} = \left\langle \dot{\underline{\underline{\sigma}}} \right\rangle$, the macroscopic incremental constitutive relations read:

$$\dot{\underline{\underline{\Sigma}}} = \mathbb{L}^{\text{hom}} : \dot{\underline{\underline{E}}} \tag{3.4}$$

The macroscopic tangent stiffness tensor is given by:

$$\mathbb{L}^{\text{hom}} = \left\langle \mathbb{L}(\underline{z}) : \mathbb{A}(\underline{z}) \right\rangle \tag{3.5}$$

Note that the homogenization procedure should further verify the energy condition of Hill, $\dot{\underline{\underline{\Sigma}}} : \dot{\underline{\underline{E}}} = \left\langle \dot{\underline{\underline{\sigma}}} : \dot{\underline{\underline{\varepsilon}}} \right\rangle$. From Eq.(3.5), one can see that for the determination of the macroscopic tangent operator, it is necessary to first define the local tangent operator and localization tensor at each material point of constituent phases, and then perform volumetric averaging of these quantities. In practice, this is nearly impossible to obtain the analytical form of such volumetric averaging and needs prohibitively high computation time for numerical evaluation. Therefore, for the effective implementation of the incremental method, an approximation of the tangent operator in each phase is needed. For this purpose, the following hypothesis is adopted: at any point $\underline{z}$ of the phase r, the relation between stress rate and strain rate can be approximated by:

$$\forall \underline{z} \in V_r \quad , \quad \dot{\underline{\underline{\sigma}}}(\underline{z}) = \mathbb{L}_r : \dot{\underline{\underline{\varepsilon}}}(\underline{z}) \tag{3.6}$$

This hypothesis comes to assume that the local tangent stiffness tensor is uniform in each material phase. It is obvious that this strong assumption represents a shortcoming of the incremental method and does not verify real fields of local stiffness which should be heterogeneously distributed inside material phases. However, this assumption makes it possible to deduce in an analytical way the macroscopic stiffness tensor. In practice, the local stiffness tensor $\mathbb{L}_r$ is evaluated for a suitable reference strain state, which is classically taken as the average value of

local strain field in the phase r, noted by $\underline{\underline{\bar{\varepsilon}}}_r$. With this reference strain state, the tangent localization laws Eq. (3.3) for each material phase (clay matrix and mineral inclusions) become:

$$\begin{cases} \dot{\underline{\underline{\varepsilon}}}_m = \mathbb{A}_m : \dot{\underline{\underline{E}}} \\ \dot{\underline{\underline{\varepsilon}}}_I = \mathbb{A}_I : \dot{\underline{\underline{E}}} \end{cases} \tag{3.7}$$

$\mathbb{A}_m$ and $\mathbb{A}_I$ are the tangent localization tensors respectively for the matrix and inclusions. Using now the Mori-Tanaka scheme (Mori & Tanaka, 1973) the tangent localization tensors are given by:

$$\begin{cases} \mathbb{A}_m = \left[f_m \mathbb{I} + f_I \left[\mathbb{I} + \mathbb{P}_I^0 : (\mathbb{L}_I - \mathbb{L}_m) \right]^{-1} \right]^{-1} \\ \mathbb{A}_I = \left[\mathbb{I} + \mathbb{P}_I^0 : (\mathbb{L}_I - \mathbb{L}_m) \right]^{-1} : \left[f_m \mathbb{I} + f_I \left[\mathbb{I} + \mathbb{P}_I^0 : (\mathbb{L}_I - \mathbb{L}_m) \right]^{-1} \right]^{-1} \end{cases} \tag{3.8}$$

The fourth order tensor $\mathbb{P}_I^0$ is called Hill tensor which only depends on the geometry of the inclusions and on the tangent stiffness tensor of the clay matrix $\mathbb{L}_m$. Alternatively the Hill tensor can be also expressed in the following form:

$$\mathbb{P}_I^0 = \mathbb{S}^{\mathrm{E}} : \mathbb{L}_m^{-1} \tag{3.9}$$

$\mathbb{S}^{\mathrm{E}}$ is the Eshelby tensor. It is important to note that due to the dependence of the local tangent stiffness on the direction of applied strain rates, $\mathbb{L}_m$ is a non linear tangent operator which characterizes the non linear response of the reference medium. Moreover, as the Hill's (or Eshelby) tensor depends on the morphology of microstructure and non linear behavior of the matrice, it is generally not possible to obtain a close form of the Hill tensor, which should be computed using a suitable numerical integration method. The computation of Hill tensor is based on the Green's function. In the case of spherical inclusions as considered here, the Hill tensor is given by the following simplified expression (Dormieux et al., 2006):

$$P_{ijkl}^0 = \frac{1}{4\pi} \int_{|\xi|=1} (C_{ijkl}^0 \xi_j \xi_l)^{-1} \xi_j \xi_l dS \tag{3.10}$$

Using a Gauss type numerical integration procedure, the integration (3.10) may be approximated by:

$$P^0_{ijkl} = \sum_{k=1}^{N} w_k (C^0_{ijkl}\xi_j\xi_l)^{-1}\xi_j\xi_l \tag{3.11}$$

where N is the number of integration points, w_k is the weight coefficient associated with the k^{th} integration point. In the case of matrix characterized by an isotropic tangent operator, it is then possible to determine a closed form of Eshelby tensor as follows (Dormieux et al., 2006):

$$\mathbb{L}_m = 3k_t\mathbb{J} + 2\mu_t\mathbb{K} \tag{3.12}$$

$$\mathbb{S}^E = \frac{3k_t}{3k_t + 4\mu_t}\mathbb{J} + \frac{6}{5}\frac{k_t + 2\mu_t}{3k_t + 4\mu_t}\mathbb{K} \tag{3.13}$$

The two coefficients, k_t and μ_t, denote the tangent compressibility and shear moduli of non linear material phase. Their values depend on the local constitutive relations and loading orientation. Using now the relations Eq. (3.6) and Eq. (3.8), the macroscopic tangent operator of the composite can be written in the following form:

$$\mathbb{L}^{\text{hom}} = f_m\mathbb{L}_m : \mathbb{A}_m + f_I\mathbb{L}_I : \mathbb{A}_I \tag{3.14}$$

As mentioned above, the matrix is described by an inelastic constitutive model, thus the tangent stiffness tensor $\mathbb{L}_m$ should be updated in each incremental loading step. $\mathbb{L}_I$ is the elastic stiffness tensor of the inclusions, which remains constant during all the loading steps.

3.2 Isotropization techniques in incremental approach

Among various approaches proposed so far, micromechanical models based on the Hill's incremental method (Hill, 1965) have been largely developed and applied to different heterogeneous materials, due to the relative mathematical simplicity and facility for numerical implementation (Doghri & Ouaar, 2003; Chaboche et al., 2005; Abou-Chakra Guéry et al., 2008). However, it is well known that the direct use of Hill's incremental method generally leads to too stiff responses of macroscopic behaviors. The main reason of such phenomenon is that the non-uniform distributions of local strains in constituents are approximated by uniform fields in the incremental method. Without developing other kinds of approaches in this stage and in order to numerically improve predictions of the incremental method, the isotropization method has been introduced. It consists of using only some isotropic part of the local tangent stiffness operator in the determination of macroscopic tangent operator for the prediction of overall responses of

homogenized material. However, different techniques of isotropization may be set up, and their efficiency should depend on local nonlinear constitutive models of constituents. This section presents a comparative study on the efficiency of these isotropization techniques. To do this, a two phase composite is considered, with an elastoplastic matrix obeying Drucker-Prager criterion and elastic inclusions.

The first step of isotropization method consists in the extraction of an isotropic part from the local tangent operator of matrix. The general decomposition method proposed by Bornert (2001) is used here. The isotropic part of tangent stiffness tensor is obtained by:

$$\mathbb{L}_m^{iso} = (\mathbb{J} :: \mathbb{L}_m)\mathbb{J} + \frac{1}{5}(\mathbb{K} :: \mathbb{L}_m)\mathbb{K} = 3k_t\mathbb{J} + 2\mu_t\mathbb{K} \tag{3.15}$$

$$k_t = \frac{1}{3}(\mathbb{J} :: \mathbb{L}_m) \;\; ; \quad \mu_t = \frac{1}{10}(\mathbb{K} :: \mathbb{L}_m) \tag{3.16}$$

Using this isotropic part of the tangent operator for the matrix phase, it is possible to consider different techniques for the evaluation of macroscopic tangent operator. In this work, the following three different techniques are considered.

Method 1:

Only the Eshelby tensor is computed with the isotropic part of the tangent stiffness tensor, i.e., Eq. (3.9) is replaced by:

$$\mathbb{P}_I^0 = \mathbb{S}^E(\mathbb{L}_m^{iso}) : \mathbb{L}_m^{-1} \tag{3.17}$$

Method 2:

The Hill tensor is calculated by the isotropic part of tangent stiffness tensor, thus Eq. (3.9) is transformed to:

$$\mathbb{P}_I^0 = \mathbb{S}^E(\mathbb{L}_m^{iso}) : (\mathbb{L}_m^{iso})^{-1} \tag{3.18}$$

Method 3:

All the computing steps for the evaluation of macroscopic tangent operator are performed using the isotropic part of the tangent operator of the matrix given by Eq.(3.15).

3.2.1 Comparison of isotropization techniques and analyses

In order to verify and compare the efficiency of isotropization methods, the three techniques mentioned above are now compared with the reference solution on the RVE. This solution is obtained by direct elastoplastic modeling of the RVE using finite element method (FEM). The microstructure of heterogeneous material is represented by some periodic assembly of 3D unit cells; each one is composed of an elastoplastic hexagonal matrix and embedded elastic spherical inclusions. A simplification is made to benefit the advantage of axial symmetry; the actual hexagonal unit cell is approximated by a cylinder one, as illustrated in Figure 3-3. Due to the symmetry, only half an axial symmetry plain is considered in the FEM simulation.

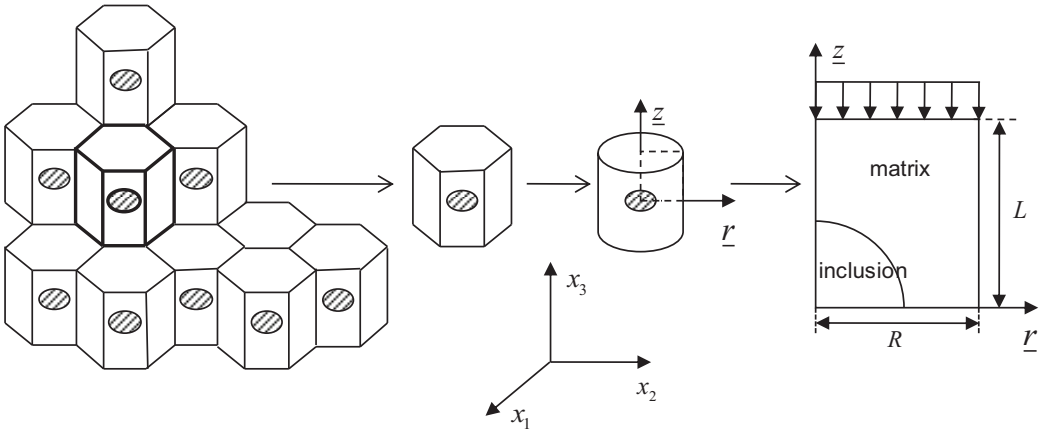

Figure 3-3: Approximation from 3D hexagonal periodic array with spherical inclusion to axi-symmetric cylinder unit cell

Uniform strain boundary conditions are applied to the unit cell as indicated in Eq. (3.19). The displacement on the top side $\overline{U_3}$ is prescribed gradually as a linear function of time. The lateral displacement $\overline{U_2}$ must keep uniform along the boundary to satisfy the uniform strain boundary condition (Huet, 1990; Hazanov & Huet, 1994; Segurado et al., 2003; Llorca & Segurado, 2004, Guery et al., 2008).

$$\begin{aligned} &U_3(r,L)=\overline{U_3}, \quad 0<r<R \\ &U_2(R,z)=\overline{U_2}, \quad 0<z<L \\ &U_3(r,0)=0, \qquad 0<r<R \\ &U_2(0,z)=0, \qquad 0<z<L \end{aligned} \tag{3.19}$$

Two cases are considered; respectively with a volumetric fraction of 5% and 15% for spherical inclusions. A classical Drucker-Prager type yield criterion with isotropic hardening is used for the description of matrix, as indicated in Eq. (3.20), and a typical set of parameters are listed in the Table 3-3-1 and Table 3-2.

$$f = \alpha I_1 + \sqrt{3J_2} - (\sigma_0 + H\gamma^b) \tag{3.20}$$

I_1 is the first invariant of stress tensor and J_2 the second invariant of deviatoric stress tensor. σ_0 denotes the initial threshold of yield stress and H the modulus for plastic hardening. Finally, γ is the plastic hardening variable which is taken as the generalized plastic shear strain.

Table 3-3-1: Typical values of parameters for matrix

$E_m(Pa)$	ν_m	α	$\sigma_0(Pa)$	$H(Pa)$	b
3.0×10^9	0.30	0.167	8.0×10^6	9.0×10^7	0.30

Table 3-2: Typical values of parameters for inclusions

$E_I(Pa)$	ν_I
9.8×10^{10}	0.15

An associated flow rule is first considered. In the Figure 3-3-4, the results for the uniaxial compression test obtained by the FEM solution are presented, together with those obtained by the micromechanical model respectively using the three different isotropization techniques and fully anisotropic tangent operator of the matrix. Similar to those shown in previous studies (Doghri & Ouaar, 2003; Chaboche, et al., 2005; Pierard & Doghri, 2006; Abou-Chakra Guéry et al., 2008), the response given by the micromechanical model using the anisotropic stiffness tensor is too stiff compared with the reference one. Also the results obtained using the isotropization methods 2 and 3 are not able to give good approximations. Only the results given by the micromechanical model with the isotropization method 1 agree very well with the reference solution. Due to this, in the following part of this study, we will take only this isotropization method will be examined.

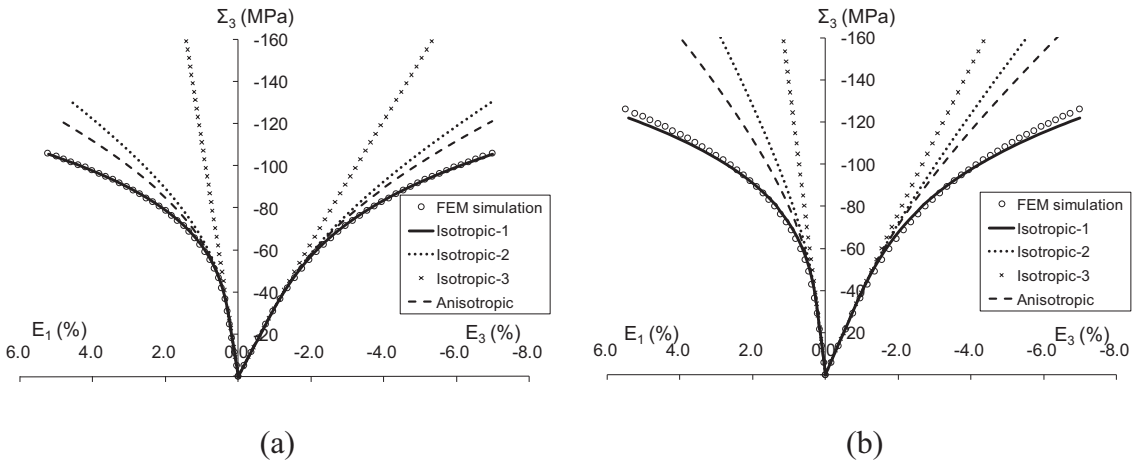

Figure 3-4: Macroscopic responses of composite in uniaxial compression test - Comparison between different isotropization techniques with the reference FEM solution; (a) $f_I = 5\%$; (b) $f_I = 15\%$.

3.2.2 Influences of local plastic flow rule

In the case of associated flow rule discussed above, it is shown that the isotropization method N°1 (only the Eshelby tensor is computed with isotropic part of tangent operator of the matrix) leads to satisfactory approximation of overall responses of heterogeneous material in the framework of incremental approach. However, in many cases such as for most geomaterials, non-associated flow rules are necessary to better describe plastic responses of materials. In this section, it is proposed to study influences of plastic flow rules on the efficiency of isotropization method in micromechanical modeling of non linear heterogeneous materials. To do this, a plastic potential is defined as expressed in Eq.(3.21):

$$g = \psi I_1 + \sqrt{3J_2} - (\sigma_0 + H\gamma^b) \tag{3.21}$$

The parameter ψ defines the so-called volumetric dilatancy coefficient. The yield function is unchanged the values of parameters are the same as those given in Table 1 and Table 2.

For each volumetric fraction of inclusions (5% and 15%), four different values of ψ values are considered. The predictions obtained by the micromechanical model with anisotropic tangent operator and isotropization technique are presented and compared with the reference solution in Figure 3-5 and Figure 3-6. It is clear that the accuracy of micromechanical modeling with isotropization technique is dependent on the flow rule of local constitutive model. With the associated flow rule (as considered above), the predictions coincide with the FEM solution very well; and with the non-associated flow rule, the efficiency of the isotropization method becomes

less confirmed as in the associated flow rule. Some less or more important scatters are observed compared with the FEM solution. However, in all the cases, the prediction using isotropization method is better than that obtained using fully anisotropic tangent operator. Note that the volumetric dilatancy parameter ψ controls plastic volumetric strain rate. It seems that there is a certain dependency of the isotropization efficiency on the plastic volumetric strain. Larger plastic volumetric strain rate will lead to soften predictions of microscopic responses while smaller plastic volumetric strain rate will induce stiffer ones.

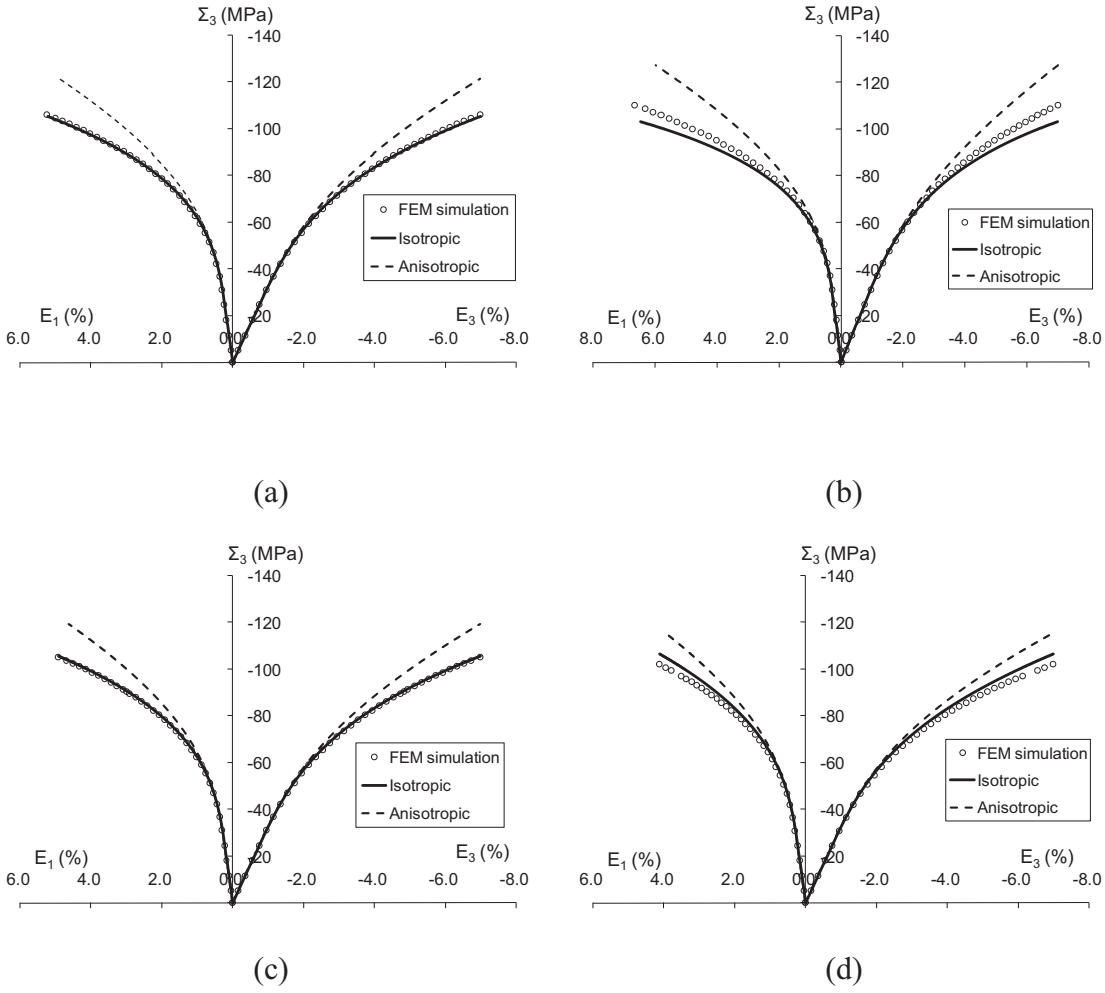

Figure 3-5: Macroscopic responses of composite in uniaxial compression test: Comparison of numerical predictions respectively using anisotropic tangent operator and isotropization method with reference FEM solution for different values of plastic dilatancy coefficient ($f_I = 5\%$); (a) $\psi = 0.167$ (associated); (b) $\psi = 0.20$; (c) $\psi = 0.15$; (d) $\psi = 0.10$

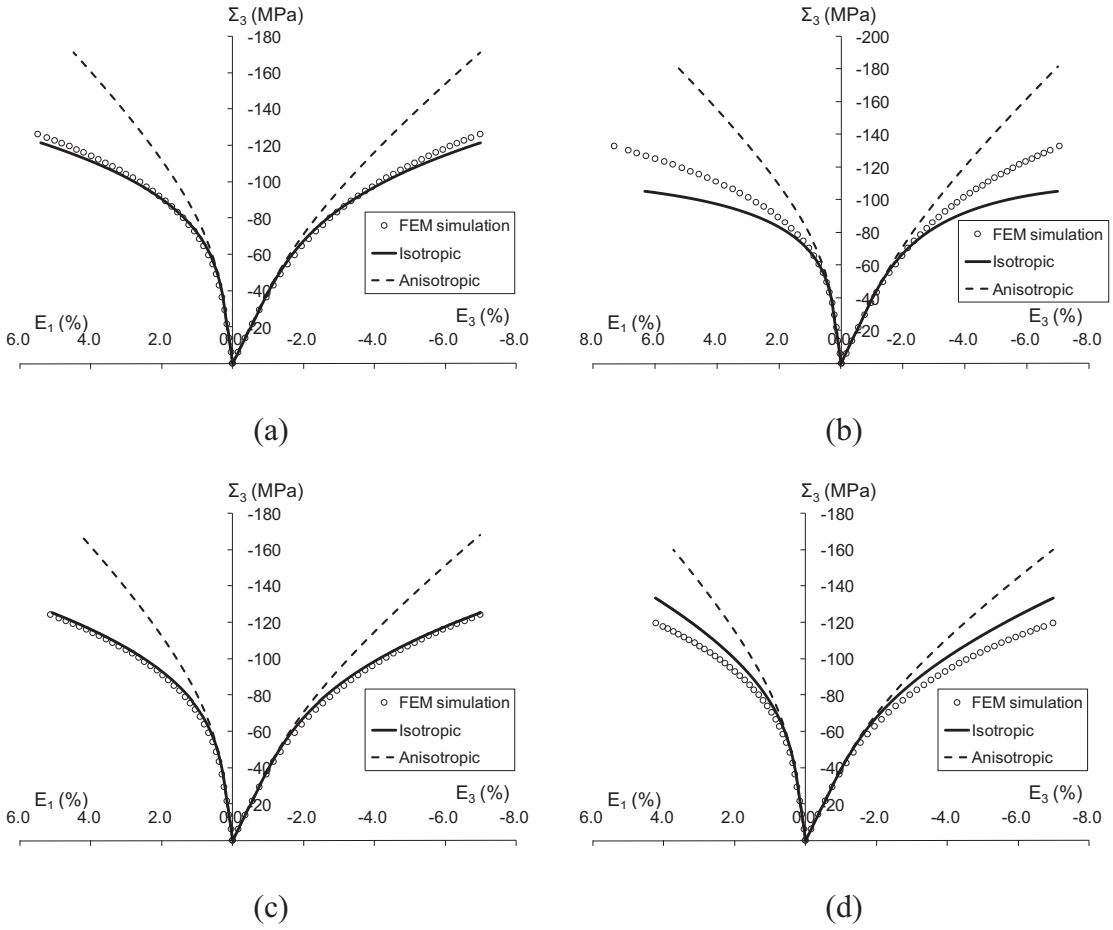

Figure 3-6: Macroscopic responses of composite in uniaxial compression test: Comparison of numerical predictions respectively using anisotropic tangent operator and isotropization method with reference FEM solution for different values of plastic dilatancy coefficient ($f_1 = 15\%$)

(a) $\psi = 0.167$ (associated); (b) $\psi = 0.20$; (c) $\psi = 0.15$; (d) $\psi = 0.10$

3.3 Application to argillite

In this section, the incremental approach is applied to micromechanical modeling of non linear behavior of the Meuse/Haute Marne (MHM) argillite seen as a heterogeneous composite. A local constitutive model is first proposed for the clay matrix.

As aforementioned, the studied argillite is considered as a two phase composite with elastic mineral inclusions embedded in the clay matrix. The behavior of clay matrix is described by an elastoplastic damage model. In this section, the local elastoplastic damage model of clay matrix is

formulated. For the sake of simplicity, an isotropic damage and isotropic plastic hardening law will be assumed. Thus, the state variables include total strain tensor, plastic strain tensor, the scalar variable for isotropic plastic hardening γ and the isotropic damage variable ω related to volumetric crack density. As in the classic plasticity theory, the total strain tensor is decomposed into an elastic part and plastic part:

$$\underline{\underline{\varepsilon}} = \underline{\underline{\varepsilon}}^{e} + \underline{\underline{\varepsilon}}^{p} \tag{3.22}$$

The total free energy function including the elastic strain energy and stored plastic hardening energy Ψ^{p} may be written as:

$$\Psi = \frac{1}{2}(\underline{\underline{\varepsilon}} - \underline{\underline{\varepsilon}}^{p}) : \mathbb{C}(\omega) : (\underline{\underline{\varepsilon}} - \underline{\underline{\varepsilon}}^{p}) + \Psi_{p}(\gamma, \omega) \tag{3.23}$$

In which the fourth order tensor $\mathbb{C}(\omega)$ denotes the elastic stiffness of the damaged material. For isotropic materials, the elastic properties are characterized by the bulk modulus $k(\omega)$ and shear modulus $G(\omega)$:

$$\mathbb{C}(\omega) = 2G(\omega)\mathbb{K} + 3k(\omega)\mathbb{J} \tag{3.24}$$

Then the stress tensor can be derived from the thermodynamic potential:

$$\underline{\underline{\sigma}} = \frac{\partial \Psi}{\partial \underline{\underline{\varepsilon}}} = \mathbb{C}(\omega) : (\underline{\underline{\varepsilon}} - \underline{\underline{\varepsilon}}^{p}) \tag{3.25}$$

The thermodynamic forces associated with the internal variables are defined by:

$$\begin{cases} -\dfrac{\partial \Psi}{\partial \underline{\underline{\varepsilon}}^{p}} = \mathbb{C}(\omega) : \underline{\underline{\varepsilon}}^{e} = \underline{\underline{\sigma}}(\underline{\underline{\varepsilon}}^{e}, \omega) \\ \dfrac{\partial \Psi}{\partial \gamma} = \dfrac{\partial \Psi_{p}}{\partial \gamma}(\gamma, \omega) = \eta(\gamma, \omega) \\ -\dfrac{\partial \Psi}{\partial \omega} = -\dfrac{1}{2}\underline{\underline{\varepsilon}}^{e} : \mathbb{C}'(\omega) : \underline{\underline{\varepsilon}}^{e} - \dfrac{\partial \Psi_{p}}{\partial \omega}(\gamma, \omega) = Y_{d} \end{cases} \tag{3.26}$$

Like most clay materials and soft rocks, the plastic behavior of clay matrix is strongly dependent on confining pressure (Shao & Henry, 1991; Pietruszczak et al., 2002). For this purpose, a curved yield surface is used and described by the following quadratic form:

$$f_p(\underline{\underline{\sigma}},\eta,\omega)=\sigma_{eq}-\eta(\gamma,\omega)P_a\left(C_s-\frac{\sigma_m}{P_a}\right)^{\frac{1}{2}}=0 \tag{3.27}$$

where P_a is a normalizing coefficient taken to be the uniaxial compression strength in the present model; and the parameter C_s represents the coefficient of material cohesion. Inspired by experimental data on various clay soils and rocks, the isotropic plastic hardening law is characterized the following hyperbolic function:

$$\eta(\gamma,\omega)=\frac{\partial\Psi_p}{\partial\gamma}(\gamma,\omega)=(1-\omega)\left[\eta_0+(\eta_m-\eta_0)\frac{\gamma}{b_1+\gamma}\right] \tag{3.28}$$

The parameters η_0 and η_m denote respectively the initial yield threshold and asymptotic state of plastic hardening, while b_1 controls the kinetics of hardening. As in many macroscopic plastic models, the hardening variable is taken as the generalized plastic shear strain defined by:

$$d\gamma=\sqrt{\frac{2}{3}de_{ij}^p:de_{ij}^p}\;;\;\; de_{ij}^p=d\varepsilon_{ij}^p-d\varepsilon_{kk}^p\delta_{ij} \tag{3.29}$$

It is known that most geomaterials exhibit volumetric contraction and dilation during plastic flow. It is generally needed to use a non-associated flow rule. In order to describe the transition from plastic contraction to dilation and inspired by the works by Pietruszczak et al. (1988), the flowing plastic potential is used:

$$Q=\sigma_{eq}+\mu_c(1-\omega)(P_aC_s-\sigma_m)\ln\left(\frac{P_aC_s-\sigma_m}{\bar{p}}\right) \tag{3.30}$$

The coefficient $\bar{p}$ corresponds to the intersection point between the plastic potential surface and the axis $(P_aC_s-\sigma_m)>0$. The parameter μ_c is related to the volumetric dilatancy.

According to the Eq. (3.26), the thermodynamic force associated with the damage can be decomposed into two parts, $Y_d=Y_d^e+Y_d^p$, respectively related to the release rate of elastic strain energy and locked plastic energy.

$$\begin{cases} Y_d^e=-\dfrac{1}{2}\underline{\underline{\varepsilon}}^e:\mathbb{C}'(\omega):\underline{\underline{\varepsilon}}^e \\ Y_d^p=-\dfrac{\partial\Psi_p}{\partial\omega}(\gamma,\omega) \end{cases} \tag{3.31}$$

Generally, for geomaterials under compressive stresses, the damage is essentially related to the

growth of microcracks generated by plastic sliding along microcracks. For simplicity, it is assumed that the damage evolution in the clay matrix is essentially controlled by the plastic shearing. As a consequence, the damage evolution depends on the plastic part of thermodynamic force Y_d^p only, which is defined by:

$$Y_d^p(\gamma) = -\frac{\partial \Psi_p}{\partial \omega} = \eta_m \gamma - (\eta_m - \eta_0) b_1 \ln\left(\frac{b_1 + \gamma}{b_1}\right) \tag{3.32}$$

For the description of damage evolution, inspired by various damage models for brittle materials, the following damage criterion is proposed here:

$$f_d(Y_d^p, \omega) = \omega_c \left[\tanh\left(B_d(Y_d^p - Y_0)\right) + \tanh(B_d Y_0)\right] - \omega = 0 \tag{3.33}$$

The two parameters B_d and Y_0 control the kinetics of damage evolution and ω_c represents the critical damage state which determines the residual strength of the material.

Generally, the elastic properties of the clay matrix are also affected by the induced damage by microcracks. According to the relevant micromechanical analysis (Nemat-Nasser & Hori, 1999; Pensée et al., 2002), the bulk modulus and shear modulus in (3.24) should be independently expressed as functions of damage variable. The unilateral effects due to crack closure should also be included in the determination of effective elastic properties. However, in the present work, we are considering essentially mechanical responses of geomaterials under compressive stresses. In this case, most microcracks are in closed position. In this case, it is found that the bulk modulus remains constant and only the shear modulus is affected by the induced damage (Pensée et al., 2002). Therefore, the following simple relations are used here:

$$\begin{cases} k(\omega) = k_0 \\ G(\omega) = G_0(1 - \omega) \end{cases} \tag{3.34}$$

The parameters k_0 and G_0 denote the initial bulk and shear modulus of undamaged clay matrix.

In the present elastoplastic damage model, the two dissipation mechanisms of plastic flow and damage evolution are coupled. Further, as a simplified choice, the damage evolution is directly related to plastic flow. Therefore, the loading/unloading conditions are the same for the two mechanisms. Generally, the plastic flow and damage evolution rates are defined by the following rules:

$$\dot{\underline{\underline{\varepsilon}}}^p = \dot{\lambda}_p \frac{\partial Q}{\partial \underline{\underline{\sigma}}} \quad ; \quad \dot{\omega} = \dot{\lambda}_d \frac{\partial f_d}{\partial Y_d^p} \tag{3.35}$$

The plastic multiplier $\dot{\lambda}_p$ and the damage multiplier $\dot{\lambda}_d$ should be determined using the consistency conditions respectively for plastic flow and damage evolution:

$$\dot{f}_p(\underline{\underline{\sigma}}, \eta, \omega) = \frac{\partial f_p}{\partial \underline{\underline{\sigma}}} \dot{\underline{\underline{\sigma}}} + \frac{\partial f_p}{\partial \eta} \frac{\partial \eta}{\partial \gamma} \dot{\gamma} + \frac{\partial f_p}{\partial \eta} \frac{\partial \eta}{\partial \omega} \dot{\omega} = 0 \tag{3.36}$$

$$\dot{f}_d(Y_d^p, \omega) = \frac{\partial f_d}{\partial Y_d^p} \dot{Y}_d^p + \frac{\partial f_d}{\partial \omega} \dot{\omega} = 0 \tag{3.37}$$

However, in the model, as only the plastic part of the thermodynamic damage force is used in the damage criterion and it is related to plastic distortion, it is then possible to relate the damage evolution rate to the plastic distortion rate. Substitute Eq. (3.32) and (3.33) for Eq. (3.37), one obtains:

$$\dot{\omega} = \frac{\partial f_d}{\partial Y_d^p} \dot{Y}_d^p = \frac{\partial f_d}{\partial Y_d^p} \frac{\partial Y_d^p}{\partial \gamma} \dot{\gamma} \tag{3.38}$$

$$\begin{cases} \dfrac{\partial f_d}{\partial Y_d^p} = \omega_c B_d \left[1 - \tanh^2 \left(B_d (Y_d^p - Y_0) \right) \right] \\ \dfrac{\partial Y_d^p}{\partial \gamma} = \eta_0 + (\eta_m - \eta_0) \dfrac{\gamma}{b_1 + \gamma} \end{cases} \tag{3.39}$$

Using the definition of $\dot{\gamma}$, one can rewrite Eq. (3.38) as follows:

$$\dot{\omega} = h_q \frac{\partial f_d}{\partial Y_d^p} \frac{\partial Y_d^p}{\partial \gamma} \dot{\lambda}_p \quad , \quad h_q = \sqrt{\frac{2}{3} (\mathbb{K} : \frac{\partial Q}{\partial \underline{\underline{\sigma}}}) : (\mathbb{K} : \frac{\partial Q}{\partial \underline{\underline{\sigma}}})} \tag{3.40}$$

Applying now the plastic consistency condition, the plastic multiplier is finally given by:

$$\dot{\lambda}_p = \frac{\dfrac{\partial f_p}{\partial \underline{\underline{\sigma}}} : \mathbb{C}(\omega) : \dot{\underline{\underline{\sigma}}}}{\dfrac{\partial f_p}{\partial \underline{\underline{\sigma}}} : \mathbb{C}(\omega) : \dfrac{\partial Q}{\partial \underline{\underline{\sigma}}} - h_q \dfrac{\partial f_d}{\partial Y_d^p} \dfrac{\partial Y_d^p}{\partial \gamma} \left(\dfrac{\partial f_p}{\partial \underline{\underline{\sigma}}} : \mathbb{C}'(\omega) : \underline{\underline{\varepsilon}}^e + \dfrac{\partial f_p}{\partial \eta} \dfrac{\partial \eta}{\partial \omega} \right) - \dfrac{\partial f_p}{\partial \eta} \dfrac{\partial \eta}{\partial \gamma}} \tag{3.41}$$

Substituting now Eq. (3.40) and (3.41) for the rate form of the constitutive relations Eq.(3.25), the local tangent operator of the clay matrix can be determined as follows:

$$\mathbb{L}_m = \mathbb{C}(\omega) + \frac{\left(h_q \frac{\partial f_d}{\partial Y_d^p} \frac{\partial Y_d^p}{\partial \gamma} \mathbb{C}'(\omega) : \underline{\underline{\varepsilon}}^e - \mathbb{C}(\omega) : \frac{\partial Q}{\partial \underline{\underline{\sigma}}} \right) \otimes \left(\frac{\partial f_p}{\partial \underline{\underline{\sigma}}} : \mathbb{C}(\omega) \right)}{\frac{\partial f_p}{\partial \underline{\underline{\sigma}}} : \mathbb{C}(\omega) : \frac{\partial Q}{\partial \underline{\underline{\sigma}}} - h_q \frac{\partial f_d}{\partial Y_d^p} \frac{\partial Y_d^p}{\partial \gamma} \left(\frac{\partial f_p}{\partial \underline{\underline{\sigma}}} : \mathbb{C}'(\omega) : \underline{\underline{\varepsilon}}^e + \frac{\partial f_p}{\partial \eta} \frac{\partial \eta}{\partial \omega} \right) - \frac{\partial f_p}{\partial \eta} \frac{\partial \eta}{\partial \gamma}} \tag{3.42}$$

3.4 Local integration scheme

The proposed micromechanical model can be easily implemented into usual computer codes, for instance, using finite element method. The local integration procedure of the micromechanical model is outlined here. The representative volume element of heterogeneous material is subjected to a uniform macroscopic strain increment, $\underline{\underline{E}}^{(n+1)} = \underline{\underline{E}}^{(n)} + \Delta \underline{\underline{E}}$, at the loading step $(n+1)$. The objective of local integration is to found the corresponding macroscopic strain increment via the macroscopic tangent stiffness tensor using (3.4). For this purpose, the following procedure is adopted. Let first denote $\Delta \underline{\underline{\bar{\varepsilon}}}_r^{(i)}$, the estimate of the average strain increment at the iteration (i) inside the material phase r (Abou-Charka Guéry, 2007).

1. Put the macroscopic strain as the initial estimate of the average strain in the inclusion phase:

$$\Delta \underline{\underline{\bar{\varepsilon}}}_I^{(0)} = \Delta \underline{\underline{E}} \tag{3.43}$$

2. Thus, at the iteration (i), the value of $\Delta \underline{\underline{\bar{\varepsilon}}}_I^{(i)}$ is known, and the local tangent operator of the inclusion phase is also determined (for instance the linear elastic tensor). Then the average strain increment in the clay matrix if given by:

$$\Delta \underline{\underline{\bar{\varepsilon}}}_m^{(i)} = \frac{\Delta \underline{\underline{E}} - f_I \Delta \underline{\underline{\bar{\varepsilon}}}_I^{(i)}}{1 - f_I} \tag{3.44}$$

3. Using this prescribed strain increment, the tangent operator of the clay matrix can be determined using the local elastoplastic damage model Eq. (3.42).

4. Hill's tensor $\mathbb{P}_I^0$ is evaluated by analytical solution Eq. (3.17) for isotropic case and by numerical calculation Eq. (3.11) for anisotropic case.

5. Update the strain localization tensors respectively for inclusion phase $\mathbb{A}_I$ and clay matrix $\mathbb{A}_m$ using Eq. (3.8). Verify now the compatibility of the average strains for each phase according to the localization tensors:

$$\underline{\underline{R}}_I^{(i)} = \mathbb{A}_I : \Delta\underline{\underline{E}} - \Delta\underline{\underline{\bar{\varepsilon}}}_I^{(i)} \tag{3.45}$$

$$\underline{\underline{R}}_m^{(i)} = \mathbb{A}_m : \Delta\underline{\underline{E}} - \Delta\underline{\underline{\bar{\varepsilon}}}_m^{(i)} \tag{3.46}$$

If the strain estimation errors $\left\|\underline{\underline{R}}_I^{(i)}\right\|$ and $\left\|\underline{\underline{R}}_m^{(i)}\right\|$ are less than the fixed convergence tolerance, then the solution is obtained. Else, a new iteration step is needed by using the new estimations of average strain in each phase:

$$\Delta\underline{\underline{\bar{\varepsilon}}}_I^{(i+1)} = \Delta\underline{\underline{\bar{\varepsilon}}}_I^{(i)} + \underline{\underline{R}}_I^{(i)} \tag{3.47}$$

$$\Delta\underline{\underline{\bar{\varepsilon}}}_m^{(i+1)} = \Delta\underline{\underline{\bar{\varepsilon}}}_m^{(i)} + \underline{\underline{R}}_m^{(i)} \tag{3.48}$$

The iterative procedure id repeated until the convergence is obtained.

6. After the convergence, the macroscopic tangent operator of homogenized material is determined and the macroscopic stress increment calculated:

$$\mathbb{L}^{\text{hom}} = (1-f_I)\mathbb{L}_m^{(i)} : \mathbb{A}_m^{(i)} + f_I\mathbb{L}_I^{(i)} : \mathbb{A}_I^{(i)} \tag{3.49}$$

$$\Delta\underline{\underline{\Sigma}}^{(n+1)} = \mathbb{L}^{\text{hom}} : \Delta\underline{\underline{E}}^{(n+1)} \tag{3.50}$$

3.5 Numerical simulation of the laboratory tests of argillite

In order to perform a first phase of validation, the proposed micromechanical model is now applied to simulate laboratory tests with various loading path performed on argillites with different mineralogical compositions. The main challenge of micromechanical modeling is the identification of local parameters for each material phase. The local mechanical behavior should be determined. This direct identification method is so far not possible because relevant data on mechanical responses at the microscopic scale are not available. An indirect identification method is then adopted. The elastic properties of quartz and calcite grains are selected from reported data in literature for these minerals. For the identification of mechanical parameters of the clay matrix,

the following procedure is used. Consider some laboratory tests as the reference tests, for example, uniaxial compression test performed on the sample with a given mineralogical composition. The model's parameters are then determined by numerical fitting with respect to these references tests. One set of parameters are then obtained, as the reference parameters. Using these ones, other laboratory tests, with different loading paths and performed on sample with different mineralogical compositions are simulated. During these simulations, all the mechanical parameters are hold constant and only the mineralogical compositions is changing. For the argillite studied here, the reference parameters are given in Table 3-3 and Table 3-4. In all the simulations presented herein, the axis $\underline{e_3}$ represents the axial direction of cylinder sample, while the axes $\underline{e_1}$ and $\underline{e_2}$ denote the radial directions.

Table 3-3: Parameters of the clay matrix

E_m(GPa)	ν_m	C_s	η_0	η_m	b_1	μ_c	Y_0	B_d	ω_c
3.0	0.30	17.0	0.0015	21.0	0.0015	1.6	0.4	3.0	0.7

Table 3-4: Parameters of the inclusion

E_I(GPa)	ν_I
98.0	0.15

3.5.1 Simulations of triaxial compression tests

The results of numerical simulation to the triaxial compression tests under different confining pressures performed on specimens from different depths are illustrated in Figure , Figure , and Figure . One can see that there is a fairly good general agreement between numerical results and experimental results. The main macroscopic characteristics of the argillite are clearly revealed in the micromechanical modeling, such as pressure dependency, transition from volumetric compressibility to dilatancy and material softening due to progressive growth of microcracks in the clay matrix. It is particularly worth noticing that the micromechanical model inherently takes into account the influences of mineralogical compositions. This is an important advantage compared with classical phenomenological models for which a set of parameters has to be determined from each group of mineralogical composition. In Figure 3-10, the simulations of triaxial compression tests with unloading cycles are also shown. The micromechanical model

seems also to be able to predict the progressive degradation of elastic modulus due to induced damage by microcracks. Some quantitative differences are observed between numerical predictions and experimental data in some tests. Note that the argillite studied here is a delicate material which is sensitive to many factors such as water content. Therefore, important scatters have been obtained during experimental investigations. The numerical prediction may be improved if more experimental investigations, in particular on the microscopic level, are available.

In Figure 3-11, the overall mechanical responses of the argillite during a triaxial compression test are compared with those of the clay matrix alone as a homogeneous material. There are significant differences between the two series of responses. The role of mineral inclusions to reinforce the composite material is clearly demonstrated. In Figure 3-12, the evolution of local damage by microcracks inside the clay matrix is shown as a function of macroscopic deviatoric stress. The local damage is responsible for progressive degradation of elastic properties and material softening of argillite at the macroscopic level.

3.5.2 Proportional triaxial compression tests and lateral extension tests

Two other typical loading paths in rock mechanics are now considered: radial extension and proportional compression tests. Numerical simulations of these tests are performed to provide a complementary validation of the model. In the proportional compression test, the axial and radial stresses are simultaneously increased with a constant ratio:

$$k = \frac{\Sigma_{33}}{\Sigma_{11}} \tag{3.51}$$

In the radial extension test, the sample is first subjected to a hydrostatic stress state to a given value, and then the radial stress is progressively decreased while the axial stress is kept constant. Comparisons between numerical predictions and experimental data for these two kinds of tests are shown in Figure 3-13 and

Figure 3-14. Again, one obtains a general good agreement and the proposed micromechanical model correctly describes the main characteristics of mechanical responses of material in these two loading paths.

In Figure 3-15, we have shown comparisons of numerical simulations respectively obtained by the present model with two material phases and that proposed by Abou-Chakra et al. (2008) with three material phases. Reminder that in the present model, the induced damage is associated

with the clay matrix while in the previous model it was included in the calcite grains. One can note that the consequence of local damage on macroscopic responses of argillite is quite different between the two models. This consequence is more significant in the present model, which is in particular able to reproduce the peak failure stress and material softening behavior in post-peak regime. This seems to more agree with experimental observations on this class of materials.

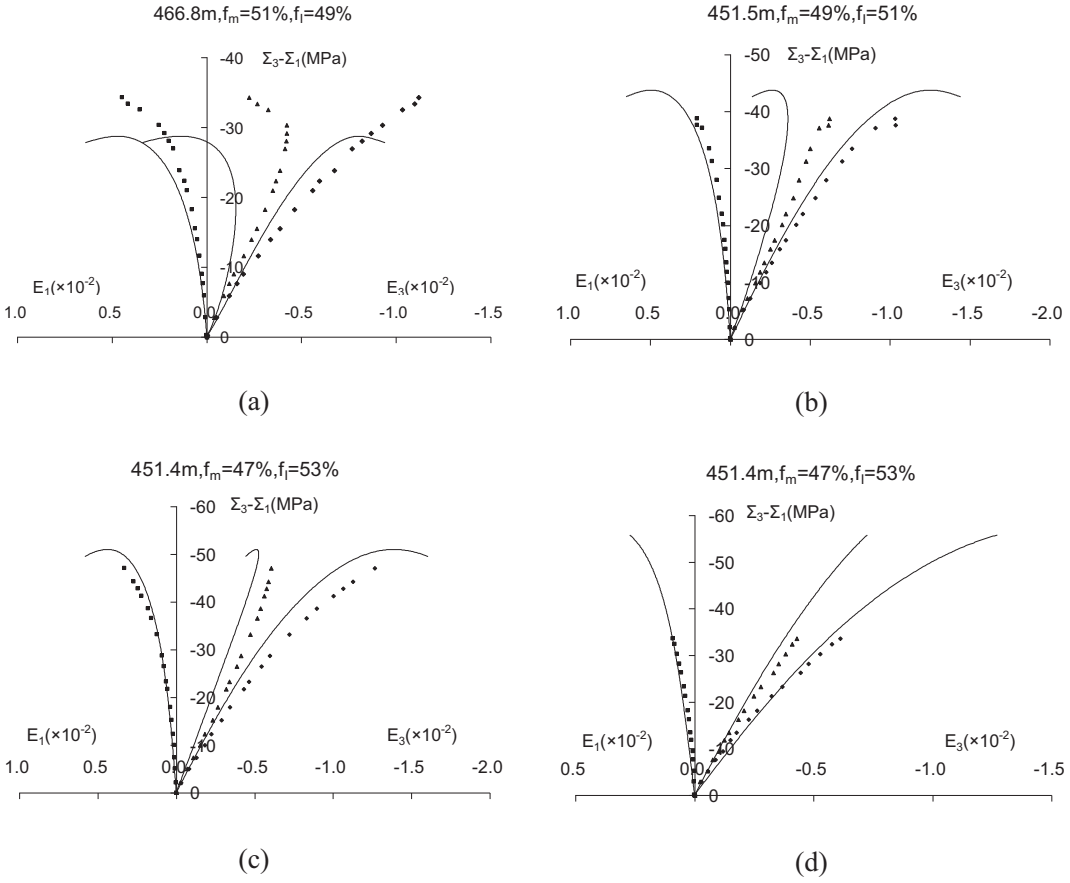

Figure 3-7: Macroscopic responses of the specimens from depth-1 (451.4m-466.8m) during triaxial compression tests with different confining pressures: (a) 0MPa; (b) 5MPa; (c) 10MPa; (d) 20MPa

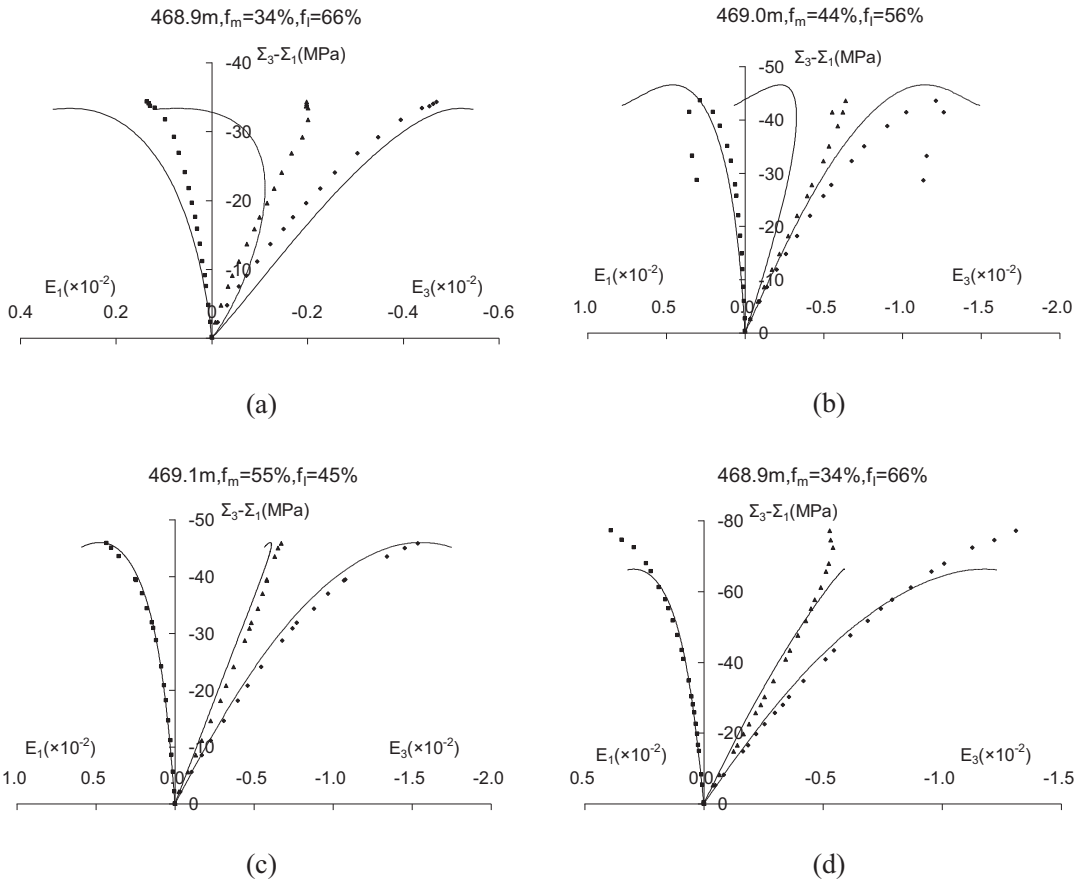

Figure 3-8: Macroscopic responses of the specimens from depth-2 (468.9m-469.1m) during triaxial compression tests with different confining pressures: (a) 0MPa; (b) 5MPa; (c) 10MPa; (d) 20MPa

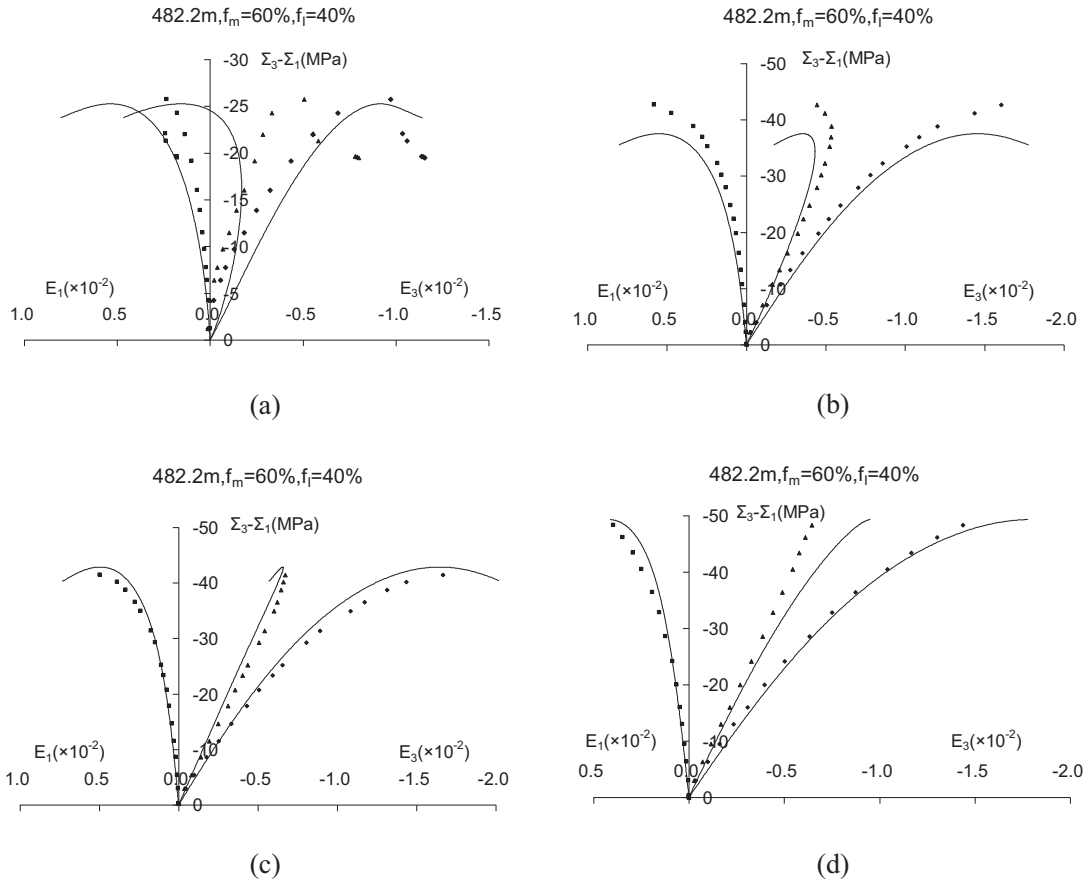

Figure 3-9: Macroscopic responses of the specimens from depth-3 (482.1m-482.4m) during triaxial compression tests with different confining pressures: (a) 0MPa; (b) 5MPa; (c) 10MPa; (d) 20MPa

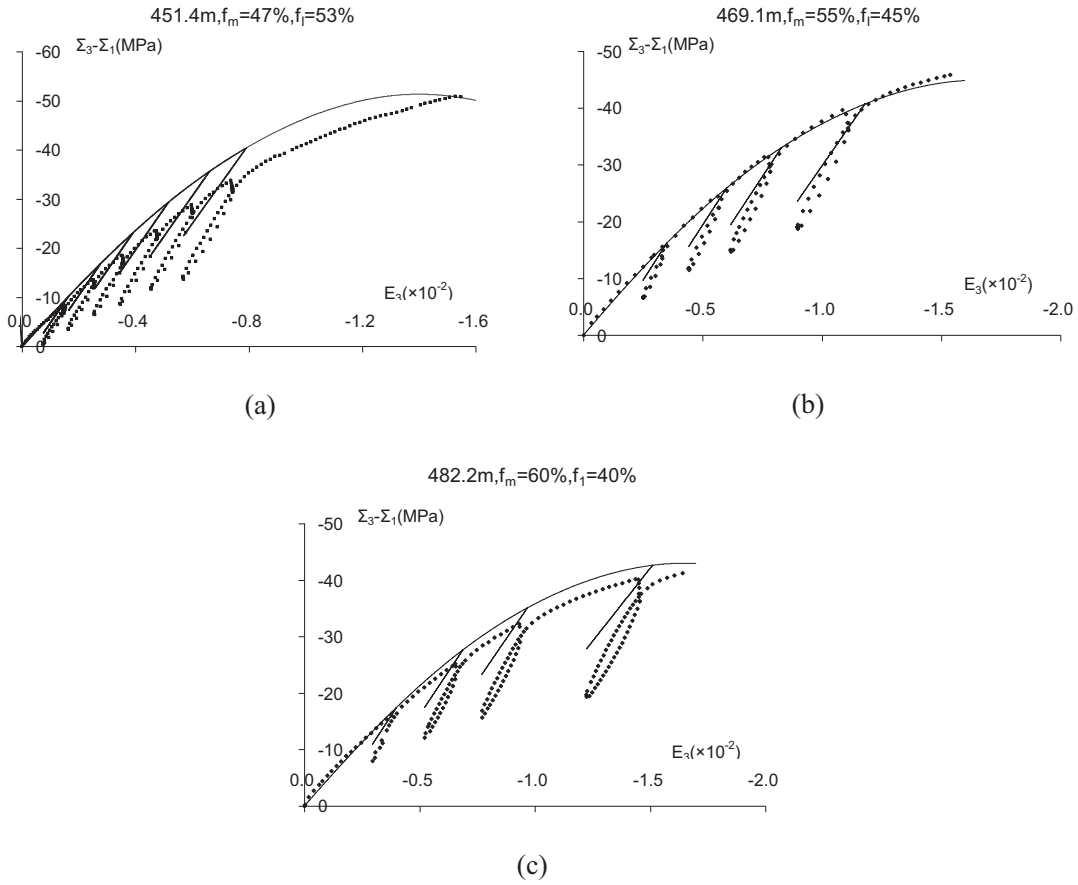

Figure 3-10: Macroscopic responses (axial strain versus deviatoric stress) of specimens from different depths during triaxial compression tests with 10MPa confining pressure and unloading – reloading cycles

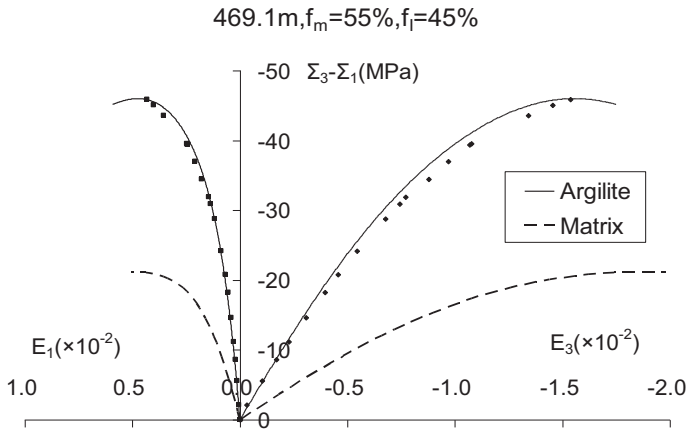

Figure 3-11: Comparison of overall responses of argillite and those of clay matrix alone during a triaxial compression test with 10MPa confining pressure – influence of mineral inclusions

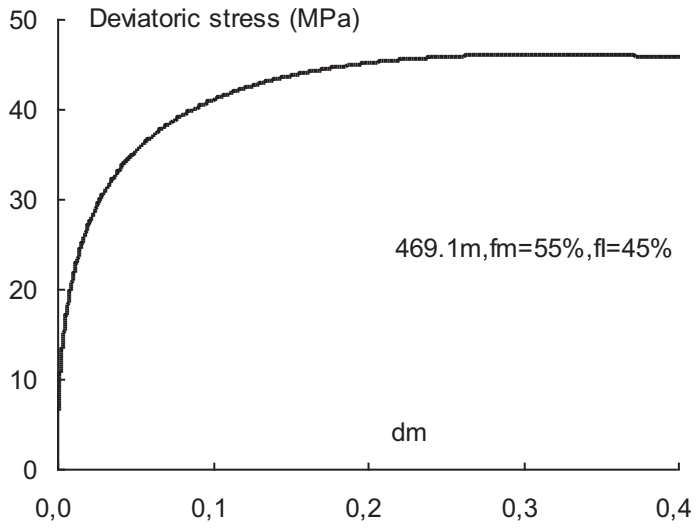

Figure 3-12: Relation of damage variable of clay matrix and macroscopic equivalent deviator stress of the specimen from depth-2 (468.9m-469.1m) with 10MPa confining pressure

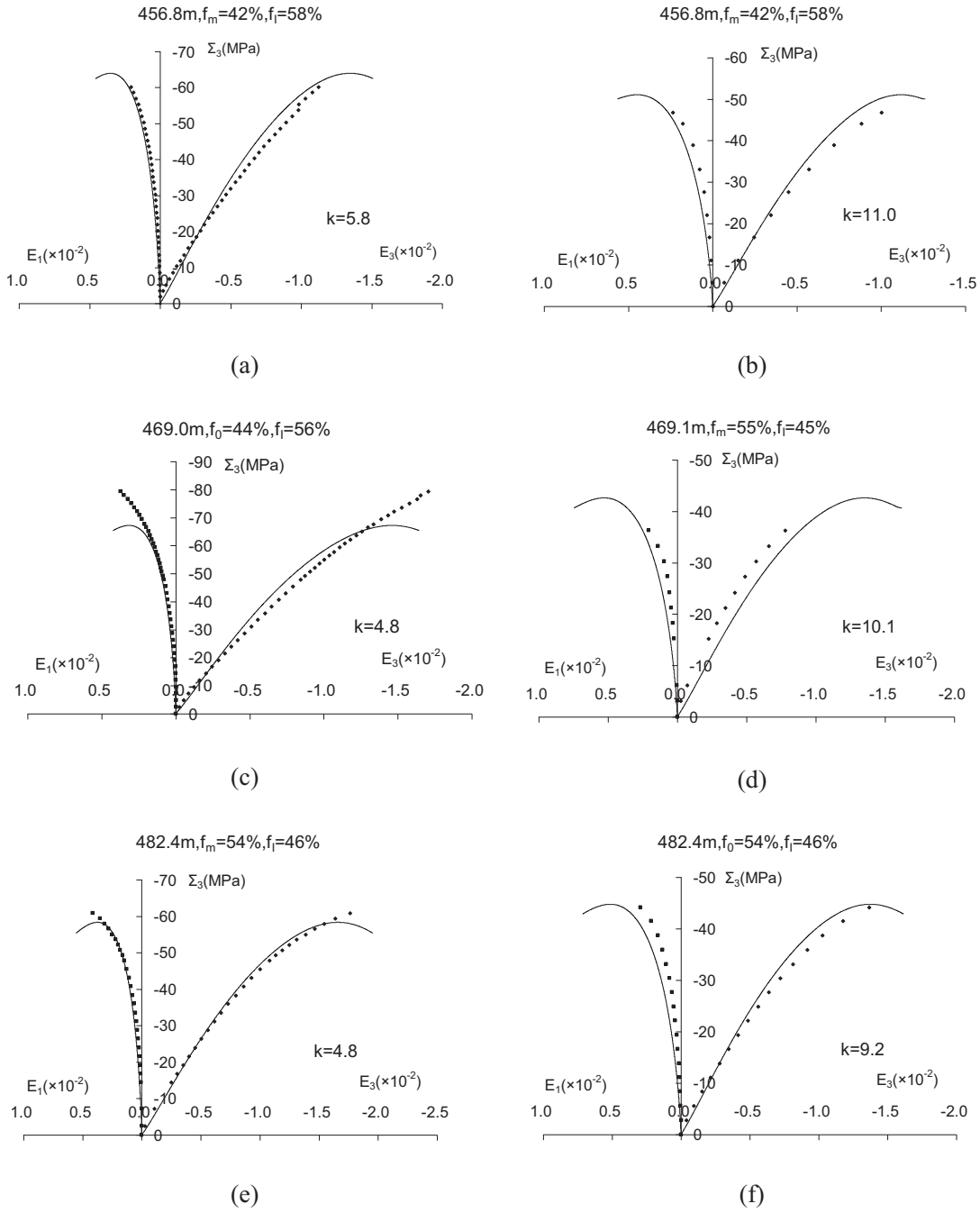

Figure 3-13: Macroscopic responses (axial and radial strains versus axial stress) of specimens from different depths during proportional compression tests

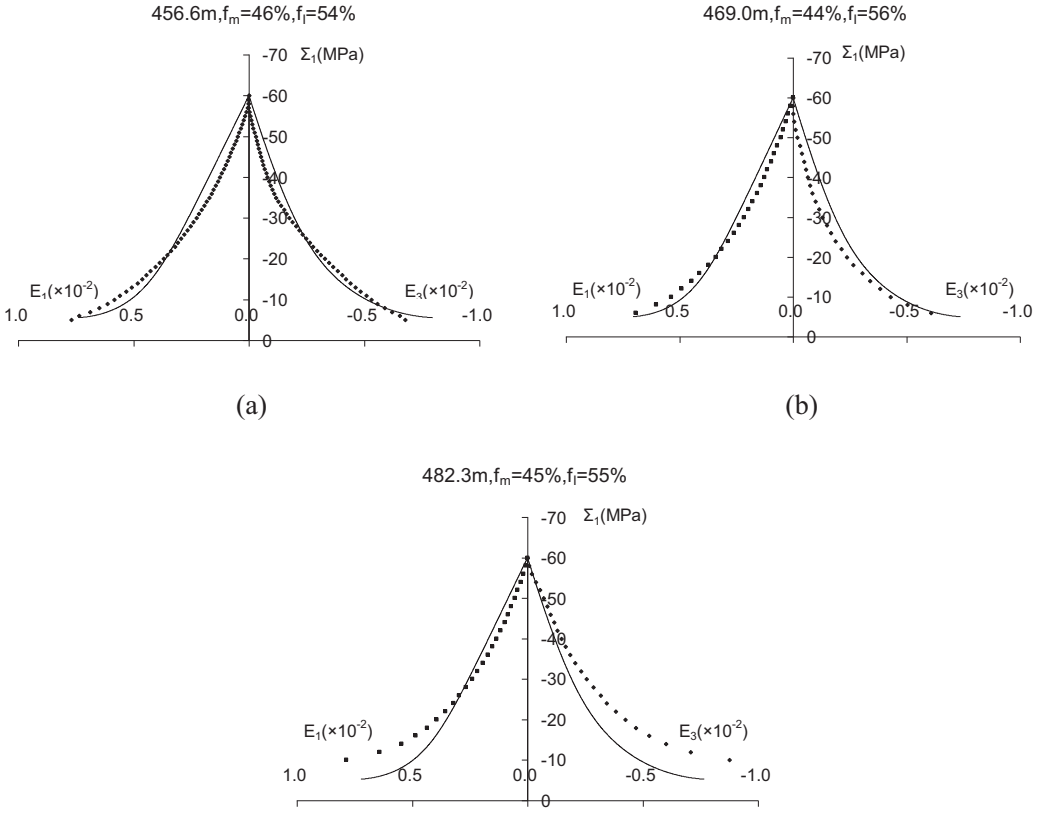

Figure 3-14: Macroscopic responses (axial and radial strains versus radial stress) of specimens from different depths during radial extension tests with initial confining pressure of 60MPa

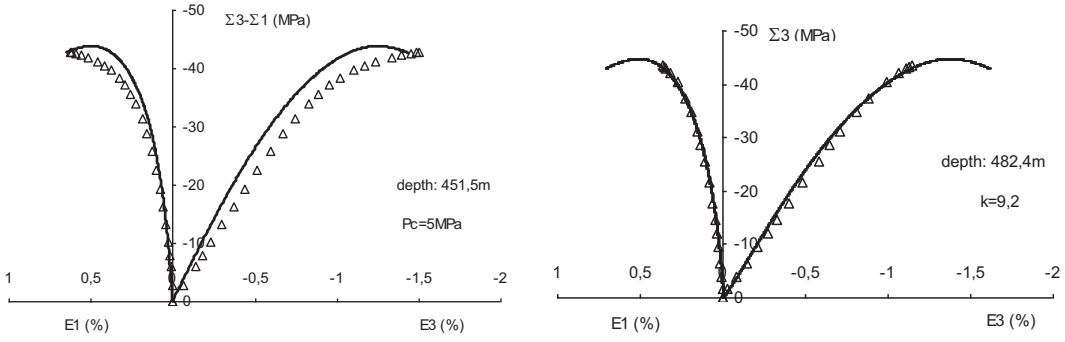

Figure 3-15: Comparison of simulations of a triaxial compression test between the micromechanical models with two (continuous lines) and three phases (symbols) ; (a) sample depth 451.5m; (b) sample depth 482.4m

3.6 Conclusions

A micromechanical model is proposed in this chapter for the description of nonlinear behavior of heterogeneous materials, in particular the elastoplastic damage geomaterial. The formulation of non linear homogenization is based on the incremental method of Hill. The proposed model is applied to hard clay which is considered as a two phase composite with the clay matrix and quartz/calcite mineral inclusions. The macroscopic tangent operation of homogenized material is obtained using Mori-Tanaka scheme. The isotropization procedure can efficiently improve the predictions of macroscopic responses of heterogeneous materials.

The validity of the proposed model is verified through the comparisons between numerical predictions and experimental data. Compared with classical macroscopic models, the micromechanical approach inherently takes into account influences of microstructure (mineralogical compositions) on macroscopic mechanical behavior of material. This is an important advantage, which allows a continuous description of spatial variations of mechanical behavior of rock materials in numerical modeling of structures. An overall good agreement between numerical predictions and experimental data has been obtained. The proposed micromechanical model seems to be able to describe main features of mechanical behaviors observed, such as pressure dependency, transition from volumetric compressibility to dilatancy, plastic damage coupling, progressive degradation of elastic properties and material softening due to induced damage by microcracks.

Chapter 4:
Non-uniform transformation field analysis (NTFA) for pressure-dependent heterogeneous elastoplastic materials

The non-uniform transformation field analysis (NTFA) initially proposed by Michel and Suquet (2003; 2004) assumed that the microscopic plastic strain field in RVE can be decomposed into a linear combination of a group of typical non-uniform plastic strain fields, called "plastic modes ". Compared with the TFA approach (Dvorak & Benveniste, 1992; Dvorak, 1992) and all the kinds of mean field approaches, the NTFA can much better describe the heterogeneity of microscopic plastic strain field. As a result, the estimation of the effective response of heterogeneous material is more accurate, and the local fields can be easily recovered after the solution of the overall structural boundary value problem (Kanouté et al. 2009).

The NTFA has so far been applied only to predict the nonlinear composites with pressure independent constituents. For heterogeneous materials composed of pressure sensitive constituents, in particular for geomaterials such as concrete, rocks, and soils, there is need for specific adaptation of the NTFA because such materials present some distinct properties, such as volumetric dilatancy, asymmetric mechanical responses to compression and tension.

Therefore, the objective of this chapter is the adaptation and application of the NTFA method to micromechanical modeling of heterogeneous geomaterials. As a starting point of this study, we will first consider nonlinear heterogeneous materials composed of pressure-sensitive matrix which is described by non associated plastic flow rule based on the classic Drucker-Prager criterion. After the presentation of local constitutive model in Section 4.1, the formulation and numerical implementation of the NTFA method are presented respectively in sections 4.2 and 4.3. In section 4.4, we will consider two specific applications; one is the composite with Drucker-Prager type matrix reinforced by elastic inclusions, the other is a porous material with Drucker-Prager matrix. The numerical results obtained from the NTFA will be compared with the reference solution from FEM simulation and those issued from other commonly used approaches.

4.1 Local elastoplastic constitutive model

The local elastoplastic constitutive model for solid matrix is formulated in the general thermodynamic framework. The state variables are composed of total strain tensor $\underline{\underline{\varepsilon}}$ and two internal variables, i.e. plastic strain tensor $\underline{\underline{\varepsilon}}^p$ and isotropic plastic hardening scale γ. The total

strain tensor is then decomposed as follows:

$$\underline{\underline{\varepsilon}} = \underline{\underline{\varepsilon}}^{e} + \underline{\underline{\varepsilon}}^{p} \tag{4.1}$$

Only isotropic hardening materials are considered in this study, thus the free energy of material is composed of two parts, energy induced by elastic deformation and isotropic hardening.

$$w(\underline{\underline{\varepsilon}}, \underline{\underline{\varepsilon}}^{p}, \gamma) = \frac{1}{2}(\underline{\underline{\varepsilon}} - \underline{\underline{\varepsilon}}^{p}) : \mathbb{C} : (\underline{\underline{\varepsilon}} - \underline{\underline{\varepsilon}}^{p}) + w^{p}(\gamma) \tag{4.2}$$

where the fourth order tensor $\mathbb{C}$ is the elastic stiffness, which can be expressed in a simple form for the isotropic material in this study.

$$\mathbb{C} = 3k\mathbb{J} + 2G\mathbb{K} \tag{4.3}$$

$$k = \frac{E}{3(1-2\upsilon)}, \quad G = \frac{E}{2(1+\upsilon)} \tag{4.4}$$

where k and G are bulk and shear modulus, E and υ are elastic modulus and Poisson ratio, respectively. Using the free energy function Eq. (4.2) as the thermodynamic potential, the standard derivation leads to the following state equations, in which the stress $\underline{\underline{\sigma}}$ and thermodynamic forces $(\underline{\underline{Y}}^{pl}, Y^{h})$ are associated with state variables as follows:

$$\underline{\underline{\sigma}} = \frac{\partial w}{\partial \underline{\underline{\varepsilon}}}(\underline{\underline{\varepsilon}}, \underline{\underline{\varepsilon}}^{p}, \gamma) = \mathbb{C} : (\underline{\underline{\varepsilon}} - \underline{\underline{\varepsilon}}^{p}) \tag{4.5}$$

$$\begin{cases} \underline{\underline{Y}}^{pl} = -\dfrac{\partial w}{\partial \underline{\underline{\varepsilon}}^{p}}(\underline{\underline{\varepsilon}}, \underline{\underline{\varepsilon}}^{p}, \gamma) = \underline{\underline{\sigma}} \\ Y^{h} = -\dfrac{\partial w}{\partial \gamma}(\underline{\underline{\varepsilon}}, \underline{\underline{\varepsilon}}^{p}, \gamma) = -\dfrac{\partial w^{p}}{\partial \gamma}(p) = -R(\gamma) \end{cases} \tag{4.6}$$

$R(\gamma)$ is the thermodynamic force associated with the internal variable γ, defining the size of elastic domain and controlling the evolution of yield surface. The classical Drucker-Prager yield function (Drucker & Prager, 1952) is written as:

$$f_{p}(\underline{\underline{\sigma}}, \gamma) = \alpha\sigma_{m} + \sigma_{eq} - R(\gamma) = 0 \tag{4.7}$$

where $\sigma_{m} = (\underline{\underline{\sigma}} : \underline{\underline{\delta}})/3$, $\sigma_{eq} = \sqrt{3\underline{\underline{s}} : \underline{\underline{s}}/2}$, $\underline{\underline{s}} = \mathbb{K} : \underline{\underline{\sigma}}$ is the deviatoric stress tensor. A non-associated flow rule is used in this study to describe the variation of plastic dilatancy:

$$g = \psi\sigma_m + \sigma_{eq} - R(\gamma) \tag{4.8}$$

The parameter ψ describes the plastic volumetric dilatancy. Then the evolution of internal variables can be derived in the general scheme of plasticity as follows:

$$\begin{cases} \dot{\underline{\underline{\varepsilon}}}^p = \dot{\lambda}\dfrac{\partial g}{\partial \underline{\underline{Y}}^{pl}} = \dot{\lambda}\dfrac{\partial g}{\partial \underline{\underline{\sigma}}} = \dot{\lambda}\left(\dfrac{1}{3}\psi\underline{\underline{\delta}} + \dfrac{3}{2}\dfrac{\underline{\underline{s}}}{\sigma_{eq}}\right) \\ \dot{\gamma} = \dot{\lambda}\dfrac{\partial g}{\partial Y^h} = \dot{\lambda}\left(-\dfrac{\partial g}{\partial R(\gamma)}\right) = \dot{\lambda} \end{cases} \tag{4.9}$$

That is, the relationship between the increments of two internal variables can be formulated as:

$$\dot{\underline{\underline{\varepsilon}}}^p = \dot{\gamma}\left(\frac{1}{3}\psi\underline{\underline{\delta}} + \frac{3}{2}\frac{\underline{\underline{s}}}{\sigma_{eq}}\right) \tag{4.10}$$

4.2 Principles of nonuniform transformation field method (NTFA) for pressure-dependent materials

4.2.1 Basic assumptions of NTFA for D-P material

As stated above, it is the main advantage of the NTFA (Michel & Suquet, 2003; 2004) that the heterogeneous plastic strain field in RVE can be considered by non uniform transformation fields. In this study, the plastic strain field of D-P material is divided into two parts, deviatoric component $\underline{\underline{\varepsilon}}_d^p(\underline{x})$, and volumetric component $\varepsilon_m^p(\underline{x})\underline{\underline{\delta}}$. Each part is decomposed of a linear combination of a group of so-called "plastic modes": $\underline{\underline{\mu}}_d^{(k)}(\underline{x})$ for deviatoric component and $\mu_m^{(k)}(\underline{x})\underline{\underline{\delta}}$ for volumetric component of the plastic strain field, respectively:

$$\begin{aligned} \underline{\underline{\varepsilon}}^p(\underline{x}) &= \underline{\underline{\varepsilon}}_d^p(\underline{x}) + \varepsilon_m^p(\underline{x})\underline{\underline{\delta}} \\ &= \sum_{k=1}^{N_d} \varepsilon_{k\_d}^p \underline{\underline{\mu}}_d^{(k)}(\underline{x}) + \sum_{k=1}^{N_m} \varepsilon_{k\_m}^p \left(\mu_m^{(k)}(\underline{x})\underline{\underline{\delta}}\right) \end{aligned} \tag{4.11}$$

where $\varepsilon_{k\_d}^p$ and $\varepsilon_{k\_m}^p$ are coefficients of linear combinations, N_d and N_m are total number of plastic modes respectively for deviatoric and volumetric part of plastic strain field. For the sake of simplicity, it is assumed that in Eq. (4.11) each plastic mode exists in only one material phase; however, every material phase can contain several plastic modes. Furthermore, there are two conditions that any two groups of plastic modes must be satisfied:

1). Orthogonal:[1]

$$\left\langle \underline{\underline{\mu}}_d^{(k)} : \underline{\underline{\mu}}_d^{(l)} \right\rangle = 0, \quad \left\langle \left(\mu_m^{(k)} \underline{\underline{\delta}} \right) : \left(\mu_m^{(l)} \underline{\underline{\delta}} \right) \right\rangle = 0 \quad (\text{if } k \neq l) \tag{4.12}$$

2). Normalized:

$$\left\langle \sqrt{\underline{\underline{\mu}}_d^{(k)} : \underline{\underline{\mu}}_d^{(k)}} \right\rangle = 1, \qquad \left\langle \left(\mu_m^{(k)} \right)^2 \right\rangle = 1 \tag{4.13}$$

To better understand the decomposition of plastic strain field, some fundamental concepts of functional analysis can be cited here (Rynne & Youngson, 2008; Lebedev & Vorovich, 2003).

Denote $\boldsymbol{H}$ being the set of all admissible plastic strain field $\underline{\underline{\varepsilon}}^p(\underline{x})$ in RVE, which can be regarded as a tensor field space (or six-dimensional vector field space) defined on $\boldsymbol{R}$. $\forall \underline{\underline{\varepsilon}}_1^p(\underline{x}),\ \underline{\underline{\varepsilon}}_2^p(\underline{x}) \in \boldsymbol{H}$, define the inner product $\langle \bullet, \bullet \rangle_{inner}$ as:

$$\left\langle \underline{\underline{\varepsilon}}_1^p(\underline{x}),\ \underline{\underline{\varepsilon}}_2^p(\underline{x}) \right\rangle_{inner} = \frac{1}{|V|} \int_V \underline{\underline{\varepsilon}}_1^p(\underline{x}) : \underline{\underline{\varepsilon}}_2^p(\underline{x})\, dV = \left\langle \underline{\underline{\varepsilon}}_1^p(\underline{x}),\ \underline{\underline{\varepsilon}}_2^p(\underline{x}) \right\rangle \tag{4.14}$$

That is, the result of volumetric average calculation can be treated as the defined inner product. It is obviously that the inner product Eq. (4.14) satisfies the "inner product axiom". Thus $\boldsymbol{H}$ is an inner product space defined on $\boldsymbol{R}$. The plastic modes, $\underline{\underline{\mu}}_d^{(k)}(\underline{x})$ $(k = 1...N_d)$, and $\mu_m^{(k)}(\underline{x})\underline{\underline{\delta}}$ $(k = 1...N_m)$ form an orthonormal basis of the plastic strain field space. Any admissible plastic strain field in the RVE can be expressed as a linear combination of the plastic modes. Then the advantage of orthonormal basis can be inherited by the plastic modes in the present study. Plastic modes can be determined either analytically or numerically. The computing method will be studied in detail in the following section.

4.2.2 Microscopic strain in elastoplastic homogenization problems

In elastic homogenization problem, the microscopic local strain tensor depends linearly on the macroscopic strain tensor, that is:

$$\underline{\underline{\varepsilon}}(\underline{x}) = \mathbb{A}(\underline{x}) : \underline{\underline{E}} \tag{4.15}$$

[1] The condition $\left\langle \underline{\underline{\mu}}_d^{(k)} : \left(\mu_m^{(l)} \underline{\underline{\delta}} \right) \right\rangle = 0$ can be satisfied automatically.

Where $\mathbb{A}(\underline{x})$ is the fourth order elastic strain localization tensor, which depends only on the properties and spatial distribution of constituents, but remains constant during all the loading history. The strain localization tensor, $\mathbb{A}(\underline{x})$, can be calculated numerically as a general method (Suquet, 1987), or obtained analytically in some specific problem, e.g. the Eshelby's problem (Eshelby, 1957). However, Eq. (4.15) is no longer valid in dealing with non linear homogenization of elastoplastic heterogeneous materials, because the influence of plastic strain field must be considered. Michel and Suquet (2003) proposed a theoretical solution by means of the non local elastic fourth order Green operator $\mathbb{G}(\underline{x},\underline{x}')$ of the heterogeneous elastic medium as:

$$\underline{\underline{\varepsilon}}(\underline{x}) = \mathbb{A}(\underline{x}) : \underline{\underline{E}} + \frac{1}{|V|}\int_V \mathbb{G}(\underline{x},\underline{x}') : \left(\mathbb{C}(\underline{x}') : \underline{\underline{\varepsilon}}^p(\underline{x}')\right) dV' \tag{4.16}$$

where $\mathbb{G}(\underline{x},\underline{x}')$ means the microscopic strain induced at the point $\underline{x}$ by a unit local stress at the point $\underline{x}'$. It is seen that the microscopic local strain in elastoplastic homogenization problem is composed of two parts that are induced by macroscopic strain and local plastic strain fields, respectively. In the elastic problem $\underline{\underline{\varepsilon}}^p(\underline{x}) = 0$, Eq. (4.16) reduces then to Eq. (4.15).

Introduce now a non local fourth order tensor $\mathbb{D}(\underline{x},\underline{x}') = \mathbb{G}(\underline{x},\underline{x}') : \mathbb{C}(\underline{x}')$ which represents the microscopic strain at the point $\underline{x}$ induced by the plastic strain at the point $\underline{x}'$ and for the sake of simplicity define a product operator '*' as follows:

$$\left(\mathbb{D} * \underline{\underline{\varepsilon}}^p\right)(\underline{x}) = \frac{1}{|V|}\int_V \mathbb{D}(\underline{x},\underline{x}') : \underline{\underline{\varepsilon}}^p(\underline{x}') dV' \tag{4.17}$$

Then the microscopic strain is formulated as:

$$\underline{\underline{\varepsilon}}(\underline{x}) = \mathbb{A}(\underline{x}) : \underline{\underline{E}} + \left(\mathbb{D} * \underline{\underline{\varepsilon}}^p\right)(\underline{x}) \tag{4.18}$$

Substituting the basic assumption of NTFA Eq. (4.11) into Eq.(4.18), the non-localized microscopic strain is obtained in terms of plastic modes:

$$\underline{\underline{\varepsilon}}(\underline{x}) = \mathbb{A}(\underline{x}) : \underline{\underline{E}} + \sum_{k=1}^{N_d}\left(\mathbb{D} * \underline{\underline{\mu}}_d^{(k)}\right)(\underline{x})\varepsilon_{k\_d}^p + \sum_{k=1}^{N_m}\left(\mathbb{D} * \left(\mu_m^{(k)}\underline{\underline{\delta}}\right)\right)(\underline{x})\varepsilon_{k\_m}^p \tag{4.19}$$

For the effective implementation of the NTFA method, a series of reduced variables should be defined in order to replace the conventional variables. Accordingly, the local constitutive model

should also be reformulated in terms of such reduced variables.

4.2.3 Reduced variables

The 'Reduced variables' means a series of macroscopic scale variables obtained by multiplying all the conventional microscopic variables (tensors), such as strain, stress, etc, by plastic modes $\underline{\underline{\mu}}_{d}^{(k)}(\underline{x})$ $(k=1...N_d)$ and $\mu_m^{(k)}(\underline{x})\underline{\underline{\delta}}$ $(k=1...N_m)$, and then performing the volumetric averaging process.

1). Reduced strain

$$e_{k\_d}=\left\langle \underline{\underline{\varepsilon}}(\underline{x}):\underline{\underline{\mu}}_{d}^{(k)}(\underline{x})\right\rangle,\quad e_{k\_m}=\left\langle \underline{\underline{\varepsilon}}(\underline{x}):\left(\mu_m^{(k)}(\underline{x})\underline{\underline{\delta}}\right)\right\rangle \tag{4.20}$$

2). Reduced plastic strain

$$e_{k\_d}^{p}=\left\langle \underline{\underline{\varepsilon}}^{p}(\underline{x}):\underline{\underline{\mu}}_{d}^{(k)}(\underline{x})\right\rangle,\quad e_{k\_m}^{p}=\left\langle \underline{\underline{\varepsilon}}^{p}(\underline{x}):\left(\mu_m^{(k)}(\underline{x})\underline{\underline{\delta}}\right)\right\rangle \tag{4.21}$$

3). Reduced stress

$$\tau_{k\_d}=\left\langle \underline{\underline{\sigma}}(\underline{x}):\underline{\underline{\mu}}_{d}^{(k)}(\underline{x})\right\rangle,\quad \tau_{k\_m}=\left\langle \underline{\underline{\sigma}}(\underline{x}):\left(\mu_m^{(k)}(\underline{x})\underline{\underline{\delta}}\right)\right\rangle \tag{4.22}$$

4). Reduced elastic localization tensor

$$\underline{\underline{a}}_{d}^{(k)}=\left\langle \underline{\underline{\mu}}_{d}^{(k)}(\underline{x}):\mathbb{A}(\underline{x})\right\rangle,\quad \underline{\underline{a}}_{m}^{(k)}=\left\langle \left(\mu_m^{(k)}(\underline{x})\underline{\underline{\delta}}\right):\mathbb{A}(\underline{x})\right\rangle \tag{4.23}$$

5). Reduced $\underline{\mathbb{D}}$ tensor

$$\begin{aligned}
D_{kl_dd}&=\left\langle \underline{\underline{\mu}}_{d}^{(k)}(\underline{x}):\left(\mathbb{D}*\underline{\underline{\mu}}_{d}^{(l)}\right)(\underline{x})\right\rangle\\
D_{kl_md}&=\left\langle \left(\mu_m^{(k)}(\underline{x})\underline{\underline{\delta}}\right):\left(\mathbb{D}*\underline{\underline{\mu}}_{d}^{(l)}\right)(\underline{x})\right\rangle\\
D_{kl_dm}&=\left\langle \underline{\underline{\mu}}_{d}^{(k)}(\underline{x}):\left(\mathbb{D}*\left(\mu_m^{(l)}\underline{\underline{\delta}}\right)\right)(\underline{x})\right\rangle\\
D_{kl_mm}&=\left\langle \left(\mu_m^{(k)}(\underline{x})\underline{\underline{\delta}}\right):\left(\mathbb{D}*\left(\mu_m^{(l)}\underline{\underline{\delta}}\right)\right)(\underline{x})\right\rangle
\end{aligned} \tag{4.24}$$

Combine Eq. (4.19) with Eq. (4.20), the following expressions can be obtained:

$$\begin{aligned} e_{k\_d} &= \left\langle \underline{\underline{\varepsilon}}(\underline{x}) : \underline{\underline{\mu}}_d^{(k)}(\underline{x}) \right\rangle \\ &= \left\langle \underline{\underline{\mu}}_d^{(k)}(\underline{x}) : \mathbb{A}(\underline{x}) \right\rangle : \underline{\underline{E}} + \sum_{l=1}^{N_d} \left\langle \underline{\underline{\mu}}_d^{(k)}(\underline{x}) : \left(\mathbb{D} * \underline{\underline{\mu}}_d^{(l)} \right)(\underline{x}) \right\rangle \varepsilon_{l\_d}^{p} \\ &\quad + \sum_{l=1}^{N_m} \left\langle \underline{\underline{\mu}}_d^{(k)}(\underline{x}) : \left(\mathbb{D} * \left(\mu_m^{(l)} \underline{\underline{\delta}} \right) \right)(\underline{x}) \right\rangle \varepsilon_{l\_m}^{p} \end{aligned} \tag{4.25}$$

$$\begin{aligned} e_{k\_m} &= \left\langle \underline{\underline{\varepsilon}}(\underline{x}) : \left(\mu_m^{(k)}(\underline{x}) \underline{\underline{\delta}} \right) \right\rangle \\ &= \left\langle \left(\mu_m^{(k)}(\underline{x}) \underline{\underline{\delta}} \right) : \mathbb{A}(\underline{x}) \right\rangle : \underline{\underline{E}} + \sum_{l=1}^{N_d} \left\langle \left(\mu_m^{(k)}(\underline{x}) \underline{\underline{\delta}} \right) : \left(\mathbb{D} * \underline{\underline{\mu}}_d^{(l)} \right)(\underline{x}) \right\rangle \varepsilon_{l\_d}^{p} \\ &\quad + \sum_{l=1}^{N_m} \left\langle \left(\mu_m^{(k)}(\underline{x}) \underline{\underline{\delta}} \right) : \left(\mathbb{D} * \left(\mu_m^{(l)} \underline{\underline{\delta}} \right) \right)(\underline{x}) \right\rangle \varepsilon_{l\_m}^{p} \end{aligned} \tag{4.26}$$

Combine Eq. (4.24) with Eq. (4.26), the reduced non-localized strain can be derived in terms of three macroscopic variables $\underline{\underline{E}}$, $\varepsilon_{k\_d}^{p}$ and $\varepsilon_{k\_m}^{p}$:

$$\begin{cases} e_{k\_d} = \underline{\underline{a}}_d^{(k)} : \underline{\underline{E}} + \sum_{l=1}^{N_d} D_{kl\_dd} \varepsilon_{l\_d}^{p} + \sum_{l=1}^{N_m} D_{kl\_dm} \varepsilon_{l\_m}^{p} \\ e_{k\_m} = \underline{\underline{a}}_m^{(k)} : \underline{\underline{E}} + \sum_{l=1}^{N_d} D_{kl\_md} \varepsilon_{l\_d}^{p} + \sum_{l=1}^{N_m} D_{kl\_mm} \varepsilon_{l\_m}^{p} \end{cases} \tag{4.27}$$

4.2.4 Constitutive model in terms of reduced variables

As stated above, the reduced scalar variables are endowed with macroscopic mechanical meaning by performing the tensor product with plastic modes and volumetric average process. Accordingly, the local constitutive model should be rewritten in terms of the reduced variables in NTFA scheme.

The local stress-strain relation for elastoplastic material is formulated as Eq. (4.5). Substitute Eq. (4.5) into Eq. (4.22), the reduced stress can be expressed as:

$$\begin{aligned}\tau_{k\_d} &= \left\langle \underline{\underline{\mu}}_d^{(k)}(\underline{x}) : \mathbb{C}(\underline{x}) : (\underline{\underline{\varepsilon}}(\underline{x}) - \underline{\underline{\varepsilon}}^p(\underline{x})) \right\rangle \qquad (k = 1...M_d) \\ \tau_{k\_m} &= \left\langle \left(\mu_m^{(k)}(\underline{x})\underline{\underline{\delta}}\right) : \mathbb{C}(\underline{x}) : (\underline{\underline{\varepsilon}}(\underline{x}) - \underline{\underline{\varepsilon}}^p(\underline{x})) \right\rangle \quad (k = 1...M_m)\end{aligned} \tag{4.28}$$

Take account of the basic NTFA assumption that each plastic mode $\underline{\underline{\mu}}_d^{(k)}(\underline{x})$ or $\left(\mu_m^{(k)}(\underline{x})\underline{\underline{\delta}}\right)$ exists in only one material phase ($r(k)$), therefore $\mathbb{C}(\underline{x})$ keeps a constant $\mathbb{C}^{(r(k))}$ in Eq.(4.28) for every definite k. $\mathbb{C}^{(r(k))}$ is the fourth order elastic stiffness tensor of the material phase $r(k)$ where the plastic mode k exist. Only isotropic material is considered in this study for simplicity; then $\mathbb{C}^{(r(k))}$ is characterized by two parameters, the bulk modulus $k^{(r(k))}$ and shear modulus $G^{(r(k))}$:

$$\mathbb{C}^{(r(k))} = 3k^{(r(k))}\mathbb{J} + 2G^{(r(k))}\mathbb{K} \tag{4.29}$$

where k and G are defined in Eq. (4.4). According to the basic NTFA assumptions, the plastic mode $\underline{\underline{\mu}}_d^{(k)}(\underline{x})$ are purely deviatoric, and $\left(\mu_m^{(k)}(\underline{x})\underline{\underline{\delta}}\right)$ are purely volumetric, so:

$$\begin{aligned}\mathbb{C}^{(r(k))} : \underline{\underline{\mu}}_d^{(k)}(\underline{x}) &= 2G^{(r(k))}\underline{\underline{\mu}}_d^{(k)}(\underline{x}) \\ \mathbb{C}^{(r(k))} : \left(\mu_m^{(k)}(\underline{x})\underline{\underline{\delta}}\right) &= 3k^{(r(k))}\left(\mu_m^{(k)}(\underline{x})\underline{\underline{\delta}}\right)\end{aligned} \tag{4.30}$$

As a result, the reduced stress-strain relation is formulated as:

$$\begin{aligned}\tau_{k\_d} &= 2G^{(r(k))}(e_{k\_d} - e^p_{k\_d}) \\ \tau_{k\_m} &= 3k^{(r(k))}(e_{k\_m} - e^p_{k\_m})\end{aligned} \tag{4.31}$$

We will now reformulate the D-P criterion in terms of reduced variables. According to Eq. (4.7) and (4.10), the local D-P yield criterion and flow rules at every microscopic point are:

$$\begin{aligned}f_p(\underline{x}) &= \alpha\sigma_m(\underline{x}) + \sigma_{eq}(\underline{x}) - R(\gamma(\underline{x})) = 0 \\ \dot{\underline{\underline{\varepsilon}}}^p(\underline{x}) &= \dot{\gamma}(\underline{x})\left(\frac{1}{3}\psi\underline{\underline{\delta}} + \frac{3}{2}\frac{\underline{\underline{s}}(\underline{x})}{\sigma_{eq}(\underline{x})}\right)\end{aligned} \tag{4.32}$$

Combined with Eq.(4.21), the reduced form of plastic strain rate can be expressed as:

$$\dot{e}^p_{k\_d} = \left\langle \frac{3}{2}\dot{\gamma}(\underline{x})\frac{\underline{\underline{\mu}}_d^{(k)}(\underline{x}) : \underline{\underline{s}}(\underline{x})}{\sigma_{eq}(\underline{x})} \right\rangle \tag{4.33}$$

$$\dot{e}^{p}_{k\_m} = \left\langle \frac{1}{3}\psi\dot{\gamma}(\underline{x})\underline{\underline{\delta}} : \left(\mu^{(k)}_{m}(\underline{x})\underline{\underline{\delta}}\right)\right\rangle = \left\langle \psi\dot{\gamma}(\underline{x}) : \mu^{(k)}_{m}(\underline{x})\right\rangle \tag{4.34}$$

Michel and Suquet (2003; 2004) studied the reduced Mises yield criterion and the corresponding flow rule in two different ways: uncoupled model and coupled model. The latter owns more advantages both in theory and in numerical accuracy. Therefore, a coupled model for D-P yield criterion and flow rule will be established in this study to predict the overall properties of elastoplastic composite or porous material. The main assumptions of coupled model rely on such intuitive mechanical concept that the k^{th} reduced stress not only controls the evolution of plastic strain on the k^{th} plastic mode, but also influences the evolution of plastic strain on the l^{th} plastic mode. All the plastic modes existing in the same material phase should be coupled. Consequently, the following simplifications have to be made:

(A). $\gamma(\underline{x})$ is independent of geometric position in every phase (r), i.e., $\gamma(\underline{x})$ can be replaced by $\gamma^{(r)}$.

(B). $\sigma_{eq}(\underline{x})$ is replaced by:

$$\bar{\sigma}^{(r)}_{eq} = \left(\frac{3}{2}\sum_{k=1}^{N_d(r)}(\tau_{k\_d})^2\right)^{\frac{1}{2}} \tag{4.35}$$

(C). $\sigma_{m}(\underline{x})$ is replaced by:

$$\bar{\sigma}^{(r)}_{m} = \frac{1}{3}\sum_{k=1}^{N_m(r)}\tau_{k\_m} \tag{4.36}$$

The simplification (A) implies that the local interne variable $\gamma(\underline{x})$ is the same value $\gamma^{(r)}$ in every material phase. The simplification (B) and (C) means that all the reduced stresses ($N_d(r)$ or $N_m(r)$) existing in the same material phase (r) are combined to form a resultant force that controls the evolution of plastic strain on all the plastic modes contained in the certain material phase (r). The reduced D-P yield criterion and flow rule can be then expressed under these simplifications as:

$$f^{(r)}_{p} = \alpha\bar{\sigma}^{(r)}_{m} + \bar{\sigma}^{(r)}_{eq} - R(\gamma^{(r)}) = 0 \tag{4.37}$$

$$\begin{cases} \dot{e}^{p}_{k\_d} = \dfrac{3}{2}\dot{\gamma}^{(r(k))}\dfrac{\tau_{k\_d}}{\bar{\sigma}^{(r)}_{eq}} \\ \dot{e}^{p}_{k\_m} = \psi\dot{\gamma}^{(r(k))}\left\langle \mu^{(k)}_{m}(\underline{x})\right\rangle \end{cases} \tag{4.38}$$

Eq. (4.37) provides the reduced form of the D-P yield criterion of every material phase (r) to estimate whether the evolution of reduced plastic strains contained in this material phase takes place. If yes, the evolution rates of reduced plastic strains are obtained according to Eq. (4.38). Combined Eq. (4.27), (4.38) and (4.31) together, the complete constitutive relations in terms of reduced variables are set up for D-P material.

4.2.5 Macroscopic stress and plastic strain

After the internal variables are determined, the macroscopic stresses and plastic strains can be then obtained as the final results of homogenized problem with uniform strain boundary condition:

Substitute Eq.(4.11) and (4.19) into Eq.(4.5), we obtain:

$$\begin{aligned} \underline{\underline{\sigma}}(\underline{x}) = &\left(\mathbb{C}(\underline{x}) : \mathbb{A}(\underline{x})\right) : \underline{\underline{E}} \\ &+\mathbb{C}(\underline{x})\left[\begin{array}{l} \left(\sum_{k=1}^{N_d}\varepsilon^{p}_{k\_d}\left(\mathbb{D} * \underline{\underline{\mu}}^{(k)}_{d}\right)(\underline{x}) + \sum_{k=1}^{N_m}\varepsilon^{p}_{k\_m}\left(\mathbb{D} * \left(\mu^{(k)}_{m}\underline{\underline{\delta}}\right)\right)(\underline{x})\right) \\ -\left(\sum_{k=1}^{N_d}\varepsilon^{p}_{k\_d}\underline{\underline{\mu}}^{(k)}_{d}(\underline{x}) + \sum_{k=1}^{N_m}\varepsilon^{p}_{k\_m}\left(\mu^{(k)}_{m}(\underline{x})\underline{\underline{\delta}}\right)\right) \end{array}\right] \end{aligned} \tag{4.39}$$

Define $\underline{\underline{\rho}}^{(k)}_{d}(\underline{x})$, $\underline{\underline{\rho}}^{(k)}_{m}(\underline{x})$ and $\mathbb{C}^{elas-\hom}$ as:

$$\begin{aligned} &\underline{\underline{\rho}}^{(k)}_{d}(\underline{x}) = \mathbb{C}(\underline{x}) : \left(\mathbb{D} * \underline{\underline{\mu}}^{(k)}_{d}\right)(\underline{x}) - \mathbb{C}(\underline{x}) : \underline{\underline{\mu}}^{(k)}_{d}(\underline{x}) \\ &\underline{\underline{\rho}}^{(k)}_{m}(\underline{x}) = \mathbb{C}(\underline{x}) : \left(\mathbb{D} * \left(\mu^{(k)}_{m}\underline{\underline{\delta}}\right)\right)(\underline{x}) - \mathbb{C}(\underline{x}) : \left(\mu^{(k)}_{m}\underline{\underline{\delta}}\right)(\underline{x}) \\ &\mathbb{C}^{elas-\hom} = \left\langle \mathbb{C}(\underline{x}) : \mathbb{A}(\underline{x})\right\rangle \end{aligned} \tag{4.40}$$

Then substituting Eq. (4.11) into Eq. (4.21):

$$
\begin{aligned}
e^p_{k\_d} &= \sum_{l=1}^{N_d} \varepsilon^p_{l\_d} \left\langle \underline{\underline{\mu}}^{(l)}_d(\underline{x}) : \underline{\underline{\mu}}^{(k)}_d(\underline{x}) \right\rangle \\
e^p_{k\_m} &= \sum_{l=1}^{N_m} \varepsilon^p_{l\_m} \left\langle \left(\mu^{(l)}_m(\underline{x})\underline{\underline{\delta}}\right) : \left(\mu^{(k)}_m(\underline{x})\underline{\underline{\delta}}\right) \right\rangle
\end{aligned}
\tag{4.41}
$$

Take account of the fact that $\left\langle \underline{\underline{\mu}}^{(k)}_d : \underline{\underline{\mu}}^{(l)}_d \right\rangle = 0$, $\left\langle \left(\mu^{(k)}_m \underline{\underline{\delta}}\right) : \left(\mu^{(l)}_m \underline{\underline{\delta}}\right) \right\rangle = 0$ (if $k \neq l$) (Eq.(4.12)), one obtains:

$$
\begin{cases}
\varepsilon^p_{k\_d} = \dfrac{e^p_{k\_d}}{\left\langle \underline{\underline{\mu}}^{(k)}_d(\underline{x}) : \underline{\underline{\mu}}^{(k)}_d(\underline{x}) \right\rangle} \\
\varepsilon^p_{k\_m} = \dfrac{\varepsilon^p_{k\_m}}{\left\langle \left(\mu^{(k)}_m(\underline{x})\underline{\underline{\delta}}\right) : \left(\mu^{(k)}_m(\underline{x})\underline{\underline{\delta}}\right) \right\rangle}
\end{cases}
\tag{4.42}
$$

Note that there is no summation with index k in Eq. (4.42). Finally, the macroscopic stress is derived as:

$$
\underline{\underline{\Sigma}} = \left\langle \underline{\underline{\sigma}}(\underline{x}) \right\rangle = \mathbb{C}^{\text{elas-hom}} : \underline{\underline{E}} + \sum_{k=1}^{N_d} \left\langle \underline{\underline{\rho}}^{(k)}_d(\underline{x}) \right\rangle \varepsilon^p_{k\_d} + \sum_{k=1}^{N_m} \left\langle \underline{\underline{\rho}}^{(k)}_m(\underline{x}) \right\rangle \varepsilon^p_{k\_m}
\tag{4.43}
$$

Left multiply each side of Eq. (4.43) by $\left(\mathbb{C}^{\text{elas-hom}}\right)^{-1}$, the following relations are deduced:

$$
\begin{aligned}
\underline{\underline{E}} - \underline{\underline{E}}^p = \underline{\underline{E}} &+ \left(\mathbb{C}^{\text{elas-hom}}\right)^{-1} : \sum_{k=1}^{N_d} \left\langle \underline{\underline{\rho}}^{(k)}_d(\underline{x}) \right\rangle \varepsilon^p_{k\_d} \\
&+ \left(\mathbb{C}^{\text{elas-hom}}\right)^{-1} : \sum_{k=1}^{N_m} \left\langle \underline{\underline{\rho}}^{(k)}_m(\underline{x}) \right\rangle \varepsilon^p_{k\_m}
\end{aligned}
\tag{4.44}
$$

Thus, the macroscopic plastic strain is obtained as:

$$
\underline{\underline{E}}^p = -\left(\mathbb{C}^{\text{elas-hom}}\right)^{-1} : \sum_{k=1}^{N_d} \left\langle \underline{\underline{\rho}}^{(k)}_d(\underline{x}) \right\rangle \varepsilon^p_{k\_d} - \left(\mathbb{C}^{\text{elas-hom}}\right)^{-1} : \sum_{k=1}^{N_m} \left\langle \underline{\underline{\rho}}^{(k)}_m(\underline{x}) \right\rangle \varepsilon^p_{k\_m}
\tag{4.45}
$$

4.3 Numerical implementation of NTFA

The numerical implementation of the NTFA is generally performed in two steps. Firstly, some preliminary computations are required to obtain the necessary static data, plastic modes, reduced elastic localization tensor, effective fourth order stiffness tensor, $\left\langle \underline{\underline{\rho}}_{d}^{(k)} \right\rangle$, $\left\langle \underline{\underline{\rho}}_{m}^{(k)} \right\rangle$ tensor in Eq. (4.43) and reduced $\mathbb{D}$ tensor. All these quantities are calculated once for all and used in all the loading process. However, for strongly non linear heterogeneous materials, these quantities inherently depend on plastic strain level. In such case, some updating computations may be necessary for different levels of applied loading. In the second stage, the local integration is performed to find the updated macroscopic stress tensor corresponding to a macroscopic strain increment via the reduced constitutive model discussed above.

4.3.1 Preliminary computations for plastic mode determination

The accuracy of the NTFA method is directly related to the choice of plastic modes. Such modes are determined from the estimations of local plastic strain fields. Generally, the analytical determination of plastic modes is very difficult; suitable numerical computations are then necessary. Various techniques can be used such as FFT method and FEM method. In this work, the plastic modes will be chosen from FEM simulations and using proper orthogonal decomposition (POD) technique.

For pressure sensitive materials, the plastic strain field is decomposed into the linear combination of two sets of plastic modes $\underline{\underline{\mu}}_{d}^{(k)}(\underline{x})\,(k=1...N_d)$ and $\mu_m^{(k)}\underline{\underline{\delta}}(\underline{x})\,(k=1...N_m)$. As mentioned above, two steps are needed to determine the plastic modes. Firstly, a set of numerical analyses are performed to determine the elastoplastic responses of RVE along representative loading paths in the macroscopic stress space. In this study, the 3D FEM analysis is performed to determine the responses of the REV along 6 typical macroscopic stress loading conditions composed of uniaxial tensile test in three directions, and three pure tests, as defined as.

$$\begin{aligned}
&\underline{\underline{\Sigma}}^{(1)} = \underline{e}_1 \otimes \underline{e}_1, \quad && \underline{\underline{\Sigma}}^{(4)} = \frac{1}{2}\left(\underline{e}_1 \otimes \underline{e}_2 + \underline{e}_2 \otimes \underline{e}_1\right) \\
&\underline{\underline{\Sigma}}^{(2)} = \underline{e}_2 \otimes \underline{e}_2, \quad && \underline{\underline{\Sigma}}^{(5)} = \frac{1}{2}\left(\underline{e}_1 \otimes \underline{e}_3 + \underline{e}_3 \otimes \underline{e}_1\right) \\
&\underline{\underline{\Sigma}}^{(3)} = \underline{e}_3 \otimes \underline{e}_3, \quad && \underline{\underline{\Sigma}}^{(6)} = \frac{1}{2}\left(\underline{e}_2 \otimes \underline{e}_3 + \underline{e}_3 \otimes \underline{e}_2\right)
\end{aligned} \tag{4.46}$$

The simulated microscopic plastic strain field $\underline{\underline{\theta}}^{(k)}(\underline{x})$ $(k=1...6)$ are analyzed when the macroscopic strain reaches a relative high value to ensure a full developed plastic strain field.

Then decompose each $\underline{\underline{\theta}}^{(k)}(\underline{x})$ into deviatoric part $\underline{\underline{\theta}}_d^{(k)}(\underline{x})$ and volumetric part $\theta_m^{(k)}\delta(\underline{x})$:

$$\underline{\underline{\theta}}^{(k)}(\underline{x}) = \underline{\underline{\theta}}_d^{(k)}(\underline{x}) + \theta_m^{(k)}(\underline{x})\underline{\underline{\delta}} \tag{4.47}$$

In the second step, an orthonormalization procedure should be realized on the sets of $\underline{\underline{\theta}}_d^{(k)}(\underline{x})$ and $\theta_m^{(k)}\delta(\underline{x})$ to generate the plastic modes $\underline{\underline{\mu}}_d^{(k)}(\underline{x})$ $(k=1...N_d)$ and $\mu_m^{(k)}(\underline{x})\underline{\underline{\delta}}$ $(k=1...N_m)$, which satisfy the condition Eq.(4.12) and (4.13), respectively. The most commonly used method, Gram–Schmidt orthogonalization method, is briefly introduced as follows:

$$\underline{\underline{\beta}}_d^{(1)}(\underline{x}) = \underline{\underline{\theta}}_d^{(1)}(\underline{x}), \quad \hat{\underline{\underline{\mu}}}_d^{(1)}(\underline{x}) = \frac{\underline{\underline{\beta}}_d^{(1)}(\underline{x})}{\sqrt{\left\langle \underline{\underline{\beta}}_d^{(1)}(\underline{x}) : \underline{\underline{\beta}}_d^{(1)}(\underline{x}) \right\rangle}} \tag{4.48}$$

$$\begin{aligned} \underline{\underline{\beta}}_d^{(n)}(\underline{x}) &= \underline{\underline{\theta}}_d^{(n)}(\underline{x}) - \sum_i^{n-1} \left\langle \underline{\underline{\theta}}_d^{(n)}(\underline{x}) : \hat{\underline{\underline{\mu}}}_d^{(i)}(\underline{x}) \right\rangle \hat{\underline{\underline{\mu}}}_d^{(i)}(\underline{x}) \\ \hat{\underline{\underline{\mu}}}_d^{(n)}(\underline{x}) &= \frac{\underline{\underline{\beta}}_d^{(n)}(\underline{x})}{\sqrt{\left\langle \underline{\underline{\beta}}_d^{(n)}(\underline{x}) : \underline{\underline{\beta}}_d^{(n)}(\underline{x}) \right\rangle}} \end{aligned} \tag{4.49}$$

Two sequences, $\hat{\underline{\underline{\mu}}}_d^{(k)}(\underline{x})$ $(k=1...N_d)$ and $\hat{\mu}_m^{(k)}(\underline{x})\underline{\underline{\delta}}$ $(k=1...N_m)$[2], respectively obtained by Eq. (4.48) and (4.49), can meet the orthogonal condition Eq. (4.12). However, they are not satisfied by the normalized condition Eq. (4.13). So a normalization process must be implemented to get the final plastic modes:

$$\underline{\underline{\mu}}_d^{(k)}(\underline{x}) = \frac{\hat{\underline{\underline{\mu}}}_d^{(k)}(\underline{x})}{\left\langle \sqrt{\hat{\underline{\underline{\mu}}}_d^{(k)}(\underline{x}) : \hat{\underline{\underline{\mu}}}_d^{(k)}(\underline{x})} \right\rangle}, \quad \mu_m^{(k)}(\underline{x})\underline{\underline{\delta}} = \frac{\hat{\mu}_m^{(k)}(\underline{x})}{\sqrt{\left\langle \left(\hat{\mu}_m^{(k)}(\underline{x}) \right)^2 \right\rangle}}\underline{\underline{\delta}} \tag{4.50}$$

4.3.2 Determination of reduced localization tensor and effective stiffness tensor

In general three-dimensional elastic homogenization problem, the fourth order strain localization tensor is usually obtained by solving such 6 linear elastic problems with uniform

[2] $\hat{\mu}_m^{(k)}(\underline{x})\underline{\underline{\delta}}$ $(k=1...M_m)$ can be obtained only by changing $\underline{\underline{\theta}}_d^{(i)}(\underline{x})$, $\underline{\underline{\beta}}_d^{(i)}(\underline{x})$ with $\theta_d^{(i)}(\underline{x})\underline{\underline{\delta}}$, $\beta_d^{(i)}(\underline{x})\underline{\underline{\delta}}$

strain boundary conditions:

$$\begin{aligned} &div(\underline{\underline{\sigma}}(\underline{x})) = 0 \\ &\underline{\underline{\sigma}}(\underline{x}) = \mathbb{C}(\underline{x}) : \underline{\underline{\varepsilon}}(\underline{x}) \\ &\left\langle \underline{\underline{\varepsilon}}(\underline{x}) \right\rangle = \underline{\underline{E}} \end{aligned} \tag{4.51}$$

with $\underline{\underline{E}} = \underline{\underline{i}}^{(11)}, \underline{\underline{i}}^{(22)}, \underline{\underline{i}}^{(33)}, \underline{\underline{i}}^{(12)}, \underline{\underline{i}}^{(13)}, \underline{\underline{i}}^{(23)}$, respectively, where:

$$i_{kl}^{(ij)} = \frac{1}{2}(\delta_{ik}\delta_{jl} + \delta_{il}\delta_{jk}) \tag{4.52}$$

$$\begin{aligned} &\underline{\underline{i}}^{(11)} = \begin{pmatrix} 1 & 0 & 0 \\ 0 & 0 & 0 \\ 0 & 0 & 0 \end{pmatrix}, \quad \underline{\underline{i}}^{(22)} = \begin{pmatrix} 0 & 0 & 0 \\ 0 & 1 & 0 \\ 0 & 0 & 0 \end{pmatrix}, \quad \underline{\underline{i}}^{(33)} = \begin{pmatrix} 0 & 0 & 0 \\ 0 & 0 & 0 \\ 0 & 0 & 1 \end{pmatrix} \\ &\underline{\underline{i}}^{(12)} = \begin{pmatrix} 0 & 1/2 & 0 \\ 1/2 & 0 & 0 \\ 0 & 0 & 0 \end{pmatrix}, \ \underline{\underline{i}}^{(13)} = \begin{pmatrix} 0 & 0 & 1/2 \\ 0 & 0 & 0 \\ 1/2 & 0 & 0 \end{pmatrix}, \ \underline{\underline{i}}^{(23)} = \begin{pmatrix} 0 & 0 & 0 \\ 0 & 0 & 1/2 \\ 0 & 1/2 & 0 \end{pmatrix} \end{aligned} \tag{4.53}$$

Let $\varepsilon_{ij}^{kl}(\underline{x})$ and $\sigma_{ij}^{kl}(\underline{x})$ denote the strain and stress solutions of Eq.(4.51) with $\underline{\underline{E}} = \underline{\underline{i}}^{(kl)}$, then the strain localization tensor, reduced strain localization tensor, and effective stiffness tensor can be obtained by:

$$A_{ijkl}(\underline{x}) = \varepsilon_{ij}^{(kl)}(\underline{x}) \tag{4.54}$$

$$a_d^{(k)}{}_{ij} = \left\langle \underline{\underline{\mu}}_{d}^{(k)}(\underline{x}) : \underline{\underline{\varepsilon}}^{(ij)}(\underline{x}) \right\rangle, \quad a_m^{(k)}{}_{ij} = \left\langle \left(\mu_m^{(k)}(\underline{x})\underline{\underline{\delta}} \right) : \underline{\underline{\varepsilon}}^{(ij)}(\underline{x}) \right\rangle \tag{4.55}$$

$$C_{ijkl}^{\text{elas-hom}} = \left\langle C_{ijmn}(\underline{x}) : A_{mnkl}(\underline{x}) \right\rangle = \left\langle \sigma_{kj}^{(kl)}(\underline{x}) \right\rangle \tag{4.56}$$

4.3.3 Determination of reduced influence tensor $\mathbb{D}$ and $\left\langle \underline{\underline{\rho}}_{d}^{(k)} \right\rangle$, $\left\langle \underline{\underline{\rho}}_{m}^{(k)} \right\rangle$ tensor

It can be seen from Eq.(4.18) that the operator $(\mathbb{D}*())(\underline{x})$ means the strain field induced by the appointed transformation plastic strain field with null averaged macroscopic strain field $\underline{\underline{E}} = \underline{\underline{0}}$. So the following linear elastic problem needs to be solved:

$$
\begin{aligned}
&div(\underline{\underline{\sigma}}(\underline{x})) = 0 \\
&\underline{\underline{\sigma}}(\underline{x}) = \mathbb{C}(\underline{x}) : \left(\underline{\underline{\varepsilon}}(\underline{x}) - \underline{\underline{\mu}}_d^{(k)}(\underline{x}) \right) \\
&\qquad or \qquad \underline{\underline{\sigma}}(\underline{x}) = \mathbb{C}(\underline{x}) : \left(\underline{\underline{\varepsilon}}(\underline{x}) - \mu_m^{(k)}(\underline{x}) \underline{\underline{\delta}} \right) \\
&\underline{\underline{E}} = \left\langle \underline{\underline{\varepsilon}}(\underline{x}) \right\rangle = \underline{\underline{0}}
\end{aligned}
\tag{4.57}
$$

The result of strain field $\underline{\underline{\varepsilon}}(\underline{x})$ obtained from this problem is $\left(\mathbb{D} * \underline{\underline{\mu}}_d^{(k)} \right)(\underline{x})$ or $\left(\mathbb{D} * \left(\mu_m^{(k)} \underline{\underline{\delta}} \right) \right)(\underline{x})$, and the stress field solution $\underline{\underline{\sigma}}(\underline{x})$ is $\underline{\underline{\rho}}_d^{(k)}(\underline{x})$ or $\underline{\underline{\rho}}_m^{(k)}(\underline{x})$ according to Eq.(4.40). Thus $(N_d + N_m)$ linear elastic problems need to be solved, the components of reduced $\mathbb{D}$ tensor D_{kl_dd}, D_{kl_md}, D_{kl_dm}, D_{kl_mm} are calculated from Eq.(4.24), and $\left\langle \underline{\underline{\rho}}_d^{(k)} \right\rangle$, $\left\langle \underline{\underline{\rho}}_m^{(k)} \right\rangle$ are obtained by performing the volumetric averaging procedures.

4.3.4 Local integration algorithm of NTFA

The NTFA can be implemented into standard computer codes, for instance, using finite element method. The core algorithm of local integration procedure is briefly outlined here. The RVE is subjected to a uniform macroscopic strain increment $\left(\underline{\underline{E}} \right)_{t+\Delta t} = \left(\underline{\underline{E}} \right)_t + \left(\Delta \underline{\underline{E}} \right)_t$ at the loading step $(t + \Delta t)$. All the variables at loading step t are assumed to be known. At the loading step $(t + \Delta t)$, $\left(e_{k\_d} \right)_{t+\Delta t}^{i}$ and $\left(e_{k\_m} \right)_{t+\Delta t}^{i}$ are then known variables for arbitrary iteration $i \geq 1$. In particular, assume the strain increments to be totally elastic for $i = 1$, then Eq. (4.27) turns to:

$$
\begin{cases}
\left(e_{k\_d} \right)_{t+\Delta t}^{(1)} = \underline{\underline{a}}_d^{(k)} : \left(\underline{\underline{E}} \right)_{t+\Delta t} \\
\left(e_{k\_m} \right)_{t+\Delta t}^{(1)} = \underline{\underline{a}}_m^{(k)} : \left(\underline{\underline{E}} \right)_{t+\Delta t}
\end{cases}
\tag{4.58}
$$

and for $i > 1$, they are obtained from the previous iteration $(i-1)$ (as done in the Step C).

– Verify the plastic yield criterion and compute the evolution of reduced internal variables $\left(\dot{\gamma}^{(r)} \right)_{t+\Delta t}^{i}$, $\left(\dot{e}_{k\_d}^{p} \right)_{t+\Delta t}^{i}$, $\left(\dot{e}_{k\_m}^{p} \right)_{t+\Delta t}^{i}$, if necessary. The detailed procedure will be presented in the following text.

– Calculate macroscopic stresses following the relations：

$$\left(\underline{\underline{\Sigma}}\right)_{t+\Delta t}^{i}=\mathbb{C}^{elas-\hom}:\left(\underline{\underline{E}}\right)_{t+\Delta t}+\sum_{k=1}^{N_d}\left\langle\underline{\underline{\rho}}_{d}^{(k)}(\underline{x})\right\rangle\left(\varepsilon_{k\_d}^{p}\right)_{t+\Delta t}^{i}+\sum_{k=1}^{N_m}\left\langle\underline{\underline{\rho}}_{m}^{(k)}(\underline{x})\right\rangle\left(\varepsilon_{k\_m}^{p}\right)_{t+\Delta t}^{i} \tag{4.59}$$

– Update $\left(e_{k\_d}\right)_{t+\Delta t}^{i}$ and $\left(e_{k\_m}\right)_{t+\Delta t}^{i}$ as follows:

$$\begin{cases}\left(e_{k\_d}\right)_{t+\Delta t}^{i+1}=\underline{\underline{a}}_{d}^{(k)}:\left(\underline{\underline{E}}\right)_{t+\Delta t}+\sum_{l=1}^{N_d}D_{kl\_dd}\left(\varepsilon_{l\_d}^{p}\right)_{t+\Delta t}^{i}+\sum_{l=1}^{N_m}D_{kl\_dm}\left(\varepsilon_{l\_m}^{p}\right)_{t+\Delta t}^{i}\\ \left(e_{k\_m}\right)_{t+\Delta t}^{i+1}=\underline{\underline{a}}_{m}^{(k)}:\left(\underline{\underline{E}}\right)_{t+\Delta t}+\sum_{l=1}^{N_d}D_{kl\_md}\left(\varepsilon_{l\_d}^{p}\right)_{t+\Delta t}^{i}+\sum_{l=1}^{N_m}D_{kl\_mm}\left(\varepsilon_{l\_m}^{p}\right)_{t+\Delta t}^{i}\end{cases} \tag{4.60}$$

– Verify the convergence:

IF

$$\begin{aligned}Max\left[\underset{k}{Max}\left(\left(e_{k\_d}\right)_{t+\Delta t}^{i+1}-\left(e_{k\_d}\right)_{t+\Delta t}^{i}\right),\ \underset{k}{Max}\left(\left(e_{k\_m}\right)_{t+\Delta t}^{i+1}-\left(e_{k\_m}\right)_{t+\Delta t}^{i}\right)\right]\\ <\chi\left\|\left(\underline{\underline{E}}\right)_{t+\Delta t}-\left(\underline{\underline{E}}\right)_{t}\right\|\end{aligned} \tag{4.61}$$

where χ is a small tolerance coefficient, for instance, $\chi=10^{-5}$. The norm of second order tensor is recommended here to use the “max norm”, defined as:

$$\left\|A\right\|_{\max}=\max_{i,j}\left\{\left|a_{ij}\right|\right\} \tag{4.62}$$

THEN

The convergent is obtained; the following quantities are updated:

$$\begin{aligned}&\left(e_{k\_d}\right)_{t+\Delta t}=\left(e_{k\_d}\right)_{t+\Delta t}^{i+1},\quad\left(e_{k\_m}\right)_{t+\Delta t}=\left(e_{k\_m}\right)_{t+\Delta t}^{i+1};\\ &\left(e_{k\_d}^{p}\right)_{t+\Delta t}=\left(e_{k\_d}^{an}\right)_{t+\Delta t}^{i+1},\quad\left(e_{k\_m}^{p}\right)_{t+\Delta t}=\left(e_{k\_m}^{an}\right)_{t+\Delta t}^{i+1};\\ &\left(\tau_{k\_d}\right)_{t+\Delta t}=\left(\tau_{k\_d}\right)_{t+\Delta t}^{i},\quad\left(\tau_{k\_m}\right)_{t+\Delta t}=\left(\tau_{k\_m}\right)_{t+\Delta t}^{i};\\ &\left(\gamma^{(r)}\right)_{t+\Delta t}=\left(\gamma^{(r)}\right)_{t+\Delta t}^{i+1};\\ &\left(\underline{\underline{\Sigma}}\right)_{t+\Delta t}=\left(\underline{\underline{\Sigma}}\right)_{t+\Delta t}^{i}\end{aligned}$$

$t = t + \Delta t$, GO TO the next load step.

ELSE

$i = i + 1$, GO TO **(A)** for the next iteration of the same loading step

END IF

Detailed procedure in Step (A):

The aim of step (A) is to determine the state evolution of reduced internal variables of iterate i in the current loading step $(t + \Delta t)$, $\left(\dot{\gamma}^{(r)}\right)_{t+\Delta t}^{i}$, $\left(\dot{e}_{k\_d}^{p}\right)_{t+\Delta t}^{i}$, $\left(\dot{e}_{k\_m}^{p}\right)_{t+\Delta t}^{i}$, from their known values at the previous loading step (t), and those of $\left(e_{k\_d}\right)_{t+\Delta t}^{i}$ $\left(e_{k\_m}\right)_{t+\Delta t}^{i}$ updated by the last iterate $(i-1)$ in the current loading step. This is composed of the following operations.

- Calculate the elastic trial stress, the superscript (e) indicates the elastic trial quantity:

$$\begin{aligned}\left(\tau_{k\_d}^{e}\right)_{t+\Delta t}^{i} &= \left(\tau_{k\_d}\right)_{t} + 2G^{(r)}\left(\left(e_{k\_d}\right)_{t+\Delta t}^{i} - \left(e_{k\_d}^{p}\right)_{t}\right)\\ \left(\tau_{k\_m}^{e}\right)_{t+\Delta t}^{i} &= \left(\tau_{k\_m}\right)_{t} + 3k^{(r)}\left(\left(e_{k\_m}\right)_{t+\Delta t}^{i} - \left(e_{k\_m}^{p}\right)_{t}\right)\end{aligned} \tag{4.63}$$

- Verify the reduced yield criterion:

$$\left(f_p^e\right)_{t+\Delta t}^{i} = \alpha\left(\overline{\sigma_m^{(r)}}^{e}\right)_{t+\Delta t}^{i} + \left(\overline{\sigma_{eq}^{(r)}}^{e}\right)_{t+\Delta t}^{i} - R\left(\left(\gamma^{(r)}\right)_{t}\right) \tag{4.64}$$

where:

$$\begin{aligned}\left(\overline{\sigma}_m^{(r)e}\right)_{t+\Delta t}^{i} &= \frac{1}{3}\sum_{k=1}^{N_m(r)}\left(\tau_{k\_m}^{e}\right)_{t+\Delta t}^{i}\\ \left(\overline{\sigma}_{eq}^{(r)e}\right)_{t+\Delta t}^{i} &= \left(\frac{3}{2}\sum_{k=1}^{N_d(r)}\left(\left(\tau_{k\_d}^{e}\right)_{t+\Delta t}^{i}\right)^2\right)^{\frac{1}{2}}\end{aligned} \tag{4.65}$$

IF $\left(f_p^e\right)_{t+\Delta t}^{i} < 0$ **THEN**

$$\left(\tau_{k\_d}\right)_{t+\Delta t}^{i}=\left(\tau_{k\_d}^{e}\right)_{t+\Delta t}^{i},\quad \left(\tau_{k\_m}\right)_{t+\Delta t}^{i}=\left(\tau_{k\_m}^{e}\right)_{t+\Delta t}^{i}$$
$$\left(e_{k\_d}^{p}\right)_{t+\Delta t}^{i}=\left(e_{k\_d}^{p}\right)_{t},\quad \left(e_{k\_m}^{p}\right)_{t+\Delta t}^{i}=\left(e_{k\_m}^{p}\right)_{t}$$
$$\left(\gamma^{(r)}\right)_{t+\Delta t}^{i}=\left(\gamma^{(r)}\right)_{t}$$

ELSE

Calculate the evolution of reduced internal variables (the deviatoric part following 'radial return' rule).

END IF

- Calculating the evolution of reduced internal variables：

a): Solve $\left(\dot{\gamma}^{(r)}\right)_{t+\Delta t}^{i}$

From Eq. (4.38) and the radial return rule, on gets:

$$\begin{cases}\left(\dot{e}_{k\_d}^{p}\right)_{t+\Delta t}^{i}=\dfrac{3}{2}\left(\dot{\gamma}^{(r)}\right)_{t+\Delta t}^{i}\dfrac{\left(\tau_{k\_d}^{e}\right)_{t+\Delta t}^{i}}{\left(\bar{\sigma}_{eq}^{(r)e}\right)_{t+\Delta t}^{i}}\\ \left(\dot{e}_{k\_m}^{p}\right)_{t+\Delta t}^{i}=\psi\left(\dot{\gamma}^{(r)}\right)_{t+\Delta t}^{i}\left\langle\mu_{m}^{(k)}(\underline{x})\right\rangle\end{cases}\tag{4.66}$$

Then the corrected reduced stresses, $\bar{\sigma}_{eq}^{(r)}$ and $\bar{\sigma}_{m}^{(r)}$, can be expressed as:

$$\begin{cases}\left(\bar{\sigma}_{eq}^{(r)}\right)_{t+\Delta t}^{i}=\left(\bar{\sigma}_{eq}^{(r)e}\right)_{t+\Delta t}^{i}-3G^{(r)}\left(\dot{\gamma}^{(r)}\right)_{t+\Delta t}^{i}\\ \left(\bar{\sigma}_{m}^{(r)}\right)_{t+\Delta t}^{i}=\left(\bar{\sigma}_{m}^{(r)e}\right)_{t+\Delta t}^{i}-3k^{(r)}\psi\left(\dot{\gamma}^{(r)}\right)_{t+\Delta t}^{i}\sum_{k=1}^{N_m(r)}\left\langle\mu_{m}^{(k)}(\underline{x})\right\rangle\end{cases}\tag{4.67}$$

Thus, a nonlinear equation for $\left(\dot{\gamma}^{(r)}\right)_{t+\Delta t}^{i}$ must be solved:

$$
\begin{aligned}
\left(f_p\right)_{t+\Delta t}^{i} &= \alpha\left(\left(\bar{\sigma}_m^{(r)e}\right)_{t+\Delta t}^{i} - 3k^{(r)}\psi\left(\dot{\gamma}^{(r)}\right)_{t+\Delta t}^{i}\sum_{k=1}^{N_m(r)}\left\langle\mu_m^{(k)}(\underline{x})\right\rangle\right) \\
&\quad + \left(\left(\bar{\sigma}_{eq}^{(r)e}\right)_{t+\Delta t}^{i} - 3G^{(r)}\left(\dot{\gamma}^{(r)}\right)_{t+\Delta t}^{i}\right) - R\left(\left(\gamma^{(r)}\right)_t + \left(\dot{\gamma}^{(r)}\right)_{t+\Delta t}^{i}\right) \\
&= \left(\alpha\left(\bar{\sigma}_m^{(r)e}\right)_{t+\Delta t}^{i} + \left(\bar{\sigma}_{eq}^{(r)e}\right)_{t+\Delta t}^{i}\right) \\
&\quad - \left(3\alpha k^{(r)}\psi\sum_{k=1}^{N_m(r)}\left\langle\mu_m^{(k)}(\underline{x})\right\rangle + 3G^{(r)}\right)\left(\dot{\gamma}^{(r)}\right)_{t+\Delta t}^{i} \\
&\quad - R\left(\left(\gamma^{(r)}\right)_t + \left(\dot{\gamma}^{(r)}\right)_{t+\Delta t}^{i}\right) \\
&= 0
\end{aligned}
\tag{4.68}
$$

In this study, the dichotomy method is used to solve this nonlinear equation. For the initial iteration, $\left(\dot{\gamma}^{(r)}\right)_{t+\Delta t}^{i}$ can be restricted into $\left(0,\ \dfrac{\left(f_p^e\right)_{t+\Delta t}^{i}}{3k^{(r)}\alpha\psi\sum_{k=1}^{N_m(r)}\left\langle\mu_m^{(k)}(\underline{x})\right\rangle + 3G^{(r)}}\right)$, where $\left(f_p^e\right)_{t+\Delta t}^{i}$ is defined in Eq.(4.64).

b): Then the reduced stress components can be computed:

$$
\begin{cases}
\left(\tau_{k\_d}\right)_{t+\Delta t}^{i} = \left(\tau_{k\_d}^{e}\right)_{t+\Delta t}^{i} - 3G^{(r)}\left(\dot{\gamma}^{(r)}\right)_{t+\Delta t}^{i}\dfrac{\left(\tau_{k\_d}^{e}\right)_{t+\Delta t}^{i}}{\left(\bar{\sigma}_{eq}^{(r)e}\right)_{t+\Delta t}^{i}} \\
\left(\tau_{k\_m}\right)_{t+\Delta t}^{i} = \left(\tau_{k\_m}^{e}\right)_{t+\Delta t}^{i} - 3k^{(r)}\psi\left(\dot{\gamma}^{(r)}\right)_{t+\Delta t}^{i}\left\langle\mu_m^{(k)}(\underline{x})\right\rangle
\end{cases}
\tag{4.69}
$$

where $\left(\bar{\sigma}_m^{(r)}\right)_{t+\Delta t}^{i}$ is calculated following the Eq.(4.67)

c): Finally the reduced plastic strain can be estimated as follows:

$$\begin{cases} \left(e^{p}_{k\_d}\right)^{i}_{t+\Delta t} = \left(e_{k\_d}\right)^{i}_{t+\Delta t} - \dfrac{\left(\tau_{k\_d}\right)^{i}_{t+\Delta t}}{2G^{(r)}} \\ \left(e^{p}_{k\_m}\right)^{i}_{t+\Delta t} = \left(e_{k\_m}\right)^{i}_{t+\Delta t} - \dfrac{\left(\tau_{k\_m}\right)^{i}_{t+\Delta t}}{3k^{(r)}} \end{cases} \tag{4.70}$$

4.4 Example of application to heterogeneous material with D-P matrix

In this section, two examples of application are presented as the first stage of validation of the NTFA method for micromechanical modeling of nonlinear composites (example I) and of porous materials (example II). The numerical results are compared with other homogenization approaches to reveal the advantage of the NTFA.

The two three-dimensional problems studied here concern both matrix-inclusion composite. In the first case, the inclusions are linear elastic material and in the second case the inclusion is replaced by pore voids. The volumetric fraction inclusion (or the porosity) is 25% in both cases; the geometrical domain studied and FEM mesh used are illustrated in Figure 4-1.

The solid matrix in the two examples is described by the same D-P plastic model. The plastic yield function and plastic potential are presented in Eq.(4.71), and the material parameters used are listed in Table 4-1. The material parameters of inclusion for the composite case are given in Table 4-2.

$$\begin{aligned} f_p &= \alpha\sigma_m + \sigma_{eq} - (\sigma_0 + H\gamma^b) = 0 \\ g &= \psi\sigma_m + \sigma_{eq} - (\sigma_0 + H\gamma^b) \end{aligned} \tag{4.71}$$

Table 4-1: Material parameters used for the solid matrix

E_m(Pa)	υ_m	σ_0(Pa)	H(Pa)	b	α	ψ
1.0×10^{10}	0.25	4.5×10^{7}	1.5×10^{8}	0.5	0.3	0.3

Table 4-2: Elastic parameters for inclusion

E_I(Pa)	ν_I
2.0×10^{10}	0.20

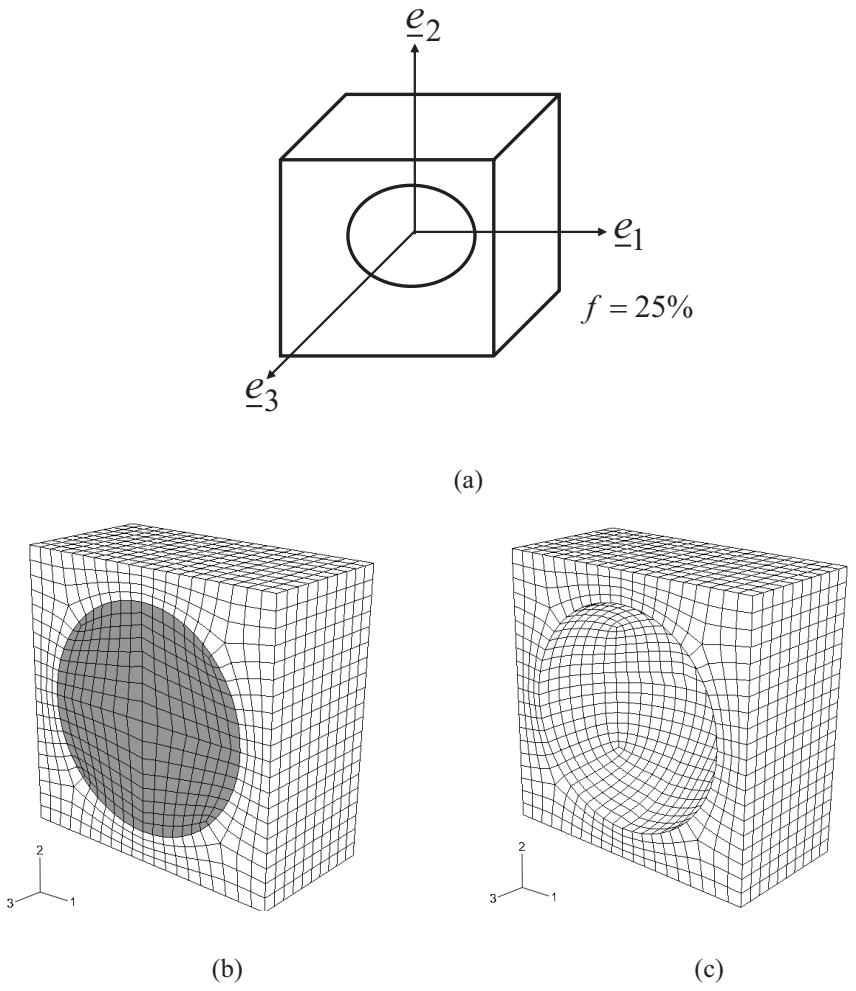

Figure 4-1: Geometry and FEM mesh (cross middle section along direction $\underline{e}_3$) of the studied unit-cell

(a) Geometry domain; (b) Mesh for composite with inclusion (Example I); (c) Mesh for porous material (Example II)

In the previous work by Michel and Suquet (Michel & Suquet, 2003; 2004) only the composite composed of Mises type matrix and elastic inclusion was discussed. For the sake of comparison, we will give an additional example (example III) for porous material with Misès type solid matrix, to show the advantage and performance of the NTFA method for different kinds of nonlinear heterogeneous materials.

4.4.1 Example I: composite with D-P matrix and elastic inclusion

In the first example, simulations of nonlinear composite composed of D-P matrix and elastic inclusion (Figure 4-1) are performed. As studied in section 4.3, the implementation is divided into two steps, the preliminary computation, and local integration process. Firstly, a set of initial numerical elastoplastic simulations are performed to decide the plastic modes. For this model six numerical simulations along different loading directions as Eq. (4.46) are executed by FEM. Then plastic modes are chosen using the method introduced in section 4.3.1. Figure 4-2 and Figure 4-3 show the six components of the first two plastic modes $\underline{\underline{\mu}}_{d}^{(1)}(\underline{x})$ and $\underline{\underline{\mu}}_{d}^{(2)}(\underline{x})$ for the deviator part, and Figure 4-4 shows the first two modes $\mu_m^{(1)}(\underline{x})$ and $\mu_m^{(2)}(\underline{x})$ for the volumetric part.

The results of uniaxial compression simulation and the finite element solutions as reference results (Michel, Moulinec, & Suquet, 1999) for the composite are illustrated in Figure 4-5. Also the results obtained by Hill's incremental method (Hill, 1965) are plotted together for comparison. Taken account of the heterogeneity of microscopic plastic strain field, the results obtained by NTFA are of a good agreement with FEM solution that can be regarded as the exact results. As anticipated above, the predictions of Hill's incremental method are unrealistically stiff, because the uniform plastic strain field is inappropriately simplified as a constant.

4.4.2 Example II: porous material with D-P matrix

Another type of nonlinear heterogeneous material, porous media has been widely researched to investigate the strength properties. For porous material composed of Mises constituent, Gurson's Model (Gurson, 1977) and other improved models, such as GTN Model (Tvergaard, 1981), can well determine the macroscopic yield surface. Nevertheless, the modeling of macroscopic strength properties for D-P porous material is still an open problem (Zaoui, 2002). In recent years, many valuable results are obtained in this area (Lee & Oung, 2000; Dormieux & Barthélémy, 2003; Trillat, Pastor, & Thoré, 2006; Pastor, Thoré, Loute, Pastor, & Trillat, 2008; Guo, Faleskog, & Shih, 2008; Maghous, Dormieux, & Barthélémy, 2009). However, the results of these analytical macroscopic strength criterions for D-P porous media proposed by different scholars vary a lot. A widely accepted and used criterion does not exist yet. Moreover all the analytical models can only predict the macroscopic yield surface, but the overall mechanical responses can not obtained from this analytical models.

In the example II, we will use the NTFA to predict the overall mechanical responses of D-P porous material. The geometric model, constitutive equations, and corresponding parameters have introduced above. Figure 4-6 and Figure 4-7 show the six components of the first two plastic modes $\underline{\underline{\mu}}_d^{(1)}(\underline{x})$ and $\underline{\underline{\mu}}_d^{(2)}(\underline{x})$ for the deviator part, and Figure 4-8 shows the first two modes $\mu_m^{(1)}(\underline{x})$ and $\mu_m^{(2)}(\underline{x})$ for the volumetric part.

The Figure 4-9 illustrates the comparison of the results obtained by FEM (as a reference result), Hill's incremental approach, and NTFA for a uniaxial compression test. We can see that the curve of NTFA coincides with the reference result very well.

The macroscopic yield surface of the studied porous material in this example obtained numerically by NTFA is plotted in Figure 4-10, accompanied by FEM solution and two typical analytical results:

Model proposed by (Dormieux & Barthélémy, 2003):

$$\frac{2+4f/3}{3T^2}\Sigma_{eq}^2+\left(\frac{3f}{2T^2}-1\right)\Sigma_m^2+2(1-f)P\Sigma_m-(1-f)^2P^2=0 \tag{4.72}$$

where f is the porosity, $T=\sqrt{\frac{2}{3}}\alpha$, $P=\sigma_0/\alpha$, α,σ_0 are defined by Eq.(4.71).

Model proposed by Guo in approximate form (2008):

$$\left(\frac{\Sigma_{eq}}{1-\alpha\Sigma_m/(1-f)^{1-s/2}}\right)^2+2f\cosh\left(\frac{2\alpha+3\,\mathrm{sgn}(\Sigma_m)}{2\alpha}\ln(1-\alpha\Sigma_m)\right)-(1+f^2)=0 \tag{4.73}$$

where $s=1+\frac{2}{3}\alpha\,\mathrm{sgn}(\Sigma_m)$.

Figure 4-10 reveals that the macroscopic yields surface obtained by NTFA follows the same trend with the two analytical models, but owns a better accordance with the finite element solution. . It can be seen that the NTFA owns a very good ability to predict the macroscopic strength property of D-P porous material besides determining the overall response of composite.

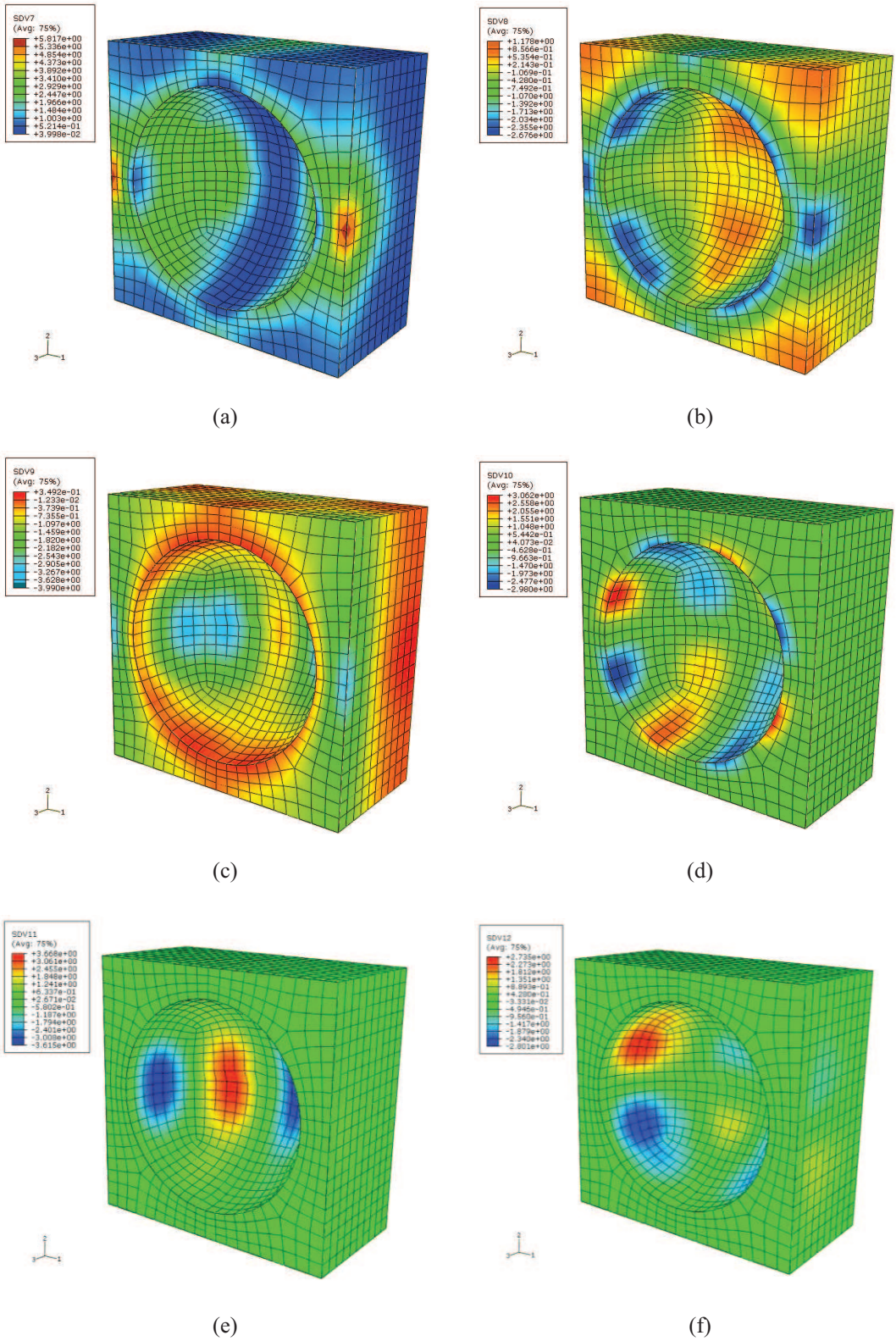

Figure 4-2: Plastic modes $\underset{=d}{\mu}^{(1)}(\underline{x})$ for the example I (only matrix is illustrated[3])

(a) $\mu_d^{(1)}{}_{11}(\underline{x})$; (b) $\mu_d^{(1)}{}_{22}(\underline{x})$; (c) $\mu_d^{(1)}{}_{33}(\underline{x})$; (d) $\mu_d^{(1)}{}_{12}(\underline{x})$; (e) $\mu_d^{(1)}{}_{13}(\underline{x})$; (f) $\mu_d^{(1)}{}_{23}(\underline{x})$

[3] The plastic mode $\underset{=d}{\mu}^{(k)}(\underline{x})$ in the linear elastic inclusion is zero, so the figure omits this part.

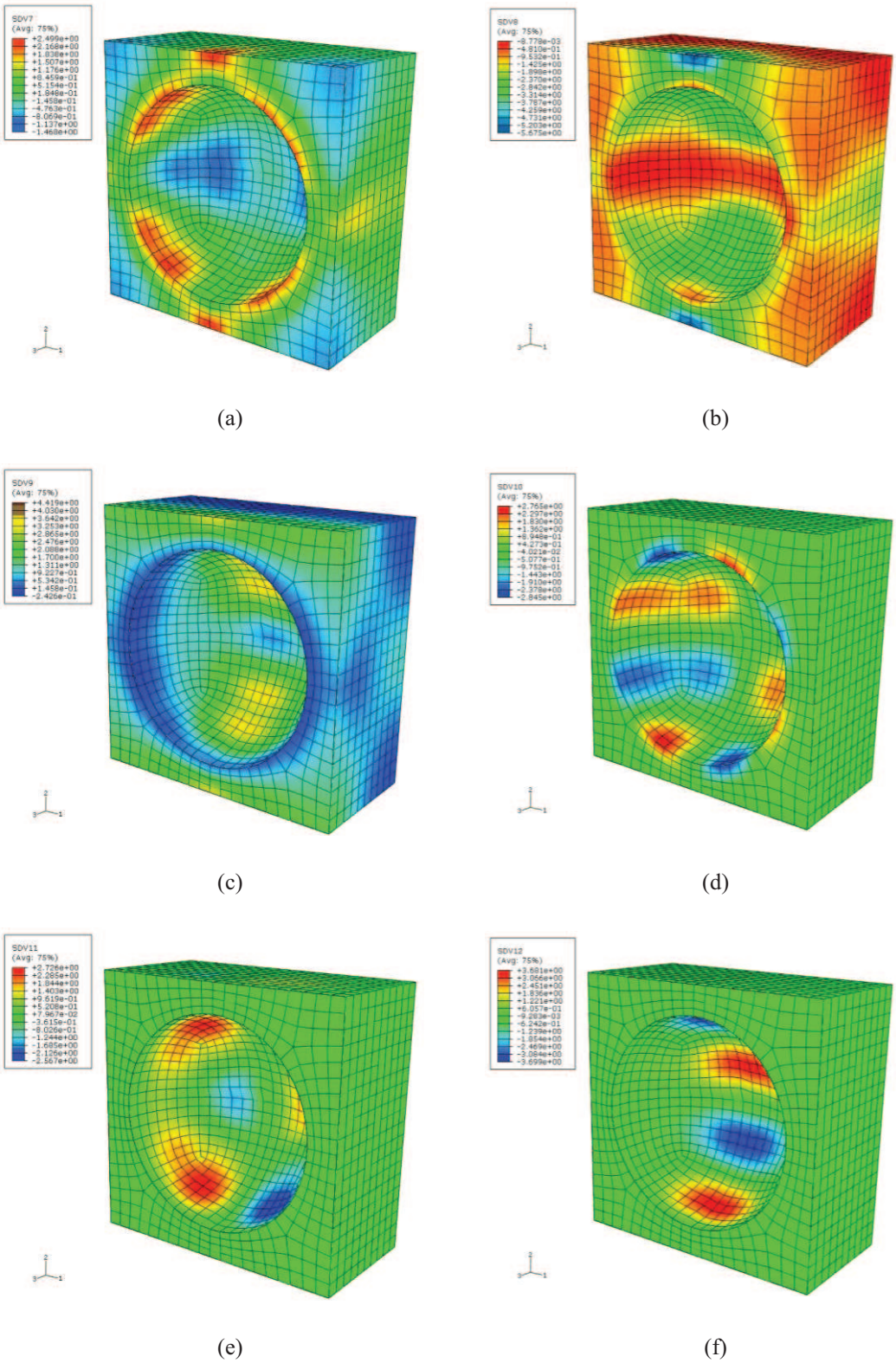

Figure 4-3: Plastic modes $\underline{\underline{\mu}}_{d}^{(2)}(\underline{x})$ for the example I (only matrix is illustrated[4])

(a) $\mu_{d}^{(2)}{}_{11}(\underline{x})$; (b) $\mu_{d}^{(2)}{}_{22}(\underline{x})$; (c) $\mu_{d}^{(2)}{}_{33}(\underline{x})$; (d) $\mu_{d}^{(2)}{}_{12}(\underline{x})$; (e) $\mu_{d}^{(2)}{}_{13}(\underline{x})$; (f) $\mu_{d}^{(2)}{}_{23}(\underline{x})$

[4] The plastic mode $\underline{\underline{\mu}}_{d}^{(k)}(\underline{x})$ in the linear elastic inclusion is zero, so the figure omits this part.

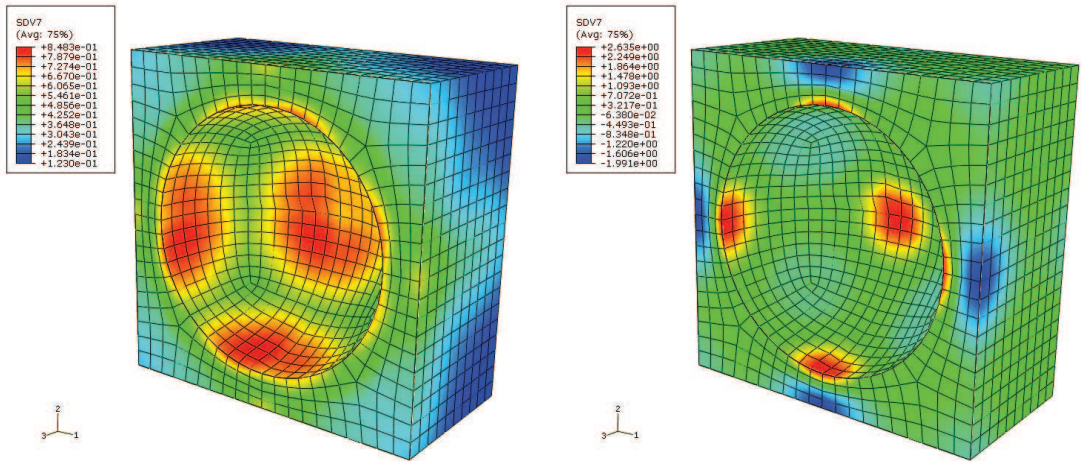

(a) (b)

Figure 4-4: Plastic modes $\mu_m^{(1)}(\underline{x})$ and $\mu_m^{(2)}(\underline{x})$ for the example I (only matrix is illustrated[5])

(a) $\mu_m^{(1)}(\underline{x})$; (b) $\mu_m^{(2)}(\underline{x})$

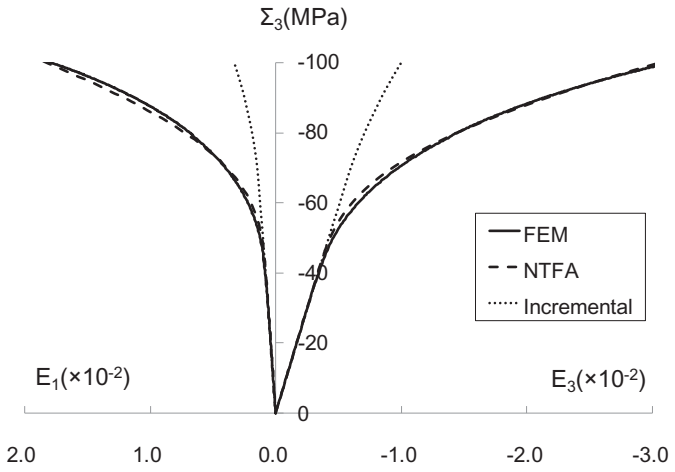

Figure 4-5: Comparison of the predicted results by NTFA with those from Hill's incremental approach and reference solution by FEM in uniaxial compression test of composite

[5] The plastic mode $\underline{\underline{\mu}}_d^{(k)}(\underline{x})$ in the linear elastic inclusion is zero, so the figure omits this part.

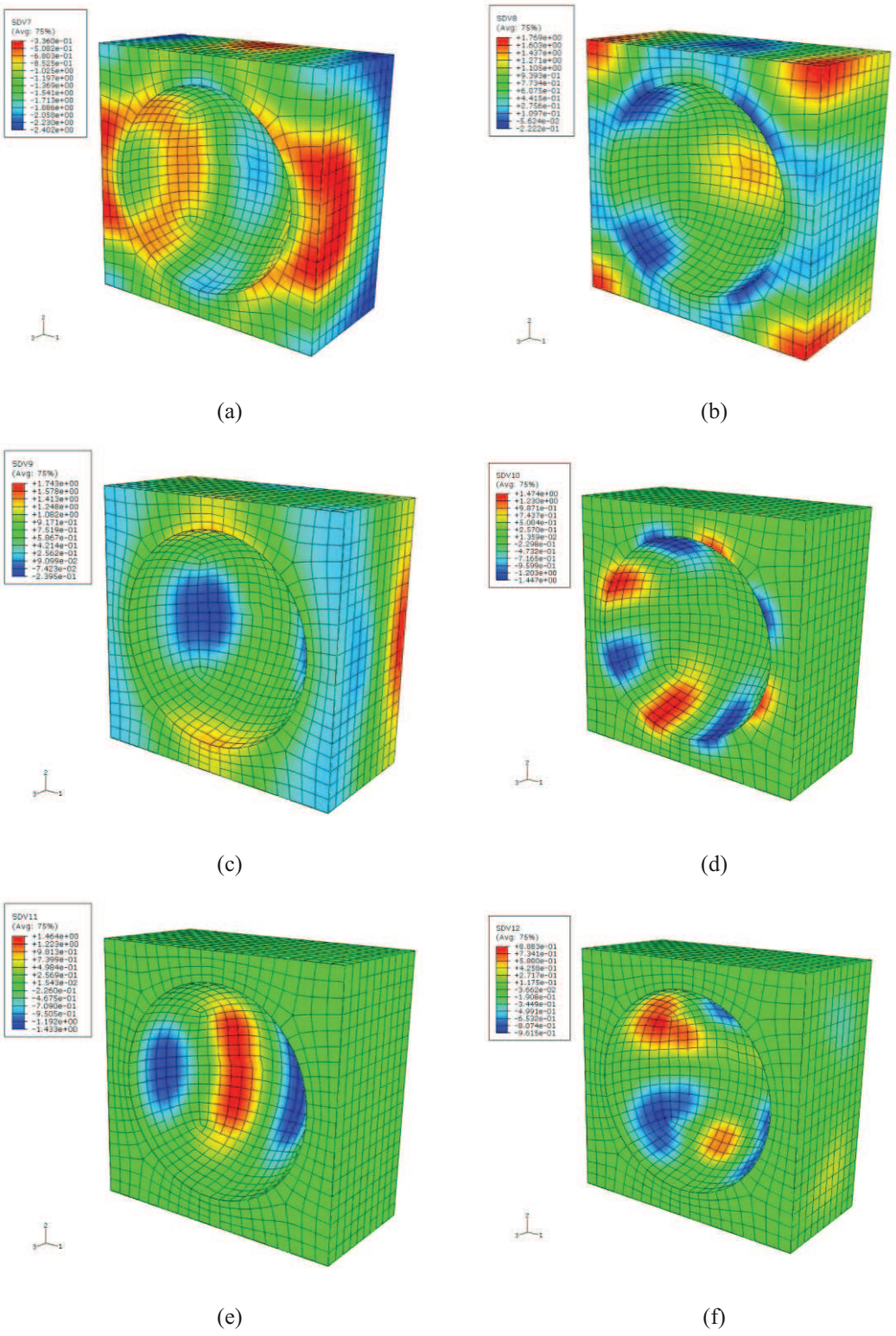

Figure 4-6: Plastic modes $\underline{\underline{\mu}}_{d}^{(1)}(\underline{x})$ for the example II (porous media)

(a) $\mu_{d}^{(1)}{}_{11}(\underline{x})$; (b) $\mu_{d}^{(1)}{}_{22}(\underline{x})$; (c) $\mu_{d}^{(1)}{}_{33}(\underline{x})$; (d) $\mu_{d}^{(1)}{}_{12}(\underline{x})$; (e) $\mu_{d}^{(1)}{}_{13}(\underline{x})$; (f) $\mu_{d}^{(1)}{}_{23}(\underline{x})$

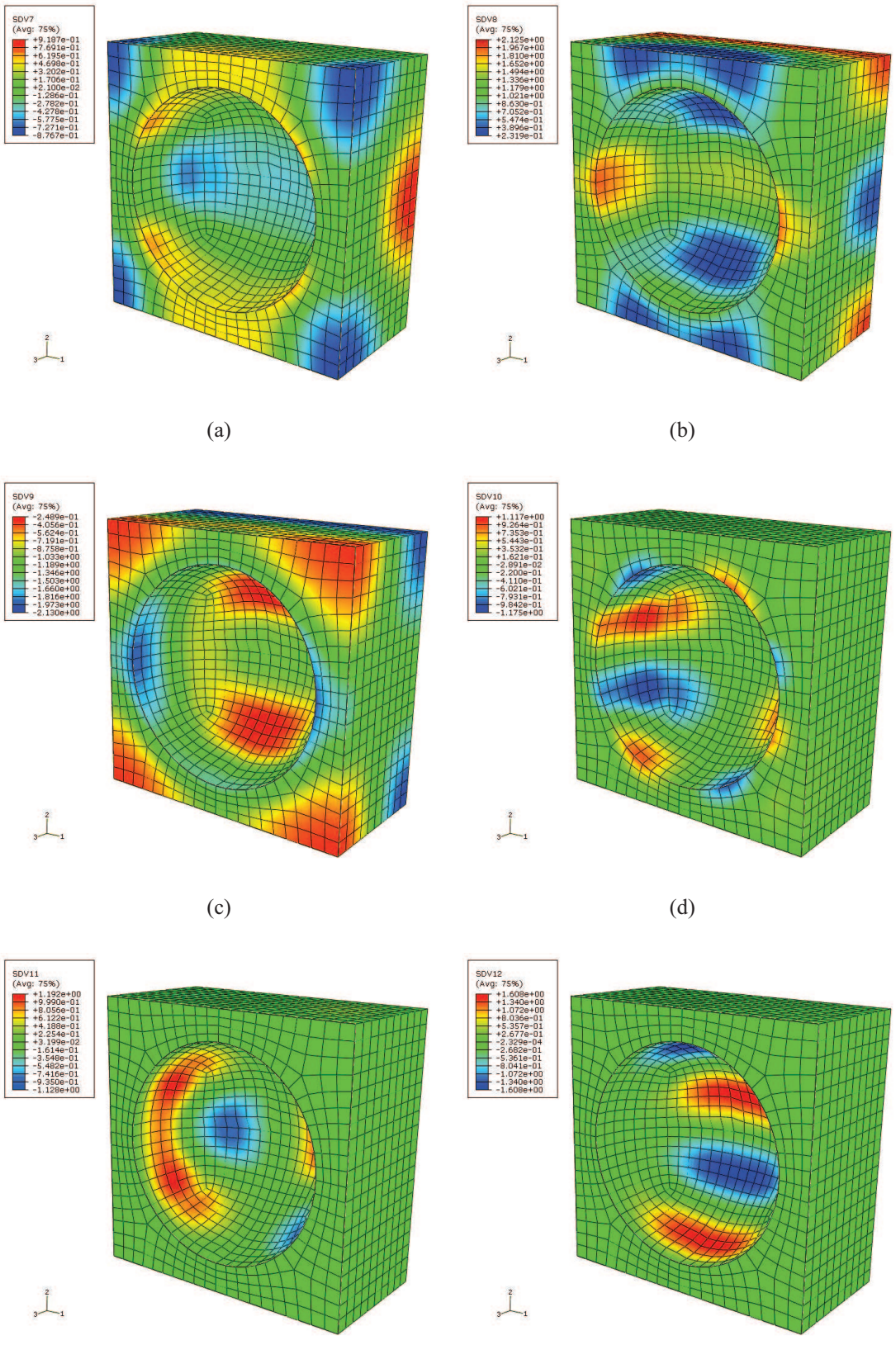

Figure 4-7: Plastic modes $\underline{\underline{\mu}}_d^{(2)}(\underline{x})$ for the example II (porous media)

(a) $\mu_d^{(2)}{}_{11}(\underline{x})$; (b) $\mu_d^{(2)}{}_{22}(\underline{x})$; (c) $\mu_d^{(2)}{}_{33}(\underline{x})$; (d) $\mu_d^{(2)}{}_{12}(\underline{x})$; (e) $\mu_d^{(2)}{}_{13}(\underline{x})$; (f) $\mu_d^{(2)}{}_{23}(\underline{x})$

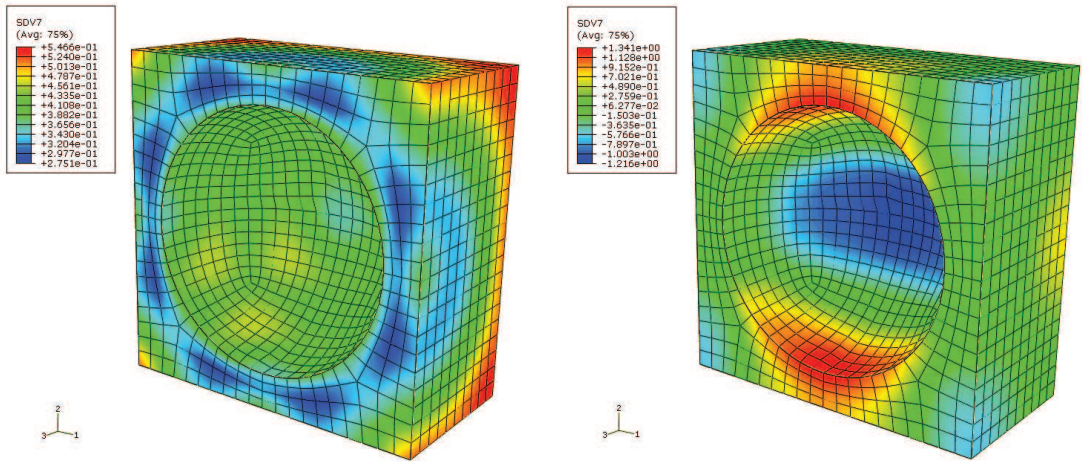

(a) (b)

Figure 4-8: Plastic modes $\mu_m^{(1)}(\underline{x})$ and $\mu_m^{(2)}(\underline{x})$ for the example II (porous media)

(a) $\mu_m^{(1)}(\underline{x})$; (b) $\mu_m^{(2)}(\underline{x})$

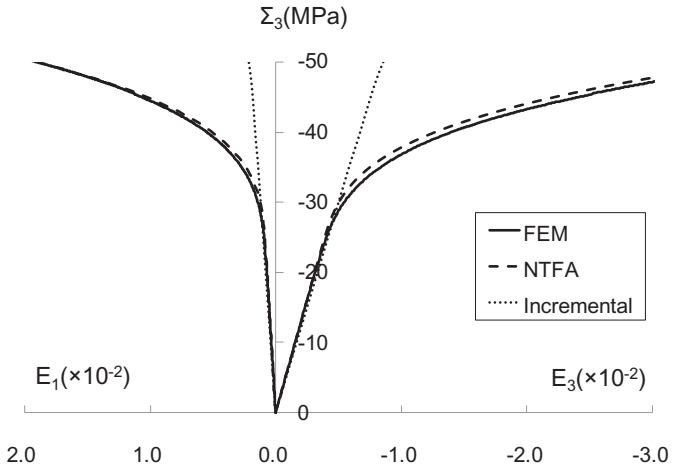

Figure 4-9: Comparison of the predicted results by NTFA with those by Hill's incremental approach and reference solution by FEM in uniaxial compression test of porous material

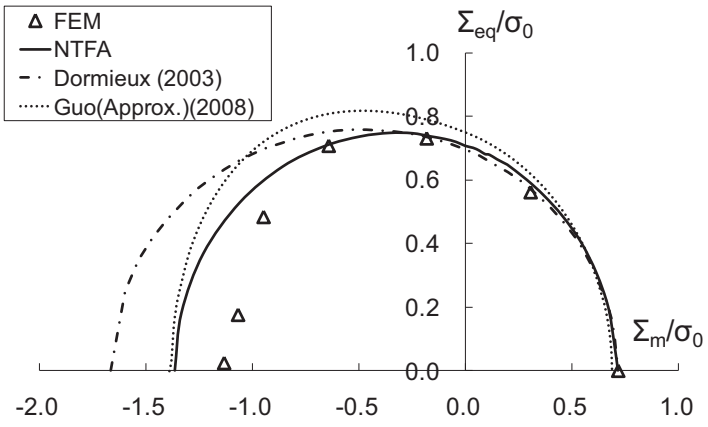

Figure 4-10: Composition of plastic yield surfaces of porous material obtained by NTFA, Dormieux's model, Guo's model, and solution by FEM simulation

4.4.3 Example III: porous material with Mises matrix

The example III concerns a porous material with Mises type solid matrix. The three-dimensional geometrical domain and FEM mesh used are illustrated as

Figure 4-11. The porosity is 10%. The plastic yield function with isotropic hardening law is given in Eq. (4.74); and the material parameters are listed in Table 4-3.

$$f_p = \sigma_{eq} - (\sigma_0 + \gamma p^b) = 0 \tag{4.74}$$

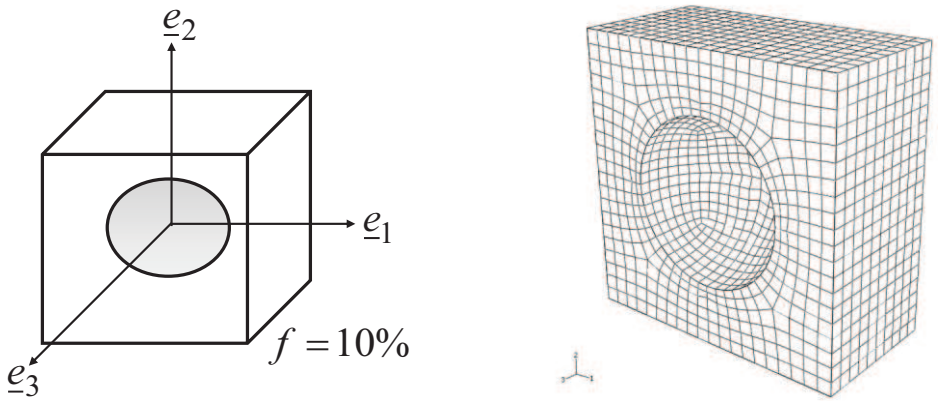

(a) (b)

Figure 4-11: Geometry domain and FEM mesh (cross middle section along direction $\underline{e}_3$) of the simulated unit-cell in example III; (a) Geometry of the model; (b) Mesh of the model

Table 4-3: Material parameters used for Mises solid matrix

E_m(Pa)	υ_m	σ_0(Pa)	H(Pa)	b
1.0×10^{10}	0.25	4.5×10^{7}	1.5×10^{8}	0.50

The result of predicting a uniaxial tension test (lateral strain was fixed to zero) of the porous media with NTFA and FEM simulation are plotted in Fig. 2. Taken as a comparison, some results of the same problem achieved by other classical homogenization approaches are also plotted in the same figure, including the Gurson's model (Gurson, 1977) expressed as Eq.(4.75), and the Hill's incremental approach (Hill, 1965) in Mori-Tanaka scheme (Mori & Tanaka, 1973). It can be seen that the prediction by Hill's incremental approach is unrealistically stiff. The reason is the incremental approach ignores the homogeneity of plastic strain field in the matrix. The result of NTFA seems to be very close to that of the FEM simulation which is regarded as a reference result.

$$\Phi = \left(\frac{\Sigma_{eq}}{\sigma_H}\right)^2 + 2f\cosh\left(\frac{3\Sigma_m}{2\sigma_H}\right) - (1+f^2) = 0 \tag{4.75}$$

$$\dot{f} = (1-f)tr(\dot{\underline{\underline{\varepsilon}}}^p)$$

$$\sigma_H = \sigma_0 + H\gamma^b \tag{4.76}$$

As mentioned in many literatures, the Gurson's model provides an upper bound of solution. The yield surface obtained from NTFA, Gurson's model, and Pastor's limit analysis results (Trillat & Pastor, 2005) (including the strain static, strain kinematic, stress static and stress kinematic results) are plotted in Figure 4-13. It seems obviously that the yield surface of NTFA is smaller than that of Gurson's model. Compared with the yield surface obtained by limit analysis, as plotted, the two vertexes of NTFA yield surface are very near with the strain results (strain static, strain kinematic), and the central part of NTFA yield surface is closed to the stress results (stress static and stress kinematic results) of limit analysis.

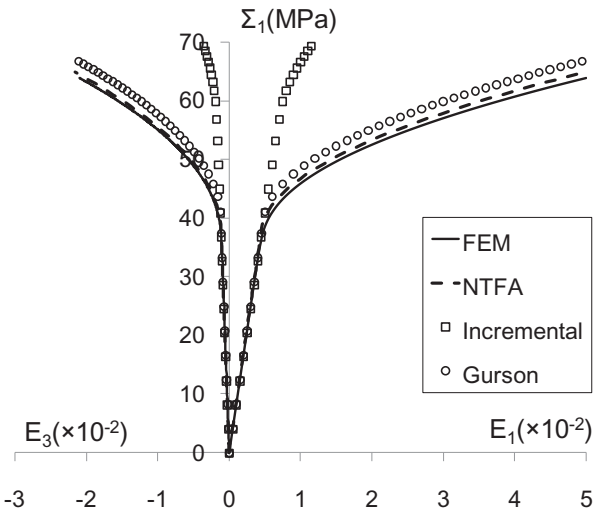

(a)

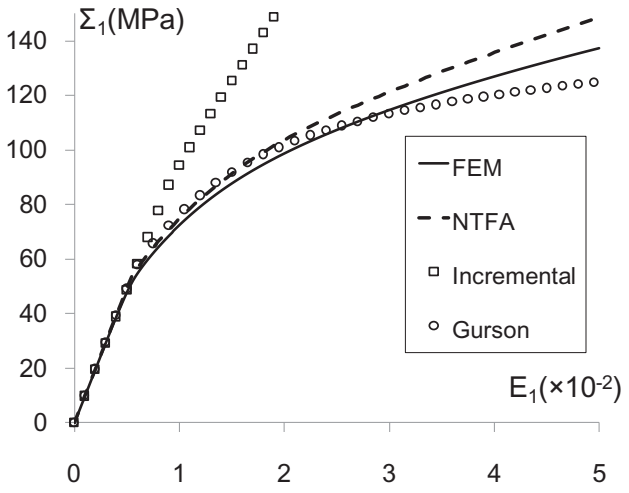

(b)

Figure 4-12: Comparison of the predicted results by NTFA with those by Gurson's model, Hill's incremental approach and reference solution by FEM in uniaxial tension test of porous media; (a) lateral free tension; (b) lateral fixed tension

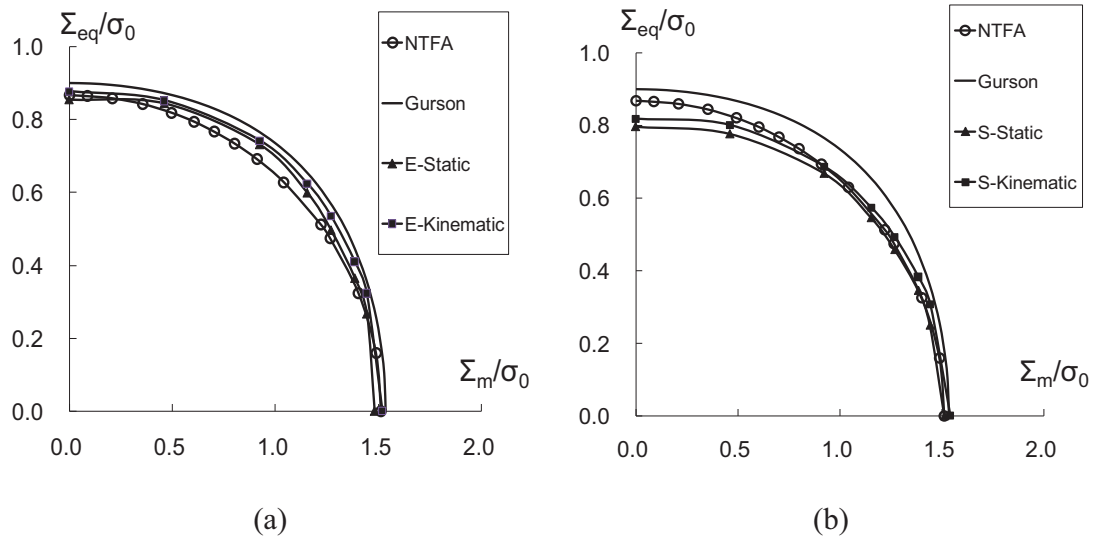

Figure 4-13: Comparison of yield surfaces of porous medium respectively obtained by NTFA, Gurson's model, and Pastor's model; (a) strain loading; (b) stress loading

4.5 Conclusions

The NTFA proposed by Michel and Suquet (2003; 2004) provides an efficient way to simulate and predict macroscopic behaviors of nonlinear heterogeneous composites and porous materials with Mises type material phases. In this chapter, the NTFA is applied to nonlinear homogenization problems with pressure-dependent constituents, in particular the D-P materials, which are commonly used in geomaterials. By decomposing the plastic strain field into volumetric and deviatoric part and then a linear combination of plastic modes, the heterogeneity of microscopic plastic strain field can be well approximated; meanwhile the number of internal variables is efficiently reduced. The D-P criterion is formulated in terms of a set of reduced variables over the plastic modes. The applications of NTFA, to the prediction of mechanical response of both matrix-inclusion composite and porous material, have shown good agreements with the reference results obtained by FEM simulations. The macroscopic yield surface of porous material has also been correctly predicted. In the next Chapter, we will present an application of the NTFA to modeling of the Callovo-Oxford argillite.

Chapter 5:
Application of NTFA to micromechanical modeling of argillite

In Chapter 3, a microscopic mechanical model based on Hill's incremental approach for the description the nonlinear behavior of argillite was proposed. The validity of the proposed model is verified through the comparisons between numerical predictions and experimental data of argillite. It seems that the proposed micromechanical model is able to describe main features of mechanical behaviors of argillite revealed in the tests, such as pressure dependency, transition from volumetric compressibility to dilatancy, and material softening.

However, as recognized by many scholars, the incremental approach owns some intrinsic theoretical defects. The most significant one is that the microscopic plastic strain filed in RVE is assumed as uniformly distributed. According to the widely accepted theory that for nonlinear heterogeneous materials the exact determination of the effective constitutive relations requires the accurate description of all microscopic plastic strain fields in RVE (Rice, 1970; Mandel, 1972; Suquet, 1985), the incremental approach can not accurately describe the overall mechanical behavior of nonlinear heterogeneous materials quantitatively. In practice, it is also noted in many researches that the direct use of Hill's incremental approach often leads to significant numerical errors. Some techniques, such as the isotropization method used in section 3.2, can be performed to improve the prediction of incremental approach.

The NTFA proposed by Michel and Suquet (2003, 2004) for pressure independent constituents and developed in chapter Chapter 4: for pressure dependent constituents, has obvious advantage that the heterogeneity of local plastic strain field in RVE can be well described by decomposing it into a linear combination of set of predicted plastic modes. Theoretically, NTFA owns the ability of accurately determining the macroscopic overall mechanical responses of nonlinear heterogeneous materials. Some examples have been presented in the previous chapter. In this chapter, the NTFA will be used to simulate some more complicated mechanical responses of argillite.

In this simulation, the studied argillite is considered as a two phase composite with elastic mineral inclusions embedded in the clay matrix. The behavior of clay matrix is described by an elastoplastic model. In section 5.1 and 5.2, the local elastoplastic model of clay matrix is formulated and validated respectively. Then the simulation of laboratory test results of argillite is presented in section 5.3.

5.1 Local constitutive model for the clay matrix of argillite

As mentioned above, some basic mechanical properties of the studied argillite have been investigated, such as an important pressure dependency of mechanical responses, a significant volumetric dilatancy following the loading increase, and the softening process after the peak strength. To describe these characters, the local constitutive model for the clay matrix is studied in this section.

The proposed local elastoplastic constitutive model is based on the thermodynamic framework discussed in section 4.1. A Drucker-Prager yield criterion is adopted to describe the character of pressure dependency:

$$f_p = \alpha\sigma_m + \sigma_{eq} - R(\gamma) = 0 \tag{5.1}$$

where γ is the internal variable, and $R(\gamma)$ acts as the isotropic hardening function. Taking account of the peak strength and softening behavior of argillite, we use such a hyperbolic tangent hardening function:

$$R(\gamma) = \sigma_0 + H_1\left(\tanh(t\gamma) - H_2\left(\tanh(t\gamma - b) + 1.0\right)\right) \tag{5.2}$$

σ_0 is the initial yield stress in uniaxial compression test. t and b control the kinetics of plastic hardening and softening; H_1 and H_2 describe the transition from hardening to softening regimes. In Figure 5-1, we show the evolution of hardening function with different values of some parameters involved in plastic hardening law. And in Table 5-1, the reference values of materials parameters are given.

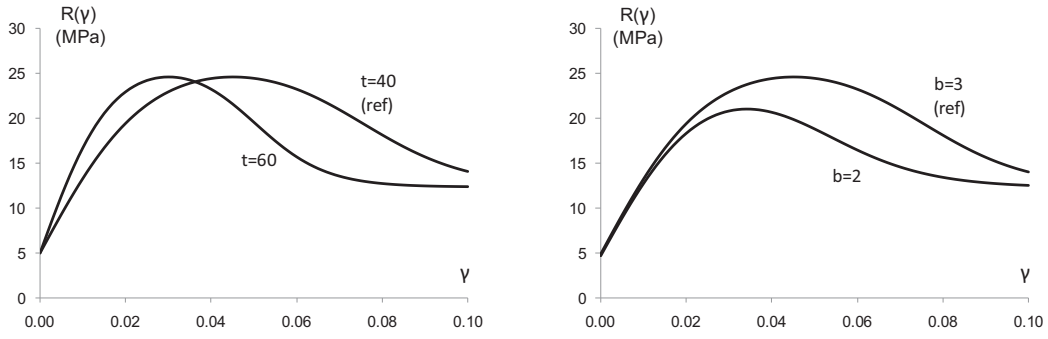

(a) (b)

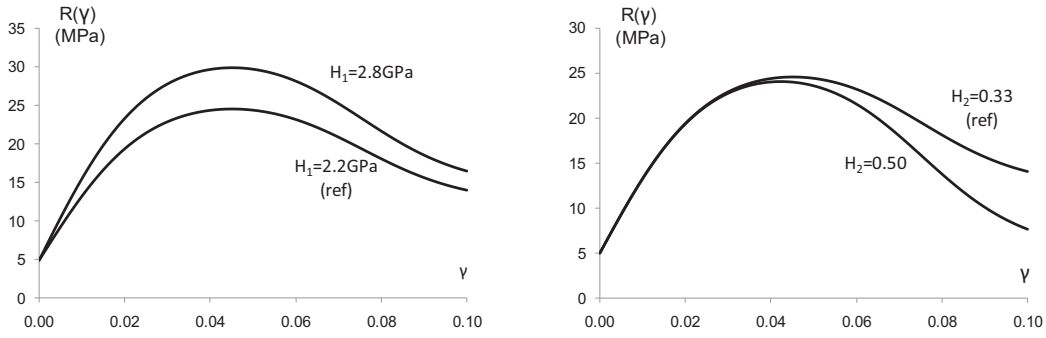

(c) (d)

Figure 5-1: Illustration of evolution of hardening function with different parameters

Table 5-1: Reference values of parameters for hardening function

σ_0(Pa)	H_1(Pa)	H_2	t	b
5.0×10^6	2.2×10^7	0.33	40	3.0

It's well known that the studied argillite exhibited significant volumetric contraction and dilation during plastic flow. In order to describe this feature, a non-associated flow rule is adopted here:

$$g = \psi(\gamma)\sigma_m + \sigma_{eq} - R(\gamma) \tag{5.3}$$

The volumetric dilatancy coefficient ψ which controls the evolution of plastic volumetric strain is a function in terms of internal variable γ. The volumetric strain features of argillite during the compression process are observed in the laboratory tests that the volumetric strain decreases in the initial loading stage, and then observably dilates with plastic flow evolution. Considering this property, the volumetric dilatancy coefficient ψ is chosen in the following form:

$$\psi(\gamma) = \psi_0 + (\psi_m - \psi_0)\tanh(t'\gamma) \tag{5.4}$$

The parameter ψ_0 and ψ_m represent the initial and asymptotic value of volumetric dilatancy coefficient. t' controls the evolution speed volumetric dilatancy coefficient. If $\psi_m = \psi_0$, then the Eq. (5.4) reduces to Eq. (4.71), in which the coefficient ψ is independent with the internal variable.

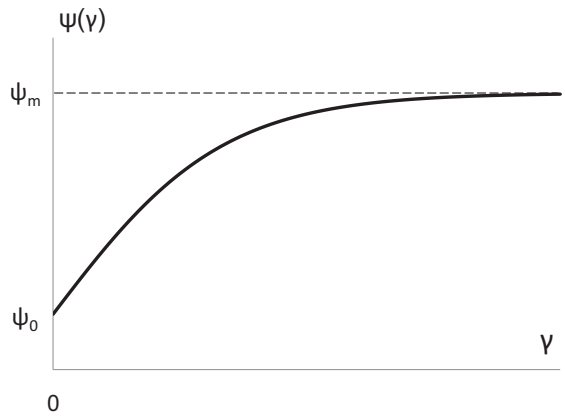

Figure 5-2: Evolution of dilatation coefficient ψ with hardening variable γ

5.2 Numerical validation

For a first verification of the NTFA to simulate composite composed of matrix obeying the proposed local constitutive equations in the previous section, and elastic inclusion, a simple numerical validation is performed in this section to compare the results obtained by NTFA and reference results by FEM.

The inclusion volumetric fraction ($f = 25\%$) and geometry of the simulated model is the same with those in section 4.4, and have been illustrated in Figure 4-1(a), (b). The parameters of matrix and inclusion are listed in Table 5-2 and Table 5-3, respectively. The results of comparison between NTFA and FEM on a uniaxial compression test are illustrated in Figure 5-3. It seems that the result obtained by NTFA coincides with the reference result by FEM. This good accordance inspires the next study of simulating the mechanical responses of argillite by NTFA with the proposed local constitutive model.

Table 5-2: Materials parameters of matrix

E_m(Pa)	υ_m	σ_0(Pa)	$H_1(MPa)$	H_2	t	b
1.0×10^{10}	0.25	2.0×10^{7}	1.5×10^{8}	0.3333	40	3.0

Table 5-2 (Continued)

α	ψ_0	ψ_m	t'
0.3	0.3	0.3	(arbitrary)

Table 5-3: Material parameters of inclusion

E_I(Pa)	υ_I
2.0×10^{10}	0.20

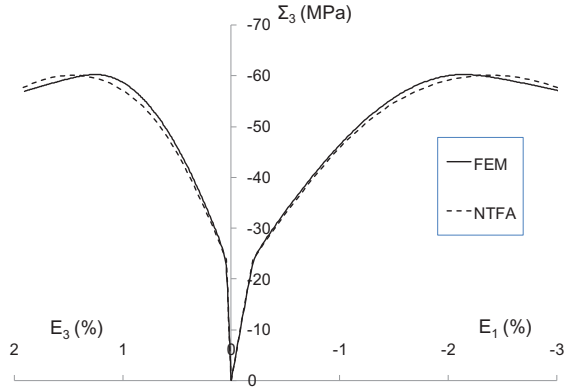

Figure 5-3: Comparison between numerical prediction by NTFA and reference solution by FEM for uniaxial tension test

5.3 Simulation of laboratory test results of argillite

In Section 3.5, the laboratory tests with various loading path performed on argillites with different mineralogical compositions were simulated by Hill's incremental method. However, although the results were fairly good after a numerical parameter fitting process, the incremental method can not accurately describe the overall mechanical behavior of nonlinear heterogeneous materials quantitatively due to it cannot describe the heterogeneous microscopic plastic strain fields in RVE. Compared with it, the NTFA well conquers this weakness and can theoretically obtain better results to simulate the mechanical responses of the nonlinear heterogeneous argillite.

As discussed in section 5.1 and 5.2, the argillite is considered as a composite composed of elastoplastic matrix (clay matrix) and linear elastic inclusions (quartz and calcite grains). In this section NTFA is used to simulate the same laboratory test results of argillite shown in section 3.5. Due to some numerical difficulties, only one mineralogical composition is calculated (matrix 60% and inclusion 40%). The parameters of each constituent cannot be determined directly because the microscopic mechanical response of each material phase is impossible to be obtained in the current experimental condition. As a result an indirect identification method has to be adopted. Firstly, the elastic parameters of quartz and calcite inclusion can be selected from the literatures of

handbook about the minerals. Then a numerical fitting process is performed to identify the parameters of clay matrix, regarding the macroscopic test results as the reference results. Finally a group of optimized local parameters are selected to simulate the macroscopic mechanical properties of argillite. The local parameters are shown in Table 5-4 and Table 5-5 for clay matrix and mineral inclusion, respectively. The simulation of triaxial compression results under different confining pressures are illustrated in Figure 5-4. We can see that the numerical simulation results are generally coincided with the test results. The main mechanical characters of argillite, such as significant plastic deformation, volumetric variation from compression to dilatancy related to plastic deformation, and the peak strength are well described by NTFA.

Table 5-4: Parameters of matrix

E_m(Pa)	υ_m	σ_0(Pa)	H_1(Pa)	H_2	t	b
3.0×10^{10}	0.30	1.0×10^{6}	1.5×10^{7}	0.4	55	3.0

(Continued)

α	ψ_0	ψ_m	t'
0.19	-0.18	0.15	30

Table 5-5: Parameters of inclusion

E_I(Pa)	υ_I
2.0×10^{10}	0.20

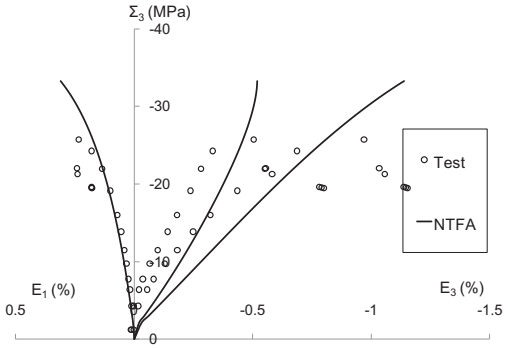

(a) Depth 482.2m, $f_m = 60\%$, $f_I = 40\%$

Uniaxial compression

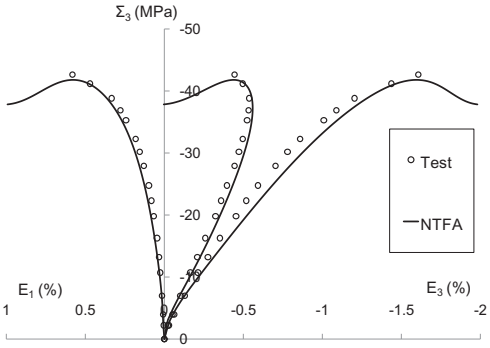

(b) Depth 482.2m, $f_m = 60\%$, $f_I = 40\%$

Triaxial compression, $\sigma_c = 5MPa$

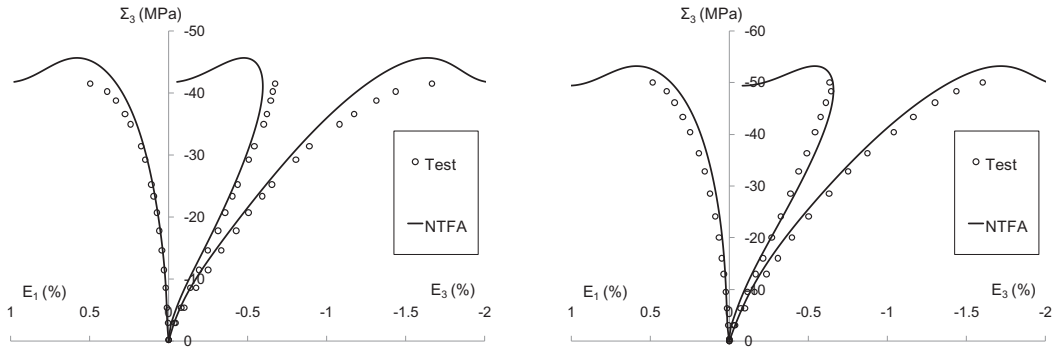

(c) Depth 482.2m, $f_m = 60\%$, $f_I = 40\%$

Triaxial compression, $\sigma_c = 10MPa$

(d) Depth 482.2m, $f_m = 60\%$, $f_I = 40\%$

Triaxial compression, $\sigma_c = 20MPa$

Figure 5-4: Comparison between the NTFA simulation and laboratory test

5.4 Conclusions

In this chapter the mechanical behavior of argillite is simulated by NTFA. The argillite is seen as a matrix-inclusion composite as mentioned in Chapter 3. For the sake of simplicity, the mechanical behavior of the clay matrix is described by an elastoplastic model with Drucker-Prager yield criterion. A specific function is used to describe the plastic hardening and softening. Further, a non-associated flow rule is adopted. A linear elastic model is used for mineral inclusion (quartz and calcite). Comparisons between numerical predictions by NTFA and experimental data have been presented for some simple cases, and a good overall agreement has been obtained. However, there are still quite important scatters for some loading paths and mineral compositions. Such scatters should be due to plastic modes used in NTFA simulations. Further works are still necessary for improve numerical prediction by more appropriate plastic modes.

Conclusions and future works

This thesis is devoted to the micromechanical modeling of nonlinear heterogeneous geomaterials with a specific application to the MHM argillite. Among various nonlinear homogenization methods, the Hill's incremental approach and non-uniform transformation field analysis (NTFA) have been adopted in this study.

As a preliminary phase of the present work, the direct FEM simulation of periodic heterogeneous materials was first performed and the obtained result served as reference solutions for comparisons and validation of two homogenization methods later developed. The unit cell of is transformed to a boundary value problem with periodic boundary conditions. The microscopic displacement fluctuations are considered as independent variables. In particular, we have focused on the cases with stress controlled loading paths in accordance with laboratory testing in geomaterials. A specific Newton-Raphson iteration method was proposed in order to obtain the corresponding macroscopic strain increment.

The Hill's incremental approach has then been studied. Combined with suitable isotropization procedures, it was seen that the incremental method seems to provide efficient predictions of macroscopic responses of non linear heterogeneous materials. In this study, several isotropization techniques have been studied and compared, and the influences of local plastic flow rule have been discussed to explore the efficiency of this approach in different situations.

Although the incremental approach associated with suitable isotropization methods provides satisfactory predictions of geomaterials (argillites) for specific cases, we cannot neglect its intrinsic limitations. The most important one is that the microscopic strain and stress fields in each material phase are assumed uniform in the incremental approach. This strong assumption is obviously far from real local fields which may be highly heterogeneous. Further, the isotropization method is not physically justified. In this study, the NTFA method proposed by Michel and Suquet was adapted. The heterogeneous local plastic strain fields are decomposed into a linear combination of several predefined plastic deformation modes. Compared with previous works, we have proposed an adaptation of the NTFA to nonlinear heterogeneous materials composed of pressure-sensitive constituents. The plastic strain field is decomposed into volumetric and deviatoric part, each of which is formulated as a linear combination of plastic modes. The computational implementation procedure of the NTFA has been studied in the context of geomaterials studied. Two examples have been presented to validate the proposed NTFA method, respectively for composite with Drucker-Prager plastic matrix and elastic inclusions, and a porous material with Drucker-Prager plastic matrix. We have shown that for the two examples

the NTFA method is able to predict correctly the overall mechanical behaviors of heterogeneous materials compared with the reference solution by FEM. Moreover, in the case of porous materials, the macroscopic yield surfaces issued from the NTFA is close to those predicted by other models.

One of the objectives of the present work is micromechanical modeling of the MHM argillite investigated in the context of feasibility study for geological storage of nuclear waste conducted by ANDRA. Two micromechanical models proposed in this work, incremental model and NTFA model, have been applied to modeling mechanical behavior of the argillite. It was considered as a composite with two phases, the elastoplastic clay matrix and linear elastic inclusions. In the case of the incremental approach associated with isotropization technique of Eshelby tensor, the numerical predictions were very close to experimental data and main features of argillite mechanical behavior have been correctly described. In particular, the influences of mineralogical compositions can be easily taken into account. Concerning the NTFA method, due to the complexity of the microstructure of argillite and time limitation of the present work, only a first phase of application to argillite was performed. It has been shown that there was also a good agreement between micromechanical predictions and experimental data. However, further investigations are still necessary to confirm the performance of the NTFA method in this situation.

As mentioned in this work, the micromechanical modeling of non linear heterogeneous geomaterials is still an open topic. It is necessary to pursue in various features. For instance, the NTFA is a promising non linear homogenization method. Further developments might be envisaged to improve its efficiency. For example, the choice of orthogonal plastic modes should be improved using more extensive numerical simulations covering more plastic deformation mechanisms or with the help of some analytical fields. As an example, in the case of porous materials, it will be interesting to use analytical strain fields issued from Eshelby solution to construct plastic deformation modes. There is also possibility of extension by using other local constitutive models such as elastoplastic damage model.

References

[1]. Abou-Chakra Guéry, A., Cormery, F., Shao, J. F., & Kondo, D. (2008). A micromechanical model of elastoplastic and damage behavior of a cohesive geomaterial. *International Journal of Solids and Structures , 45* (5), 1406-1429.

[2]. Abou-Charka Guéry, A. (2007). Contributions à la modélisation micromécanique du comportement non linéaire de l'argilite du Callovo-Oxfordien. Doctoral Thesis . USTL, Lille, France.

[3]. Adams, D. F., & Doner, D. R. (1967). Transverse normal loading of a unidirectional composite. Journal of Composite Materials , 1 (2), 152-167.

[4]. Berveiller, M., & Zaoui, A. (1979). An extension of the self-consistent scheme to plastically flowing polycrystal. J. Mech. Phys. Solids , 6, 325-344.

[5]. Bornert, M., Bretheau, T., & Gilormini, P. (2001). Homogénéisation en mécanique des matériaux 1- Matériaux aléatoires élastiques et milieux périodiques. Hermes Sciences Europe Ltd.

[6]. Bornert, M., Vales, F., & Halphen, B. (2001). Géomicromécanique des argillites du site Meuse/Haute Marne – Extensométrie. Report LMS-ANDRA N°BRP0LMS2001 -01/A.

[7]. Bossart, P., Meier, P. M., Moeri, A., Trick, T., & Mayor, J. C. (2002). Geological and hydraulic characterisation of the excavation disturbed zone in the Opalinus Clay of the Mont Terri Rock Laboratory. Engineering Geology , 66, 19-38.

[8]. Chaboche, J. L., Kanouté, P., & Roos, A. (2005). On the capabilities of mean-field approaches for the description of plasticity in metal matrix composites. International Journal of Plasticity , 21, 1409-1434.

[9]. Chaboche, J. L., Kruch, S., Maire, J. F., & Pottier, T. (2001). Towards a micromechanics based inelastic and damage modeling of composites. International Journal of Plasticity , 17, 411-439.

[10]. Chiarelli, A. S. (2000). Etude expérimentale et modélisation du comportement mécanique de l'argilite de l'Est. Thèse de l'Université des Sciences et Technologies de Lille .

[11]. Chiarelli, A. S., Shao, J. F., & Hoteit, N. (2003). Modeling of elastoplastic damage behavior of a claystone. International Journal of Plasticity , 19 (1), 23-45.

[12]. Conil, N., Djeran-Maigre, I., Cabrillac, R., & Su, K. (2004). Poroplastic damage model for claystones. Appl. Clay Sci , 26, 473-487.

[13]. Delay, J., Forbes, P. L., & Roman, J. (2007). The Meuse/Haute-Marne underground research laboratory: seven years of scientific investigations. Retrieved from http://www.andra.fr
http://www.andra.fr/lille2007/abstract_lille2007/donnees/pdf/007_008_O_01_1.pdf

[14]. Delay, J., Rebours, H., Vinsot, A., & Robin, P. (2007). Scientific investigation in deep wells for nuclear waste disposal studies at the Meuse/Haute Marne underground research laboratory, Northeastern France. Physics and Chemistry of the Earth , 32, 42-57.

[15]. Delay, J., Vinsot, A., Krieguer, J., Rebours, H., & Armand, G. (2007). Making of the underground scientific experimental programme at the Meuse/Haute-Marne underground research laboratory, North Eastern France. Physics and Chemistry of the Earth , 32, 2-18.

[16]. Doghri, I., & Ouaar, A. (2003). Homogenization of two-phase elasto-plastic composite materials and structures. Study of tangent operators, cyclic plasticity and numerical algorithms. International Journal of Solids and Structures , 40, 1681-1712.

[17]. Dormieux, L., & Barthélémy, J. -F. (2003). Détermination du crière de rupture macroscopique d'un milieu poreux par homogénéisation non linéaire. CR. Méc. Acad. Sci. Paris , 334, 271-276.

[18]. Dormieux, L., Kondo, D., & Ulm, F.-J. (2006). Microporomechanics. Wiley.

[19]. Drucker, D. -C., & Prager, W. (1952). Soil mechanicsand plastic analysis or limit design. Quartely of Appl. Math. , 157-175.

[20]. Dvorak, G. (1992). Transformation field analysis of inelastic composite materials. Proc. R. Soc. Lond. , A431, 89-110.

[21]. Dvorak, G., & Benveniste, Y. (1992). On transformation strains and uniform fields in multiphase elastic media. Proc. R. Soc. Lond. , A437, 291-310.

[22]. Dvorak, G., & Zhang, J. (2001). Transformation field analysis of damage evolution in composite materials. J. Mech. Phys. Solids. , 49, 2517-2541.

[23]. Dvorak, G., Baihe-El-Din, Y., & Wafa, A. (1994). Inplementation of the transformation field analysis for inelastic composite materials. Comput. Mech. , 68 (5), 201-228.

[24]. Eshelby, J. (1957). The determination of the elastic field of an ellipsoidal inclusion,

and related problems. Proc. Roy. Soc. , A 241, 376-396.

[25]. Fish, J., & Yu, Q. (2002). Computational mechanics of fatigue and life predictions for composite materials and structures. Comput. Methods. Appl. Mech. Eng. , 191, 4827-4849.

[26]. Fish, J., Shek, K., Pandheeradi, M., & Shepard, M. (1997). Computational plasticity for composite structures based on mathematical homogenisation: theory and practice. Comput. Methods. Appl.Mech. Eng. , 148, 53-73.

[27]. Gonzalez, C., Segurado, J., & Llorca, J. (2004). Numerical simulation of elasto-plastic deformation of composites: evolution of stress microfields and implications for homogenization models. Journal of the Mechanics and Physics of Solids , 52, 1573-1593.

[28]. Guo, T. F., Faleskog, J., & Shih, C. F. (2008). Continuum modeling of a porous solid with pressure-sensitive dilatants matrix. Journal of the Mechanics and Physics of Solids , 56, 2188-2212.

[29]. Gurson, A. L. (1977). Continuum theory of ductile rupture by void nucleation and growth: Part I – yield criteria and flow rules for porous ductile media. ASCE J. Engineering Materials Technology , 99, 2-15.

[30]. Hazanov, S., & Huet, S. (1994). Order relationships for boundary condition effects in heterogeneous bodies smaller than the representative volume. Journal of the Mechanics and Physics of Solids , 42, 1995-2011.

[31]. Hill, R. (1965). Continuum micro-mechanics of elastoplastic polycrystals. Journal of Mechanics and Physics of Solids , 13, 89-101.

[32]. Hoxha, D., Giraud, A., Homand, F., & Auvray, C. (2007). Saturated and unsaturated behaviour modelling of Meuse-Haute/Marne argillite. International Journal of Plasticity , 23 (5), 733-766.

[33]. Huet, C. (1990). Application of variational concepts to size effects in elastic heterogeneous bodies. Journal of the Mechanics and Physics of Solids , 8, 813-841.

[34]. Jiang, T., & Shao, J. F. (2009(b)). On the incremental approach for nonlinear homogenization of composite and influence of isotropization. Computational Materials Science ,46(2), 447-451.

[35]. Jiang, T., Abou-Chakra Guéry, A., Kondo, D., & Shao, J. F. (2009(a)). Multi-scale modeling for inelastic behavior of a cohesive geomaterial. Mechanics Research Communications , 36(6),673-681.

[36]. Kanouté, P., Boso, D. P., Chaboche, J. L., & Schrefler, B. A. (2009). Multiscale Methods for composites: a review. Arch. Comput. Methods. Eng. , 16, 31-75.

[37]. Kattan, P., & Voyiadjiis, G. (1993). Overall damage and elastoplastic deformation in fibrous metal matrix composites. Int. J. Plast. , 9, 931-949.

[38]. Lahellec, N., & Suquet, P. (2007). On the effecive behavior of nonlinear inelastic composites: I. Incremental variational principles. Journal of the Mechanics and Physics of Solids , 55 (9), 1932-1963.

[39]. Lahellec, N., & Suquet, P. (2007). On the effective behavior of nonlinear inelastic composites: II: A second-order procedure. Journal of the Mechanics and Physics of Solids , 55 (9), 1964-1992.

[40]. Lebedev, L. P., & Vorovich, I. I. (2003). Functional Analysis in Mechanics. New York: Springer-Verlag.

[41]. Lee, J. H., & Oung, J. (2000). Yield functions and flow rules for porous pressure-dependent strain-hardening polymeric materials. Journal of Engineering Mechanics , 67, 288-297.

[42]. Li S. and Wang G. (2008). Introduction to Micromechanics and Nanomechanics. World Scientific publishing

[43]. Lielens, G. (1999). Micro-macro modeling of structured materials. Ph.D thesis . Université Catholique de Louvain, Belgium.

[44]. Llorca, J., & Segurado, J. (2004). Three-dimensional multiparticle cell simulations of deformation and damage in sphere-reinforced composites. Materials Science and Engineering , A365, 267–274.

[45]. Maghous, S., Dormieux, L., & Barthélémy, J. F. (2009). Micromechanical approach to the strength properies of frictional geomaterials. European Journal of Mechanics A/Solids , 28 (1), 179-188.

[46]. Mandel, J. (1972). Plasticité classique et Viscoplasticité, CISM Lecture Notes (Vol. 97). Wien: Springer-Verlag.

[47]. Masson, R. (1998). Estimations non linéaires du comportement global de matériaux hétérogénes. Thése de doctorat . Ecole Polytechnique.

[48]. Masson, R., Bornert, M., Suquet, P., & Zaoui, A. (2000). An affine formulation for the prediction of the effective properties of nonlinear composites and polycrystals. Journal of the Mechanics and Physics of Solids , 48, 1203-1227.

[49]. Michel, J. C., & Suquet, P. (2004). Computational analysis of nonlinear composite

structures using the nonuniform transformation field analysis. Comput. Methods Appl. Mech. Engrg. , 193, 5477-5502.

[50]. Michel, J. C., & Suquet, P. (2003). Nonuniform transformation field analysis. International Journal of Solids and Structures , 40, 6937-6955.

[51]. Michel, J. C., Galvanetto, U., & Suquet, P. (2000). Constitutive relations involving internal variables based on a micromechanical analysis. In G. A. Maugin, R. Drouot, & F. Sidoroff (Eds.), Continuum Thermomechanics: The Art and Science of Modelling Material Behavior. Kluwer Acad. Pub.

[52]. Michel, J. C., Moulinec, H., & Suquet, P. (1999). Effective properties of composite materials with periodic microstructure: a computational approach. Comput. Methods. Appl. Mech. Engrg. , 172, 109-143.

[53]. Mori, T., & Tanaka, K. (1973). Average stress in matrix and average elastic energy of materials with misfitting inclusions. Acta Metallurgica , 21, 571-574.

[54]. Moulinec, H., & Suquet, P. (1994). A fast numerical method for computing the linear and nonlinear properties of composites. C.R. Acad. Sci. Paris , II 318, 1417-1423.

[55]. Moulinec, H., & Suquet, P. (1998). A numerical method for computing the overall respinse of nonlinear composites with complex microstructure. Comput. Mithods. Appl. Mech. Engng , 157, 69-94

[56]. Multon G.W. (2004). The theory of composites. Cambridge University Press

[57]. Needleman, A. (1972). Void growth in an elasti plastic medium. Journal of Applied Mechanics , 39, 964-970.

[58]. Nemat-Nasser, S. H., & Hori, M. (1999). Micromechanics: Overall Properties of Heterogeneous Materials. North-Holland.

[59]. Pastor, F., Thoré, P., Loute, E., Pastor, J., & Trillat, M. (2008). Convex optimization and limit analysis: Application to Gurson and porous Drucker-Prager materials. Engineering Fracture Mechanics , 75, 1367-1383.

[60]. Pensée, V., Kondo, D., & Dormieux, L. (2002). Micromechanical analysis of anisotropic damage in brittle materials. Journal of Engineering Mechanics ASCE , 128 (8), 889-897.

[61]. Pierard, O., & Doghri, I. (2006). A study of various estimates of the macroscopic tangent operator in the incremental homogenization of elasto-plastic composites. International Journal for Multiscale Computational Engineering , 4, 521-543.

[62]. Pierard, O., Frieble, C., & Doghri, I. (2004). Mean-field homogenization of

multi-phase thermo-elastic composites: a general framework and its validation. Compos. Sci. Technol. , 64 (10-11), 1587-1603.

[63]. Pierard, O., Gonzalez, C., Segurado, J., Llorca, J., & Doghri, I. (2007). Micromechanics of elasto-plastic materials reinforced with ellipsoidal inclusions. International Journal of Solids and Structures , 44, 6945-6952.

[64]. Pierard, O., Llorca, J., Segurado, J., & Doghri, I. (2007). Micromechanics of particle-reinforced elasto-viscoplastic composites: Finite element simulations versus affine homogenization. International Journal of Plasticity , 23, 1041-1060.

[65]. Pietruszczak, S., Jiang, J., & Mirza, F. A. (1988). An elastoplas tic constitutive model for concrete. International Journal of Solids and Structures , 24, 705-722.

[66]. Pietruszczak, S., Lydzba, D., & Shao, J. F. (2002). Modelling of inherent anisotropy in sedimentary rocks. International Journal of Solids and Structures , 39 (3), 637-648.

[67]. Rice, J. R. (1970). On the structure of stress-strain relations for time-dependent plastic deformation in metals. J. Appl. Mech. , 37, 728-737.

[68]. Roussette, S., Michel, J. C., & Suquet, P. (2008). Nonuniform transformation field analysis of elastic-viscoplastic composites. Composites Science and Technology , 69 (1), 22-27.

[69]. Rynne, B. P., & Youngson, M. A. (2008). Linear Functional Analysis (Second Edition ed.). London: Springer-Verlag.

[70]. Segurado, J., & Llorca, J. (2005). A computational micromechanics study of the effect of interface decohesion on the mechanical behavior of composites. Acta Materialia , 53, 4931-4942.

[71]. Segurado, J., & Llorca, J. (2004). A new three-dimensional interface finite element to simulate fracture in composites. International Journal of Solids and Structures , 41, 2977–2993.

[72]. Segurado, J., & Llorca, J. (2001). A numerical approximation to the elastic properties of sphere-reinforced composites. Journal of the Mechanics and Physics of Solids , 50, 2107-2121.

[73]. Segurado, J., & Llorca, J. (2002). A numerical approximation to the elastic properties of sphere-reinforced composites. Journal of the Mechanics and Physics of Solids , 50, 2107-2121.

[74]. Segurado, J., & Llorca, J. (2006). Computational micromechanics of composites: The effect of particle spatial distribution. Mechanics of Materials , 38, 873-883.

[75]. Segurado, J., Gonzalez, C., & Llorca, J. (2003). A numerical investigation of the effect of particle clustering on the mechanical properties of composites. Acta Materialia , 51, 2355-2369.

[76]. Segurado, J., Llorca, J., & Gonzalez, C. (2002). On the accuracy of mean-field approaches to simulate the plastic deformation of composites. Scripta Materialia , 46, 525-529.

[77]. Shao, J. F., & Henry, J. P. (1991). Development of an elastoplastic model for porous rock. International Journal of Plasticity , 6 (1), 1-13.

[78]. Shao, J. F., Hoxha, D., Bart, M., Homand, F., Duveau, G., Souley, M., et al. (1999). Modelling of induced anisotropic damage in granite. International Journal of Rock Mechanics and Mining Sciences , 36 (8), 1001-1012.

[79]. Shao, J. F., Zhou, H., & Chau, K. T. (2005). Coupling between anisotropic damage and permeability variation in brittle rocks. International Journal for Numerical and Analytical Methods in Geomechanics , 29, 1231-1247.

[80]. Suquet, P. (1997). Effective properties of nonlinear composites. In P. Suquet (Ed.), Continuum Micromechanics, CISM Lecture Notes (Vol. 377, pp. 197-264). New York: Springer Verlag.

[81]. Suquet, P. (1987). Elements of homogenization for inelasic solid mechanics. In A. Zaoui (Ed.), Homogenization techniques for composite media, Lecture nots in physics (Vol. 272, pp. 193-278). New York: Springer-Verlag.

[82]. Suquet, P. (1985). Local and global aspects in the mathematical theory of plasticity. In A. Sawczuk, & G. Bianchi, Plasticity Today: Modelling Methods and Applications (pp. 279-310). London: Elsevier.

[83]. Tandon, G. P., & Weng, G. J. (1988). A theory of particle-reinforced plasticity. J. Appl. Mech. , 55 (1), 126-135.

[84]. Torquato, S. (2001). Random heterogeneous materials. Springer.

[85]. Trillat, M., & Pastor, J. (2005). Limit analysis and Gurson's model. European Journal of Mechanics A/Solids , 24, 800-819.

[86]. Trillat, M., Pastor, J., & Thoré, P. (2006). Limit analysis and programming: 'porous Drucker-Prager' material and Gurson's model. Comptes Rendus Mécanique , 334, 599-604.

[87]. Tvergaard, V. (1981). Influence of voids on shear bands instabilities under plane strain conditions. Int. J. Fracture , 17, 389-407.

[88]. Zaoui, A. (2002). Continuum micromechanics: survey. Journal of Engineering Mechanics , 128 (8), 808-816.

[89]. Zaoui, A. (2000). Matériaux hétérogènes et composites. Teaching material of l'Ecole Polytechnique.

Contribution to the micromechanical modelling of inelastic behaviors of heterogeneous geomaterials

This study is devoted to the micromechanical modelling of inelastic behaviors of heterogeneous geomaterials. A kind of hard clay rock (argillite) is taken as an example to validate the micromechanical modelling. A short review of main homogenization techniques developed for multi-scale modeling of nonlinear heterogeneous materials is presented in the first chapter. Then some numerical results from direct FEM simulation are given in the second chapter. In the following chapter, one of the most commonly used approaches of nonlinear homogenization methods for nonlinear heterogeneous materials, Hill's incremental approach, is studied and applied to simulate the mechanical behaviors of argillite with various compositions under different loading paths. Considering some theoretical limitations of the incremental approach, a new homogenization method named nonuniform transformation field analysis (NTFA) firstly proposed by Michel and Suquet is adopted and developed to adapt the pressure-dependent geomaterials in chapter 4. In this chapter the formulation and numerical implementation of the NTFA for a typical pressure-dependent heterogeneous materials composed of Drucker-Prager matrix and elastic inclusion are presented. Next, in chapter six a more complicated application is performed to simulate the mechanical behavior of argillite to verify the validity of the proposed NTFA method.

Key words: Micromechanics, homogenization, multi-scale modelling, plasticity, geomaterials, rocks, Drucker-Prager criterion

Contribution à la modélisation micromécanique des comportements inélastiques des géomatériaux hétérogènes

Cette étude est consacrée à la modélisation micromécanique de comportement inélastique des géomatériaux hétérogènes . Une sorte de roche d'argile dure (argilite) est considérée comme un exemple pour valider la modélisation micromécanique. Un bref aperçu des principales techniques d'homogénéisation pour la modélisation multi-échelles développées de matériaux non-linéaire hétérogènes est présenté dans le premier chapitre. Puis quelques résultats numérique des simulations directes FEM sont donnés dans le deuxième chapitre. Dans le chapitre suivant, l'une des approches les plus couramment utilisée de méthodes d'homogénéisation non-linéaire des matériaux hétérogènes non linéaires, approche incrémentale de Hill, est étudiée et appliquée pour simuler le comportement mécanique de l'argilite avec des divers compositions sur différents parcours de chargement. Compte tenu des certains limites théoriques de l'approche incrémentale, une nouvelle méthode d'homogénéisation nommé analyse des champs avec transformation non-uniforme (NTFA) proposé d'abord par Michel et Suquet est adoptée et développée pour s'adapter aux géomatériaux pression-dépendants dans Chapitre 4. Dans ce chapitre, la formulation et la mise en œuvre numérique de la NTFA pour des matériaux hétérogènes composés d'une matrice pression-dépendante de type Drucker-Prager et une inclusion élastique sont présentés. Ensuite, dans le chapitre six une application plus compliquée est réalisée pour simuler le comportement mécanique de l'argilite afin de valiter de la méthode proposée NTFA.

Mots clés: micromécanique, homogénéisation, modélisation multi-échelles, plasticité, géomatériaux, roches, critère de Drucker-Prager